Confirmatory Appendices

APPENDIX I: ANSI/ANS JET MODEL

APPENDIX II: CONFIRMATORY DEBRIS GENERATION ANALYSES

The Nuclear Energy Institute (NEI) guidance contains recommendations that will determine the quantities of insulation debris generated with the zone of influence (ZOI). These recommendations include the size of the ZOI based on the insulation destruction pressure and the fraction of the insulation located within the ZOI that subsequently is damaged into the small-fine-debris category. Confirmatory research was performed to ascertain whether the NEI recommendation would reliably result in conservative estimates for the volumes of debris generated within the ZOI. This appendix documents the confirmatory research estimates for the volumes of small fine debris. The confirmatory research for determining the size of the ZOI is the subject of Appendix I. Both the NEI guidance and the confirmatory research used the ANSI/ANS-58.2-1988 standard to calculate the jet isobar volumes with very similar results. The confirmatory research issues addressed herein include the following.

- The NEI guidance recommends the assumption that 60% of the fibrous and 75% of the reflective metal insulation (RMI) volume contained within the ZOI becomes small fine debris. Confirmatory research was performed that integrated the insulation damage versus jet pressures over the ZOI volume to determine the fraction of the insulation within the ZOI that would become small fine debris based on available debris generation data.

- The NEI guidance recommends adapting the debris-size distribution for NUKON™ to other types of fibrous insulation that have a destruction pressure higher than that of NUKON™. The size distribution confirmatory research provides partial justification that supports that NEI recommendation.

- The applicability of air-jet-determined destruction pressures to two-phase pressurized-water-reactor (PWR) loss-of-coolant-accident (LOCA) jets has been questioned. NUREG/CR-6762 (Vol. 3) noted that data from the Ontario Power Generation (OPG) two-phase debris generation tests indicated that the destruction pressure could be lower for a two-phase jet than for an air jet and that the resultant debris could be finer. Therefore, it may be prudent to apply a safety factor to accommodate the uncertainty. This confirmatory analysis estimates the volume fractions for small fine debris if an alternate lower destruction pressure were used than those in the NEI guidance.

II.1 COMPARISON OF JET ISOBAR VOLUME CALCULATIONS

Three calculations of the jet isobar volumes were available for comparison.[*] The calculations were the following.

- The volumes determined from the NEI guidance recommended values for ZOI radii versus the destruction pressures in NEI baseline guidance's Table 3-1. The destruction pressure represents the jet isobar pressure for each particular ZOI radii.
- The volumes determined from the confirmatory research (Appendix I) for the ZOI radii versus the jet pressure.

[*] The volumes are actually presented in terms of the break diameter cubed (D^3) corresponding to an equivalent spherical radius in terms of r/D (i.e., $4/3\ \pi\ r^3/D^3$).

- The volumes determined from the boiling-water-reactor owners' group (BWROG) recommendation documented in their utility resolution guidance (URG). Although these volumes apply to a BWR steam jet rather than a PWR two-phase jet, the volumes are compared here to demonstrate the differences between PWR and BWR LOCA jets.

Both the NEI guidance and the confirmatory research volume calculations used the ANSI/ANS-58.2-1988 standard method, whereas the BWROG URG method used the computational-fluid-dynamics (CFD) code, NPARC, to evaluate the volumes. The equivalent spherical radii for these three methods are compared in Figure II-1.

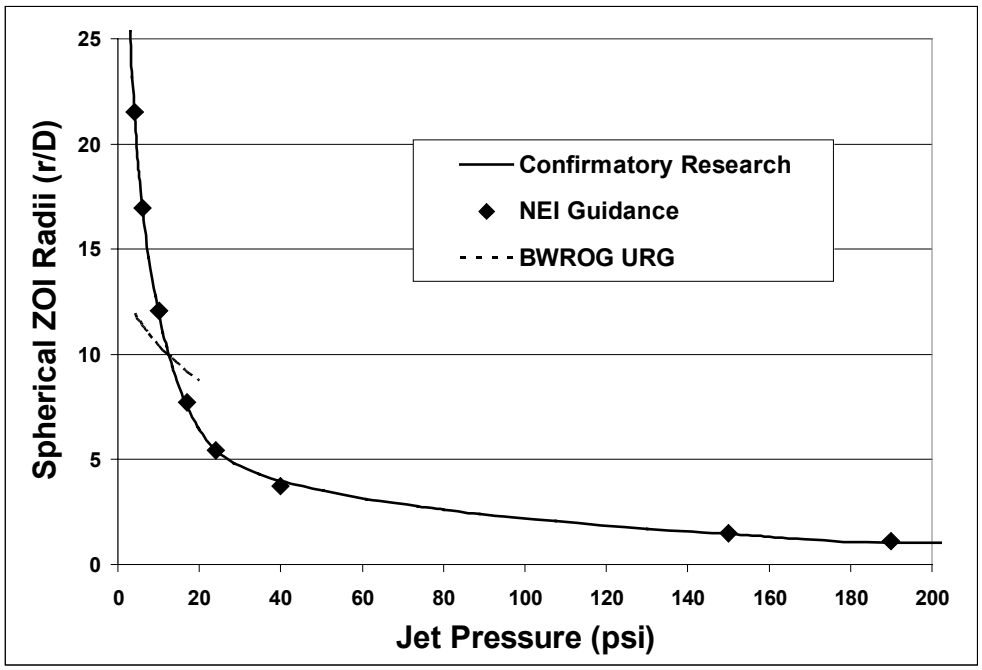

Figure VI-1. Comparison of Jet Isobar Volumes.

As shown, at the lower jet pressures, the pressure isobar volumes are much larger for the PWR two-phase LOCA jet than for the BWR steam jet. A principal reason for this difference is the higher energy associated with the higher pressure of a PWR reactor coolant system (RCS) than with a BWR RCS; however, another consideration is the accuracy of the ANSI/ANS-58.2-1988 standard at the lower pressures. For example, the validity of the assumption in the ANSI/ANS-58.2-1988 standard that the jet expands at a half angle of 10 degrees once the jet expansion has reached the asymptotic plane becomes more important at the lower expansion pressures. The accuracy of the debris volumes of insulations that damage significantly at the lower jet pressures is subject to the accuracy of this assumption. Note that the confirmatory research and NEI-recommended-equivalent spherical ZOI radii are in good agreement.

II.2 METHOD OF DETERMINING ZOI DEBRIS-SIZE DISTRIBUTIONS

The volume of debris generated within a ZOI depends on the following three factors: (1) the size of the ZOI defined by the spherical radius, (2) the concentration of a particular insulation within the ZOI, and (3) the fraction of the ZOI insulation that is damaged into a particular debris-size

classification. The size distribution and spherical ZOI radius are interdependent. The threshold damage pressure and the jet volumes determine the size of the ZOI (Appendix I). The insulation concentration within a ZOI is determined by plant-specific information (i.e., the volume of a particular insulation within the ZOI divided by the volume of the ZOI).

Integration of experimental debris generation data is required to determine the fraction of the ZOI insulation that is damaged into a particular debris-size classification (e.g., NEI small fine debris). A generalized equation was offered in NUREG/CR-6808 for this integration. A slightly expanded version of this equation is

$$F_{ZOI} = \frac{3}{r_{ZOI}^3} \int_0^{r_{ZOI}} f_d\left(P_{jet}(r)\right) r^2 \, dr \quad ,$$

where

F_{ZOI} = the fraction of the ZOI insulation type i that is damaged into a particular debris-size classification;

f_d = the fraction of debris damaged into a particular debris size as a function of the jet pressure P_{jet}, which is a function of the spherical radius, r, within the ZOI; and

r_{ZOI} = the outer radius of the ZOI.

Implicit in this integration is the assumption that the insulation is uniformly distributed within the ZOI, which may not be realistic. Because the functional information needed for this integration is not available in an equation form simple enough for a formal integration to proceed, the following simplification is used:

$$F_{ZOI} = \frac{1}{r_{ZOI}^3} \sum_j \left[\frac{f_{fines}\left(P_{jet}(r_j)\right) + f_{fines}\left(P_{jet}(r_{j-1})\right)}{2} \left(r_j^3 - r_{j-1}^3\right) \right] \quad ,$$

where

f_{fines} = the fraction of debris damaged into a particular debris size as a function of the jet pressure P_{jet} at a radius of r_j.

The spherical ZOI is first subdivided into numerous spherical shells (j). The precision of the integration increases with the number of subdivisions. In a spreadsheet, the jet pressure is listed in increasing values and then the spherical radii are determined, followed by the damage fraction evaluated at each r_j. For the intervals, the average damage across the interval and the volume of the interval is determined. Multiplying the average interval damage by the interval volume, summing, and dividing by the total ZOI volume results in the debris fraction for the ZOI.

II.3 EVALUATION OF DEBRIS SPECIFIC DAMAGE FRACTIONS AND POTENTIAL DEBRIS VOLUME

Potential debris volumes were calculated for fibrous, RMI, and particulate debris types and compared with the NEI baseline model to determine whether the baseline is conservative. The

potential volume of debris is defined as the fraction of the ZOI debris damaged into a particular debris size multiplied by the total volume of the sphere, as

$$V_{Potential} = F_{ZOI}\left(\frac{4}{3}\pi\right) r_{ZOI}^3 \quad .$$

Note that to calculate the volume of small fine debris generated, the potential volume must be multiplied by the concentration of insulation ($C_{insulation}$), i.e., the fraction of the ZOI actually occupied by the insulation, and by the pipe break diameter cubed. Again, it is assumed that the insulation type in question is uniformly distributed over the ZOI, regardless of the size of the ZOI, as

$$V_{Fines} = C_{Insulation}\, V_{Potential}\, D^3 \quad .$$

II.3.1 Fibrous Debris

The fibrous insulation types evaluated include NUKON™, Transco (Transco Products, Inc., or TPI), Temp-Mat, K-wool, and Knauf. Table II-1 shows the NEI-guidance-recommended destruction pressures and an alternate set of values used herein to test the sensitivity of the potential debris volumes to the destruction pressures.

Table VI-1. Fibrous Insulation Destruction Pressures

Insulation	NEI Recommendation	Alternate Lower Pressure
NUKON™	10 psi	6 psi
TPI	10 psi*	6 psi
Knauf	10 psi	6 psi
Temp-Mat	17 psi	10 psi
K-wool	40 psi	17 psi

II.3.1.1 Low-Density Fiberglass (LDFG) Debris

A review of the air jet testing debris generation data, both the BWROG Air Jet Impact Testing (AJIT) data (BWROG URG) and the drywell debris transport study (DDTS) data [NUREG/CR-6369, 1999], demonstrates that NUKON™, TPI, and Knauf fiberglass insulations underwent similar damage. These insulations have approximately the same as-manufactured density (~2.4 lb/ft^3), and their recommended minimum pressures for destruction are usually taken to be the same pressure. Therefore, these insulations have been grouped together as LDFG insulation.

The fractions for the small fines from the AJIT debris generation test data are plotted in Figure II-2 as a function of the jet centerline pressure for these three types of LDFG insulations. A curve was drawn through the data to continuously represent the damage for use in the damage integration over the ZOI. One set of seven data points was from tests (in the DDTS) that used a

* NEI guidance considers TPI fiber blankets to behave similarly to NUKON™ blankets.

4-in. nozzle, whereas the remainder used a 3-in. nozzle. The 4-in. nozzle data from the DDTS generally shows more damage than do the 3-in. nozzle tests. The basic reason for the higher damage was that with the larger-diameter jet, more of the target insulation blanket was exposed to higher pressures. Note that the data were correlated by the estimated jet centerline pressure but that the pressure on the blanket decreased outward from the centerline. When the blanket was placed in close to the jet, the ends of the blanket were hit with substantially less force of flow than the centerline for which the data were correlated. For example, for the 3-in. nozzle data point for NUKON™ at a jet pressure of 20 psi, only ~7% of the insulation was damaged into small fine debris, whereas the TPI blankets in the 4-in. nozzle were totally destroyed at this pressure. Apparently, testing blanket destruction for insulations requiring a pressure higher than ~17 psi needs a jet nozzle larger than 3 in. For LDFG, any jet pressure larger than ~17 psi will totally destroy the blanket into small fine debris, whereas the NEI guidance cited an OPG two-phase jet test with 52% of the insulation damaged into small fine debris as their basis of conservatism.

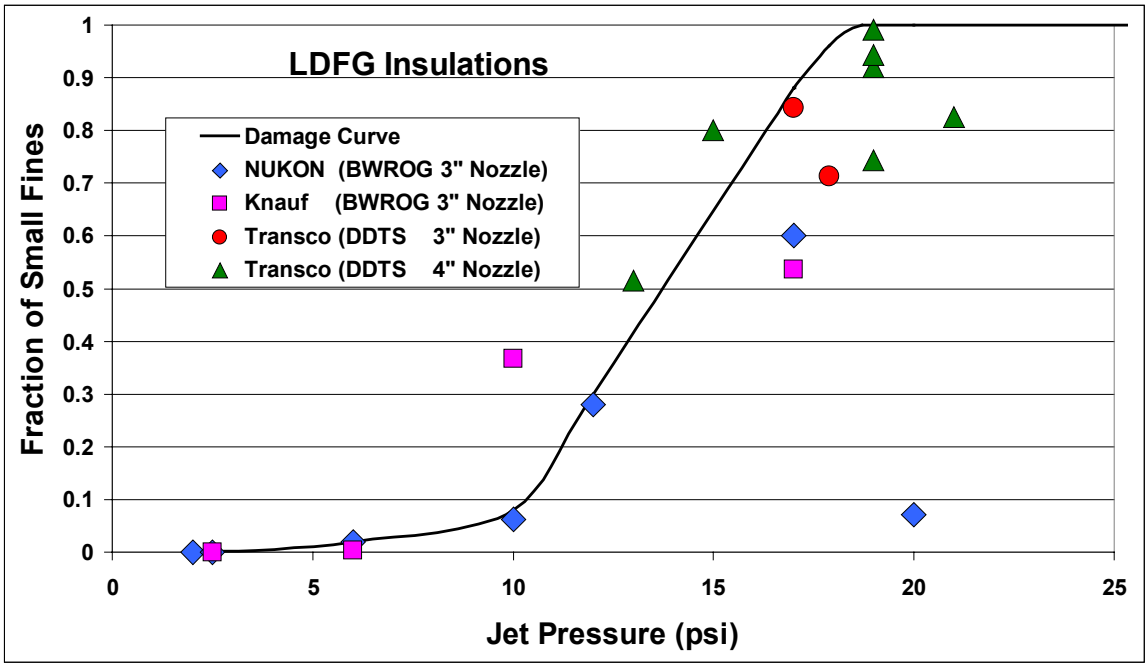

Figure VI-2. LDFG Damage Curve for Small Fine Debris.

Another significant point of discussion is that the threshold of damage for LDFG insulation has been specified as 10 psi, where Figure II-2 clearly shows damage at jet pressures <10 psi. Apparently, neglecting the tail of the damage curve was considered acceptable for the BWR strainer resolution because of the lesser BWR jet volumes at lower pressures, as shown in Figure II-1. However, the much larger jet volumes below 10 psi for the PWR jet shown in Figure II-1 make the neglect of the tail less acceptable.

The results of debris-size distribution integration over the ZOI are provided in Table II-2. A lower alternate damage pressure results in a larger equivalent spherical ZOI; however, a lesser fraction of the debris is damaged into small fine debris. The use of the alternate damage pressures over the NEI-recommended damage pressures for PWR analyses would result in

~16% more small fine debris. The potential debris volumes are compared in Figure II-3, along with an estimate using the baseline guidance. The baseline estimate is simply 60% of 4/3 π $(12.1/D)^3$. As shown, the baseline guidance appears to be conservative, but not overly so.

Table VI-2. Results of Debris-Size Distribution Integration for LDFG Insulations

Jet Pressure Isobar Volume Calculation	Radius of Sphere (r/D)	Fraction Small Fines	Potential Debris Volumes (V/D^3)
NEI-Recommended Damage Pressures			
BWROG Steam Jet	10.4	0.83	3910
PWR Two-Phase Jet (Confirmatory)	11.9	0.53	3790
Alternate Damage Pressures			
BWROG Steam Jet	11.4	0.65	3980
PWR Two-Phase Jet (Confirmatory)	17.0	0.22	4410

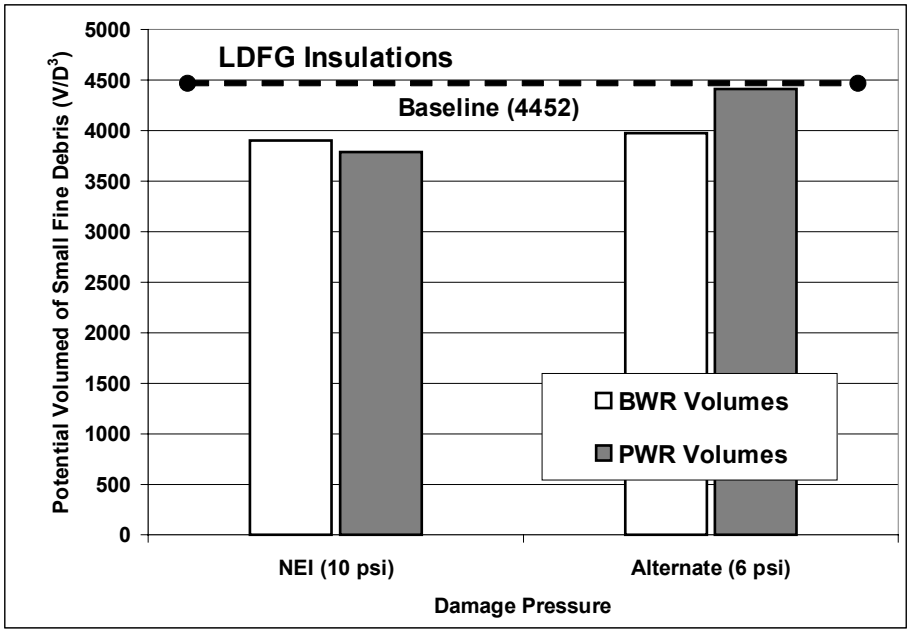

Figure VI-3. Potential Volumes of Small Fines LDFG Debris. fix y axis label (volumes)

The NEI baseline guidance completely neglects the transport of large debris to the sump screen; however, some plants will likely need to consider large debris transport as part of a more realistic evaluation. Therefore, the following equation is provided to estimate the volume of large debris generated within the ZOI:

$$V_{Large} = C_{Insulation}\left(1 - F_{ZOI}\right)\left(\frac{4}{3}\pi\right) r_{ZOI}^3 \, D^3 \quad .$$

Also, plants that must perform more realistic evaluations may need to subdivide the baseline small-fine-debris class into fines and small-piece debris, where the fines (e.g., individual fibers) remain suspended in the pool and the small-piece debris sinks to the pool floor where the debris may or may not transport to the sump screen. The baseline guidance has the inherent assumption that all of its small fine debris essentially remains suspended.

During the debris generation tests conducted during the DDTS, 15% to 25% of the debris from a completely disintegrated TPI fiberglass blanket was classified as nonrecoverable. The nonrecoverable debris either exited the test chamber through a fine-mesh catch screen or deposited onto surfaces in such a fine form that it could not be collected by hand (it was collected by hosing off the surfaces). Therefore, it would be reasonable to assume that 25% of the baseline small fine debris (i.e., F_{ZOI}) is in the form of individual fibers and that the other 75% is in the form of small-piece debris.

II.3.1.2 Temp-Mat Debris

Temp-Mat is much higher-density insulation (~11.8 lb/ft^3) than the LDFG insulation and requires a significantly higher-pressure jet pressure to damage the insulation. The Temp-Mat insulation debris fractions for the small fine debris from the AJIT tests are shown in Figure II-4. This figure shows six data points for Temp-Mat, two of which were tests where no significant damage was noted. The test with the maximum damage had ~36% of the insulation damaged into small fine debris, with the remainder of the insulation forming large-piece debris. Unfortunately, no tests were conducted with jet pressures high enough to complete the damage curve to total destruction into small fine debris, as was done for the LDFG insulations. Therefore, a conservative extrapolation of the data is required to perform the debris generation integration over the equivalent ZOI sphere. The extrapolation used herein is shown as a dashed line in Figure II-4. The selection of the NEI-guidance damage pressure of 17 psi is also illustrated in Figure II-4, where it is seen that significant small fine debris is generated at jet pressures below 17 psi.

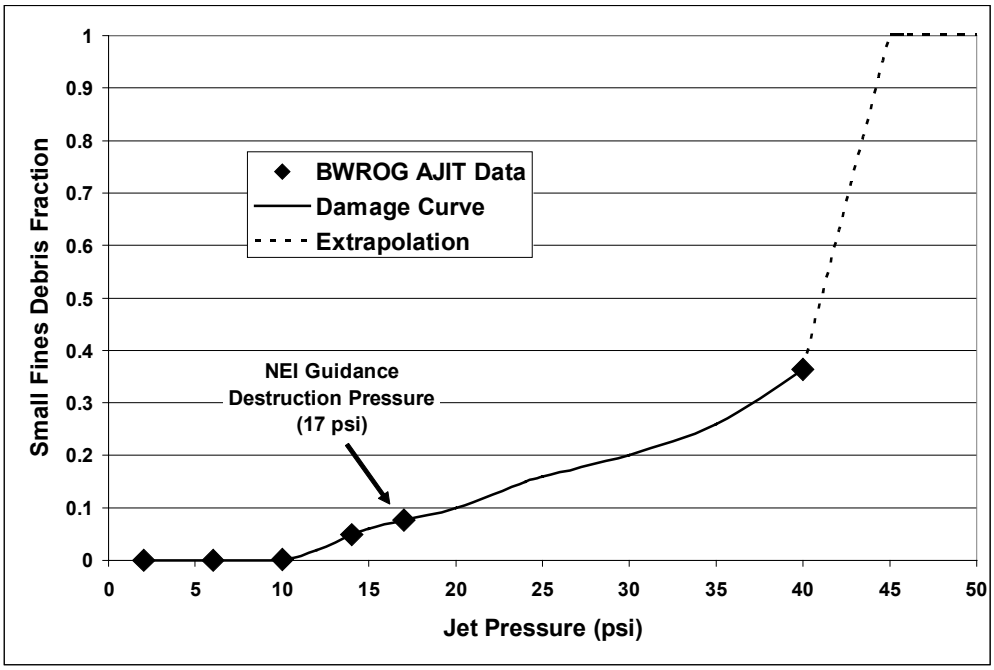

Figure VI-4. Temp-Mat Damage Curve for Small Fine Debris. fix x axis to "fine"

The results of the Temp-Mat debris-size distribution integration over the ZOI are provided in Table II-3. The potential debris volumes are compared in Figure II-5, along with an estimate using the baseline guidance [60% of 4/3 π $(7.8/D)^3$]. A lower alternate damage pressure results in a larger equivalent spherical ZOI; however, a lesser fraction of the debris is damaged into small fine debris. The use of the alternate damage pressures over the NEI-recommended damage pressures for PWR analyses would result in ~36% more estimated small fine debris. For Temp-Mat insulation, the baseline is conservative with respect to both the NEI-guidance damage pressure of 17 psi and the alternate pressure of 10 psi.

The debris-size estimate for Temp-Mat has more uncertainty associated with the estimate than does the similar calculation for LDFG, primarily because of more limited data. The negative uncertainties include the neglect of the damage curve tail by the NEI-recommended damage pressure (quantified using the alternate damage pressure) and the fact that the BWROG AJIT tests used the small 3-in. nozzle, which makes it difficult to subject the entire target blanket to the characteristic jet pressure (near the centerline pressure) when the blanket is located close to the nozzle. The positive uncertainty is the sharp extrapolation of the damage curve to 100% destruction at 45 psi. In this case, it is possible that the positive uncertainty overshadows the negative uncertainties.

Table VI-3. Results of Debris-Size Distribution Integration for Temp-Mat Insulation

Jet Pressure Isobar Volume Calculation	Radius of Sphere(r/D)	Fraction Small Fines	Potential Debris Volumes (V/D^3)
NEI Recommended Damage Pressures			
PWR Two-Phase Jet (Confirmatory)	7.5	0.25	448
Alternate Damage Pressures			
PWR Two-Phase Jet (Confirmatory)	11.9	0.086	608

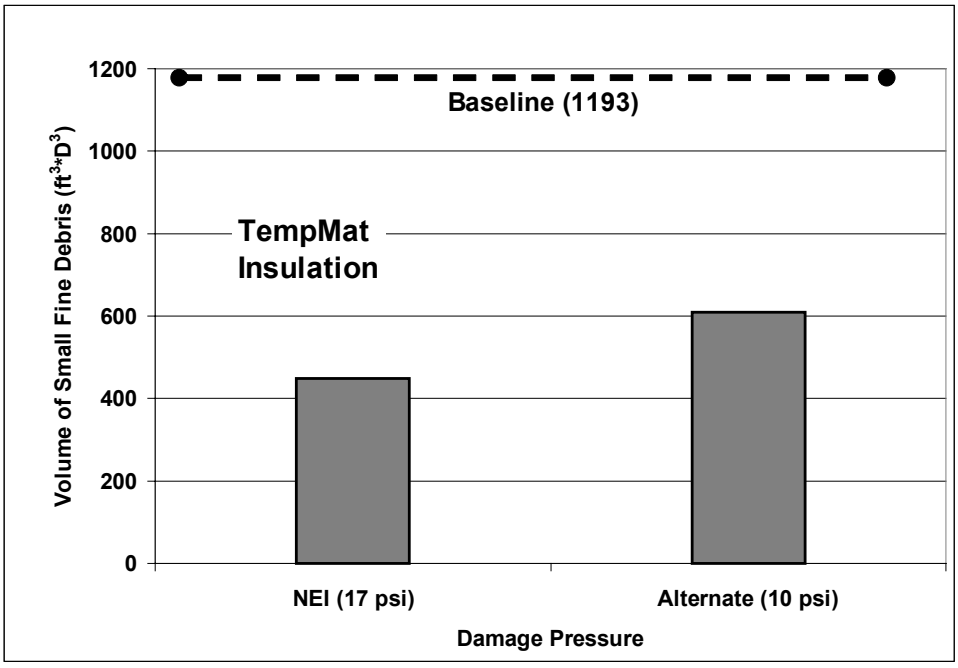

Figure VI-5. Potential Volumes of Small Fine Temp-Mat Debris.

II.3.1.3K-wool Debris

K-wool is also higher-density insulation (~10 lb/ft^3) than the LDFG insulation and requires an even higher-pressure jet pressure to damage the insulation. The NEI-recommended damage pressure for K-wool is 40 psi. The K-wool insulation debris fractions for the small fine debris from the AJIT tests are shown in Figure II-6. This figure shows only four data points for K-wool, two of which were tests where no significant damage was noted. The test with the maximum damage had ~7.1% of the insulation damaged into small fine debris, with much of the remainder of the insulation still contained in the blanket cover and still attached to the target mount. As with the Temp-Mat data, the K-wool damage curve is incomplete because the highest jet pressure tested was that of the NEI-recommended damage pressure. To perform the debris generation integration over the equivalent ZOI sphere, the test data were conservatively extrapolated, as shown in Figure II-6.

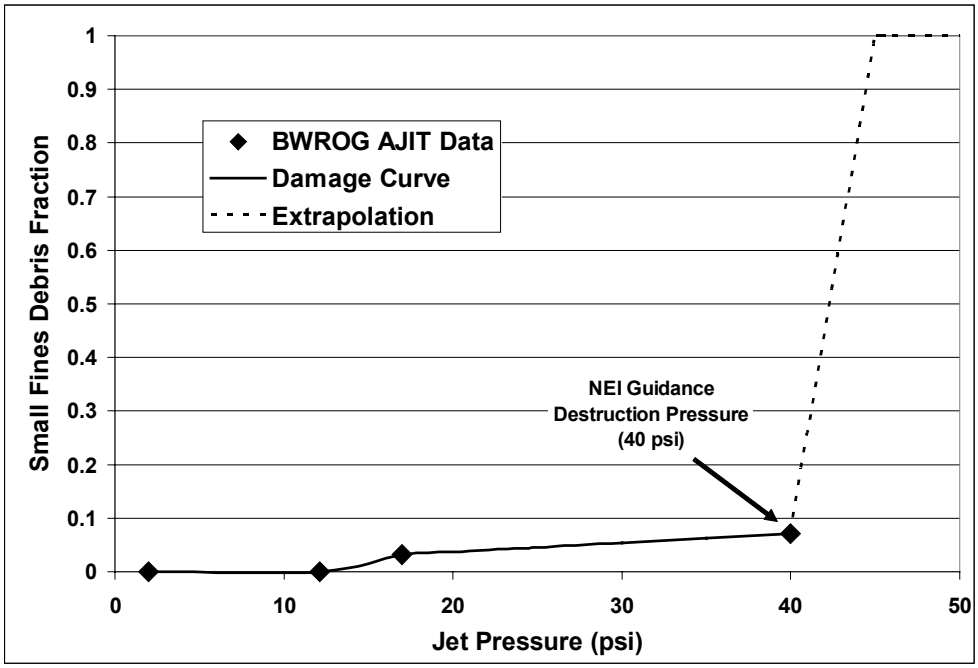

Figure VI-6. K-wool Damage Curve for Small Fine Debris. fix x axis label to "fine"

The results of the K-wool debris-size distribution integration over the ZOI are provided in Table II-4. The potential debris volumes are compared in Figure II-7, along with an estimate using the baseline guidance [60% of 4/3 π $(3.8/D)^3$]. The difficulty with the K-wool integration is that there is no debris generation data for a jet pressure higher than the NEI-recommended destruction pressure of 40 psi. Therefore, to ensure conservative debris-size integration, it must necessarily be assumed that the insulation is completely destroyed at a pressure higher than 40 psi (the integration herein assumed 100% at 45 psi). However, this assumption may be overly conservative. For K-wool insulation, the baseline is not conservative with respect to either the NEI-guidance damage pressure of 40 psi or the alternate pressure of 17 psi.

Table VI-4. Results of Debris-Size Distribution Integration for K-wool Insulation

Jet Pressure Isobar Volume Calculation	Radius of Sphere(r/D)	Fraction Small Fines	Potential Debris Volumes (V/D^3)
NEI-Recommended Damage Pressures			
PWR Two-Phase Jet (Confirmatory)	4.0	0.92	246
Alternate Damage Pressures			
PWR Two-Phase Jet (Confirmatory)	7.5	0.17	307

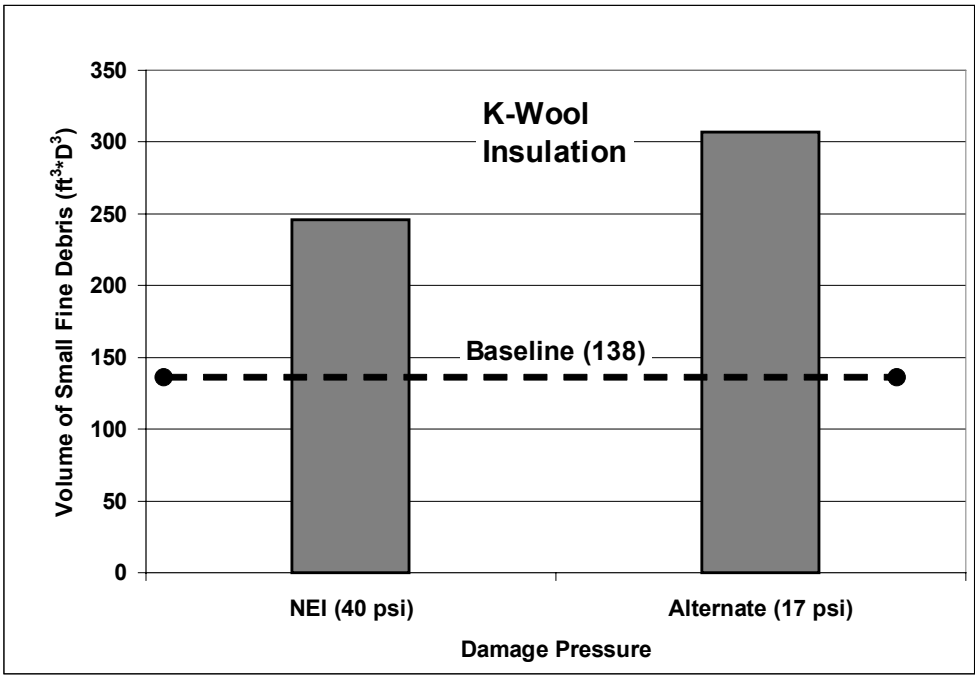

Figure VI-7. Potential Volumes of Small Fine K-wool Debris.

II.3.1.4 Correlation between Debris Size and Destruction Pressure

The NEI guidance contains the assumption that it is conservative to adapt the debris-size distribution for NUKON™ to other types of insulations that have a higher destruction pressure than NUKON™ (e.g., Temp-Mat and K-wool). This assumption is examined by comparing the debris generation data for LDFG, Temp-Mat, and K-wool, as shown in Figure II-8.

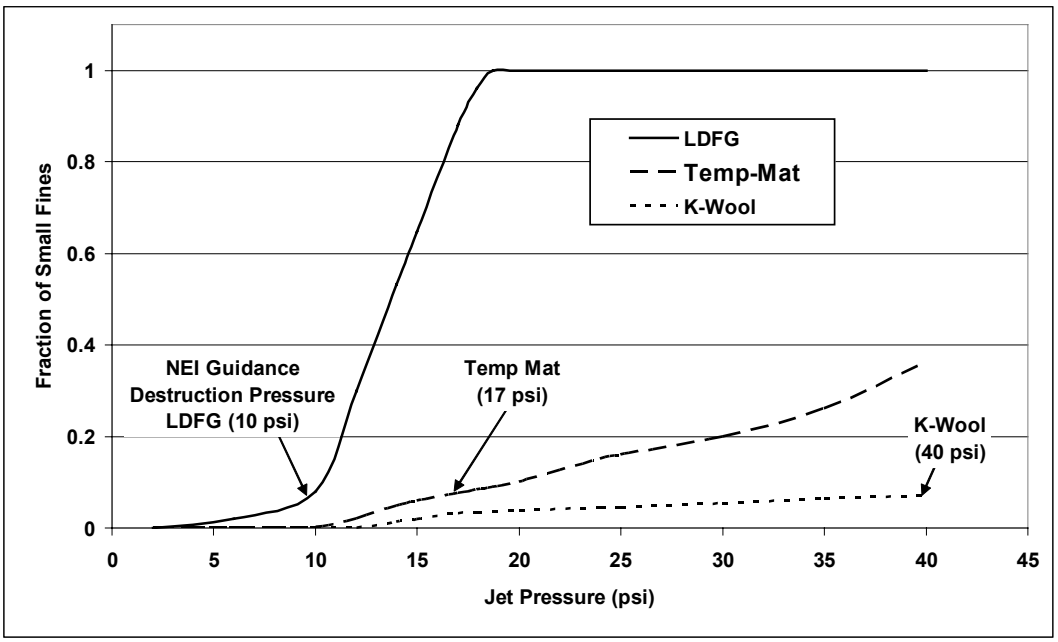

Figure VI-8. Comparison of Fibrous Insulation Damage Curves.

This damage curve comparison for LDFG, Temp-Mat, and K-wool does seem to support the concept that a higher destruction pressure results in the fractions of small fines being increasingly smaller as the destruction pressure increases. Certainly this is the case for Temp-Mat, where the baseline guidance is conservative relative to the integration herein where both the fractions of small fine debris and the potential debris volumes are smaller than the baseline guidance. Although this case is likely true for K-wool as well, it cannot be conclusively proven because of the complete lack of data beyond the NEI-recommended destruction pressure.

II.3.2 RMI Debris

The NEI guidance contains recommendations for three types of RMI insulation:

1. DARMET® manufactured by Darchem Engineering, Ltd.;
2. RMI manufactured by TPI; and
3. Mirror® marketed by Diamond Power Specialty Company (DPSC).

The NEI recommends that 75% of the RMI insulation contained in the equivalent spherical ZOI should be assumed to be turned into small fine debris. Table II-5 shows the NEI-recommended destruction pressures and the corresponding NEI-recommended radii for those pressures. Note that the ZOI for DARMET® and TPI are quite small compared with the ZOI for DPSC Mirror®.

Table VI-5. NEI-Recommended RMI Insulation Destruction Pressures and ZOI Radii

RMI Insulation	Destruction Pressures (psi)	ZOI Radius (r/D)
DARMET®	190 psi	1.3
TPI	190 psi	1.3
DPSC Mirror®	4 psi	21.6

Nearly all the debris generation data used to justify the NEI recommendations came from the BWROG Air Jet Impact Testing (AJIT) data [BWROG URG]; therefore, the NEI recommendations must be anchored to the insulation types as tested. Besides the BWROG AJIT tests, a single Nuclear Regulatory Commission (NRC)-sponsored test* was conducted using a stainless-steel DPSC Mirror® RMI cassette at the Siemens AG Power Generation Group (KWU) test facility in Karlstein am Main, Germany (1994 and 1995**can't find these as references in this section**) [SEA-95-970-01-A:2, 1996]. The cassettes and their closures, as tested in the AJIT tests with the cassettes mounted perpendicular to the jet centerline,† are provided in Table II-6. All of the cassettes tested had stainless-steel sheaths.

*The NRC-sponsored test involved a stainless-steel Mirror® cassette mounted directly on a device designed to simulate a double-ended guillotine break (DEGB) such that the discharge impinged on the inner surface of the RMI target as it would an insulation cassette surrounding a postulated pipe break. This NRC-sponsored test was performed with a high-pressure blast of two-phase water/steam flow from a pressurized vessel connected to a target mount by a blowdown line with a double-rupture disk. In this test, the cassette was completely destroyed into debris that can be considered small fine debris.

†Two tests were conducted, with the cassette mounted parallel to the jet centerline.

A review of the data indicates that the stainless-steel sheaths were not directly penetrated by the air jet; rather, the sheaths disassembled at the seams, such as with rivet failures. Those cassettes secured by stainless-steel bands in addition to latches and strikes generally remained relatively intact. The severity of the damage, in terms of the generation of small fine debris, depends on the degree or ease of disassembling the cassette. However, when considering large-piece debris, all detached cassettes, disassembled or not, become large-piece debris.

Table VI-6. BWROG AJIT RMI Insulations Tested

Insulation	RMI Foils Tested	Cassette Closures
DARMET®	Stainless-Steel Foils	Darchem Stainless-Steel Bands and CamLoc® Latches and Strikes
TPI	Aluminum Foils	Latch and Strike Closures
TPI	Stainless-Steel Foils	Latch and Strike Closures
DPSC Mirror®	Aluminum Foils	Latch and Strike Closures
DPSC Mirror®	Stainless-Steel Foils	Latch and Strike Closures
DPSC Mirror®	Stainless-Steel Foils	Latch and Strike Closures and Sure-Hold Band Closures

II.3.2.1 DARMET®, Manufactured by Darchem Engineering, Ltd.

The NEI-recommended destruction pressure of 190 psi for stainless-steel DARMET®, manufactured by Darchem Engineering, Ltd. and held in place by Darchem stainless-steel bands and CamLoc® latches and strikes, is based on two AJIT tests, Tests 25-1 and 25-2 with jet centerline pressures on target of 190 and 590 psi, respectively. In both of these tests, the cassettes, although deformed, remained intact and attached to the target mount. In effect, no debris was generated. This result indicates that a pressure greater than 590 psi is required to generate debris, with the exception of a cassette mounted over the break, where the jet would enter the inside of the cassette. This scenario would almost certainly result in complete destruction of that cassette. Another possible exception could be a jet approximately parallel to the cassette sheath that could penetrate through the ends—a configuration that has not been tested. It is apparent that the baseline recommendation of assuming 75% of this insulation within a 1.3/D spherical radius becomes small fine debris is conservative.

II.3.2.2 RMI Manufactured by Transco Products, Inc.

TPI manufactures stainless-steel and aluminum RMI insulation. The NEI guidance recommends a destruction pressure of 190 psi for the TPI RMI. The TPI cassettes tested included both aluminum and stainless-steel foils encased in stainless-steel sheaths secured with latches and strikes (no bands were used). Although the recommended destruction pressure is 190 psi, a small amount of fine debris was noted for jet pressures as low as 10 psi (Test 21-3). On the other hand, only small quantities of fine debris (i.e., <0.5%) were found for tests with jet pressures as high as 600 psi. Figure II-9 shows the debris generation fractions for TPI stainless-steel RMI small fines.

Table II-8 **Table II-7?** shows a comparison of potential debris volumes when estimated using the NEI baseline guidance and when acknowledging debris generation at jet pressures as low as 10 psi. Recall that to get actual volumes of debris, the potential volumes must be multiplied by the insulation concentration and again by D^3. For the baseline estimate, the volume

associated with a ZOI radius of 1.3/D is multiplied by 75% to get the baseline potential volume. For the alternate estimate, the ZOI volume out to a jet pressure of 10 psi was multiplied by 0.5% to get the alternate potential volumes. The application of the alternate pressure results in approximately three times as much small fine debris as using the baseline guidance. However, even these quantities are not very large compared with such insulations as LDFG.

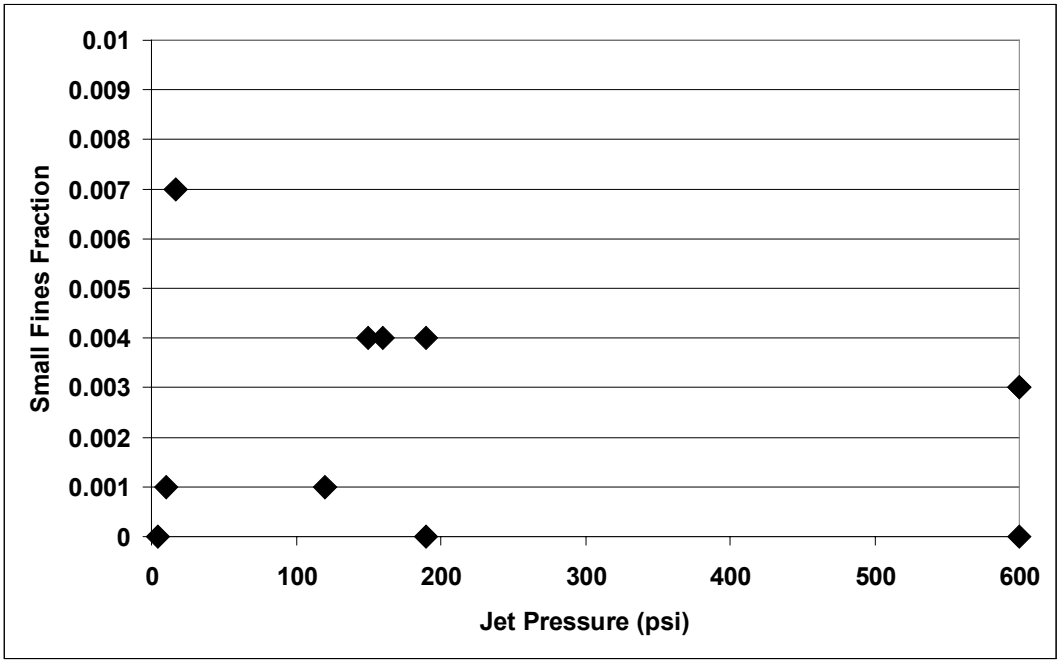

Figure VI-9. TPI Stainless-Steel RMI Small-Fine-Debris Fractions. fix y axis label (should be small-fine-debris fraction, not fines)

Table VI-7. Comparison of TPI Potential Debris Volumes

Guidance	Damage Pressure (psi)	Radius of ZOI (r/D)	Damage Fraction	Potential Volume of Debris (V/D^3)
Confirmatory Recommended Jet Isobar Volumes				
NEI Guidance	190	1.5	0.75	10.6
Alternate	10	11.9	0.005	35.3

However, if the transport of large-piece TPI RMI debris becomes necessary to the strainer blockage evaluation, the use of 190 psi to define the ZOI is totally inadequate. Although the TPI stainless-steel sheaths may effectively contain the foils, their latches and strikes do not effectively keep the cassettes attached to the mounts (or pipes). AJIT Test 21-2, with a jet pressure of only 4 psi, shows the two cassette half sections detached from the target mount, i.e., the cassettes become large-piece debris. At 4 psi, the ZOI radius would be ~21.6/D; therefore, numerous cassettes in various degrees of damage would be expected on the break-room floor. If the transport flow velocities were sufficient to move cassettes, then these cassettes could become a significant problem.

II.3.2.3 DPSC Mirror®, Manufactured by Diamond Power Specialty Company

DPSC manufactures stainless-steel and aluminum RMI insulations marketed as Mirror® insulations. The Mirror® cassettes tested included both aluminum and stainless-steel foils encased in stainless-steel sheaths secured with latches and strikes with or without "Sure-Hold" bands. The NEI guidance recommends a destruction pressure of 4 psi for the DPSC Mirror® insulations. The apparent reason that Mirror® cassettes form debris at much lower pressures than does the TPI RMI is the construction of the sheaths, i.e., the cassette integrity depends on strength of the seams.

The debris fractions for the small fine debris from the AJIT tests are shown in Figure II-10. The small fine debris was correlated here as pieces <6 in., although the NEI guidance specified RMI small fines as <4 in.; therefore, a small measure of conservatism was added to the comparison. Figure II-10 shows six data points for Mirror®, with two of those tests generating very minor quantities of small fines. It should perhaps be noted that with the lower pressure test where the RMI cassette was exposed to a jet pressure of only 2 psi (AJIT Test 18-3), the cassette was still detached from the target mount, leaving two half cassettes on the chamber floor. The test with the largest quantity of small fine debris (AJIT Test 17-1) had only 10.6% of the foils turned into pieces <6 in., with the remaining foils becoming large-piece debris. The conservative extrapolation shown in Figure II-10 to complete the spherical ZOI debris fraction integration assumes complete destruction at a jet pressure of 130 psi. Note that in the single NRC-sponsored Mirror® debris generation test conducted at the KWU test facility, the test article was completely destroyed.

The results of the Mirror® debris-size distribution integration over the ZOI are provided in Table II-8. The potential debris volume of $661/D^3$ is quite low compared with an estimate using the baseline guidance [75% of $4/3\ \pi\ (21.6/D)^3$] of $31660/D^3$. Although this insulation is damaged at jet pressures as low as 4 psi, a relatively small amount of small debris is formed at pressures less than ~120 psi, and when the debris damage data are applied to the larger ZOI radius of 21.6/D, only a small fraction of the insulation in that sphere becomes small fine debris. For DPSC Mirror® RMI insulation, the NEI-baseline-guidance assumption that 75% of the insulation within a 21.6/D ZOI sphere would become debris <4 in. in size (i.e., $31{,}660/D^3$) is overly conservative. However, the quantities of large-piece debris, including nearly intact cassettes, could be very large because even 2 psi can detach the cassettes, which could become very important in containments where the transport velocities are high enough to move this heavier debris significantly.

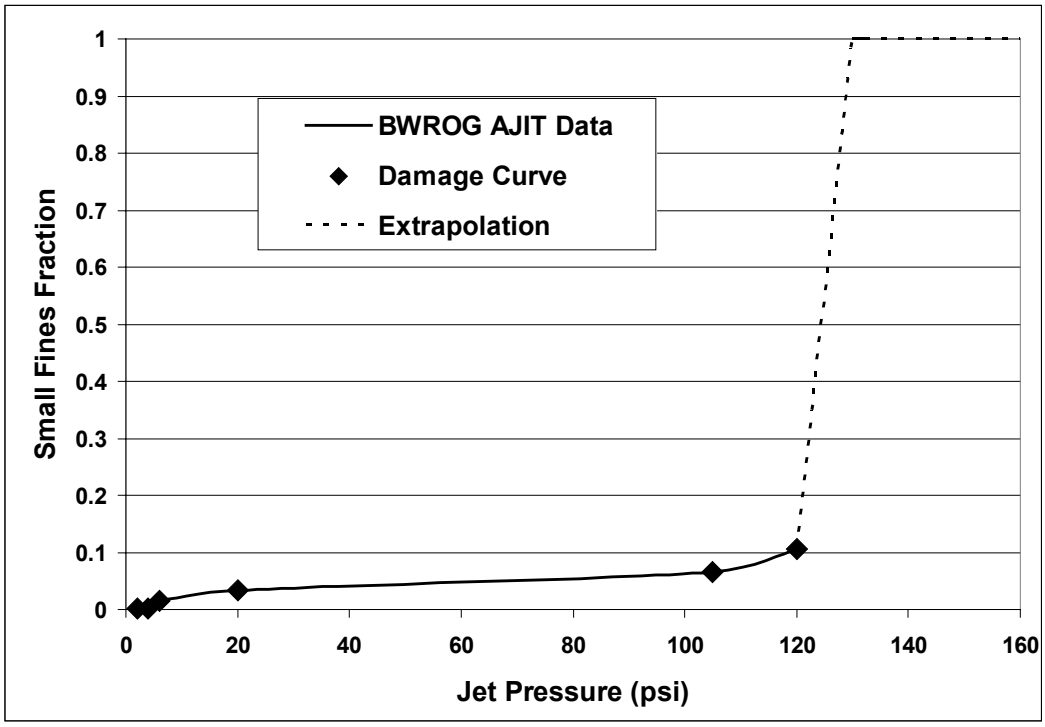

Figure VI-10. DPSC Mirror Damage Curve for Small Fine Debris.

Table VI-8. Results of Debris-Size Distribution Integration for DPSC Mirror® Insulation

Jet Pressure Isobar Volume Calculation	Radius of Sphere (r/D)	Fraction Small Fines	Potential Debris Volumes (V/D^3)
NEI-Recommended Damage Pressures			
PWR Two-Phase Jet (Confirmatory)	21.6	0.016	658

II.3.3 Particulate Insulation Debris

II.3.3.1 Min-K Debris

The NEI baseline guidance recommends the assumption that 100% of the Min-K insulation located inside a ZOI defined by the destruction pressure of 4 psi, corresponding to a radius of 21.6/D, becomes small fine debris. The basis for this recommendation apparently is the single Min-K BWROG AJIT debris generation test, Test 9-1. In this test, ~70% of the Min-K insulation became small fine debris. In fact, most of this debris was not recovered, apparently because it was too fine.[*] Based on the extensive damage to this Min-K blanket at 4 psi, it does not seem reasonable to assume that the threshold of damage is 4 psi.

[*] It was noted that a cloud of debris was observed to exit the test chamber through the exhaust screen and that the venting of the chamber to clear the dust required more than 15 minutes.

At jet pressures substantially higher than 4 psi, it seems likely that the Min-K would be totally destroyed. At jet pressures <4 psi, the damage to Min-K would continue but would decrease in severity until the pressure became insufficient to cause damage. However, that pressure is not known. It is unlikely that the NEI baseline guidance is conservative with respect to the Min-K blanket tested. On the other hand, Min-K insulation protected by a metal jacket secured with steel bands would most likely be substantially less damaged than the unjacketed blanket tested.

II.3.3.2 Calcium Silicate Debris

The NEI baseline guidance recommends the assumption that 100% of the calcium silicate insulation located inside a ZOI defined by the destruction pressure of 24 psi (corresponding to a radius of 5.5/D) becomes small fine debris. The OPG debris generation tests [N-REP-34320-10000-R00] were cited to justify the 24-psi destruction pressure. The OPG tests involved impacting aluminum-jacketed calcium silicate insulation targets with a two-phase water/steam jet. The jacketing was secured with stainless-steel bands, and the jacketing seams were typically oriented at 45 degrees from the jet centerline—an orientation that appeared to maximize damage. The OPG data, illustrated in Figure II-11, only cover a limited range of damage pressures (~24 to 65 psi).

The damage curve shown in Figure II-12 was generated by summing all four debris categories in Figure II-11 to get the OPG debris fractions shown and then constructing a plausible curve through the data that was conservatively extrapolated at both ends. The results of the calcium silicate debris-size distribution integration over the ZOI are provided in Table II-9. The potential debris volumes are compared in Figure II-13, along with an estimate using the baseline guidance [100% of $4/3\ \pi\ (5.45/D)^3$]. A lower alternate damage pressure results in a larger equivalent spherical ZOI, but a lesser fraction of the debris is damaged into small fine debris. The use of the alternate damage pressures over the NEI-recommended damage pressures for PWR analyses would result in ~43% more estimated small fine debris. For calcium silicate insulation, the baseline is conservative with respect to both the NEI guidance damage pressure of 24 psi and the alternate pressure of 20 psi.

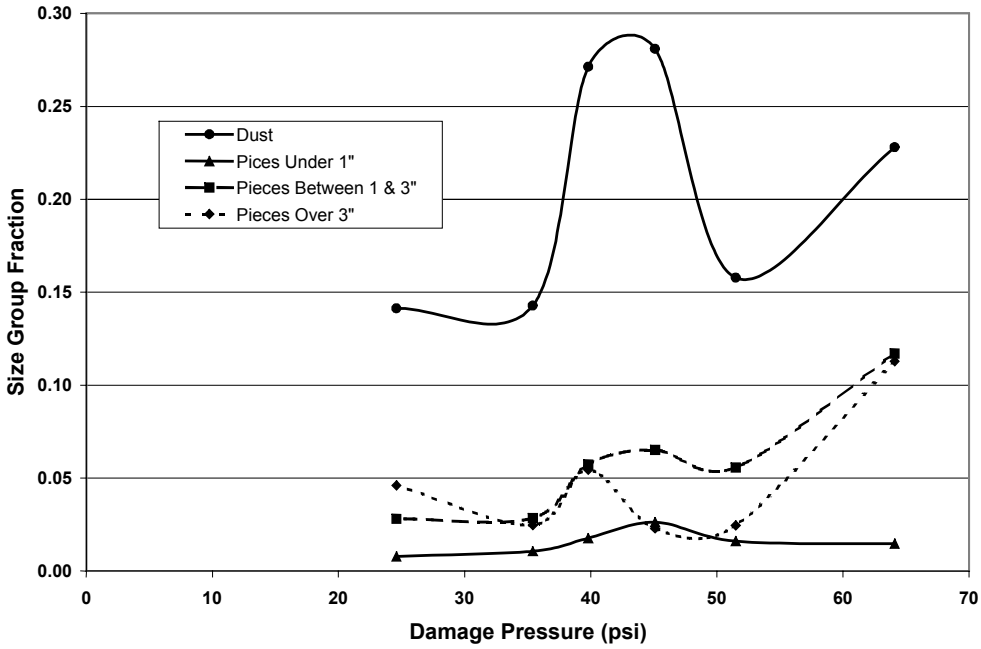

Figure VI-11. Debris-Size Distributions for OPG Calcium Silicate Tests.

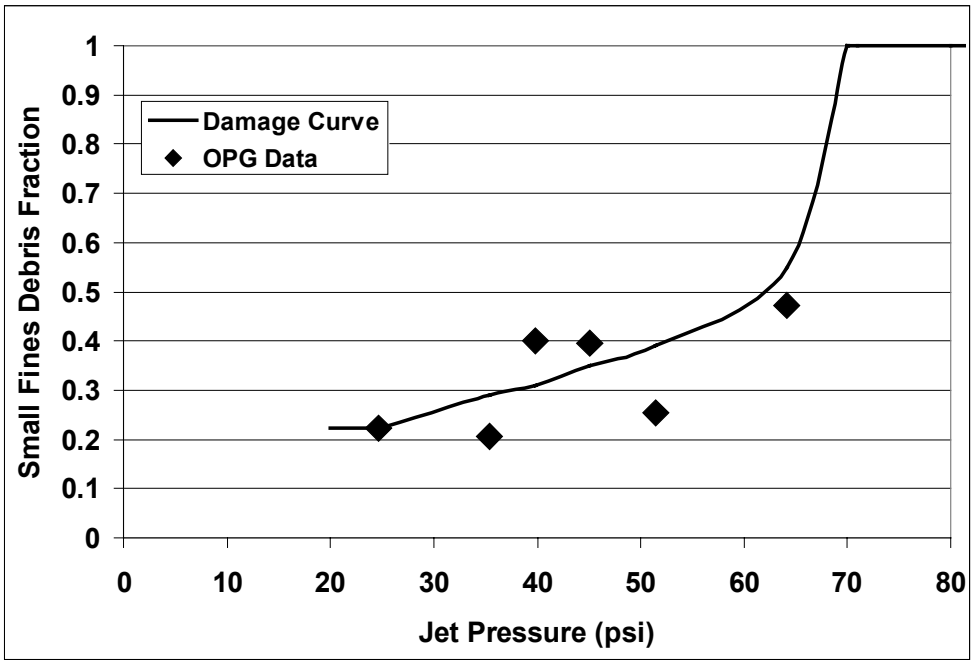

Figure VI-12. Calcium Silicate Damage Curve for Small Fine Debris.

Table VI-9. Results of Debris-Size Distribution Integration for Calcium Silicate Insulation

Jet Pressure Isobar Volume Calculation	Radius of Sphere (r/D)	Fraction Small Fines	Potential Debris Volumes (V/D^3)
NEI-Recommended Damage Pressures			
PWR Two-Phase Jet (Confirmatory)	5.4	0.42	273
Alternate Damage Pressures			
PWR Two-Phase Jet (Confirmatory)	6.4	0.34	372

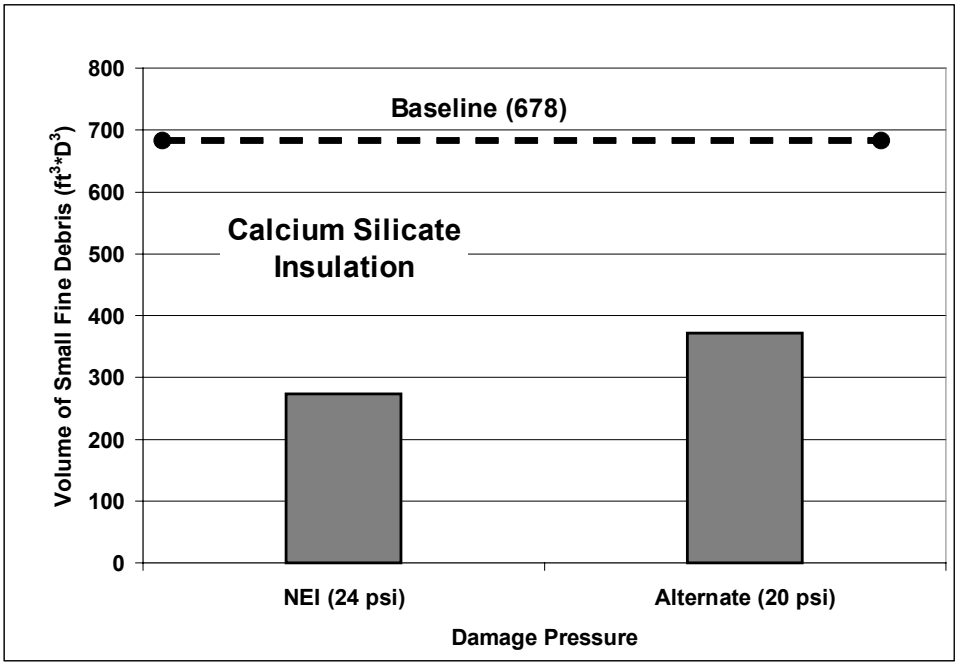

Figure VI-13. Potential Volumes of Small Fine Calcium Silicate Debris.

The BWROG AJIT tests also contain four tests of calcium silicate with aluminum jacketing secured by four ¾-in. stainless steel bands; however, these tests indicated that a jet of 150 psi was needed to cause significant damage. The reason(s) that a much higher pressure was needed to cause significant damage in the AJIT calcium tests than in the OPG tests has not been determined but is likely due to the differences in jacketing thickness, seam orientation, and strength of the bands. Here the destruction pressure depends more on the pressure needed to remove the jacket and expose the insulation than on the pressure required to erode the calcium silicate.

II.4 SUMMARY AND CONCLUSIONS

Confirmatory research was performed to ascertain whether the NEI recommendations for ZOI destruction pressures and debris fractions would reliably result in conservative estimates for the volumes of debris generated within the ZOI. Specifically, the NEI guidance recommends the assumption that 60% of the fibrous and 75% of the RMI insulation volume contained within the ZOI becomes small fine debris for ZOI radii defined by their recommended destruction pressures. The NEI guidance recommends adapting the debris-size distribution for NUKON™ to other types of fibrous insulation that have a destruction pressure higher than that of NUKON™.

Available debris generation data were used to define debris fractions versus jet pressure curves for the insulations examined. Difficulties encountered when correlating these data include aspects of protective jacketing and banding, as well as the variability in insulations. Before the insulation is subjected directly to jet flow forces, the flow must penetrate the protective coverings. Steel bands securing a metal jacket can require a rather high jet pressure to open the jacket before insulation debris is generated. The seam orientation affects the ease with which an edge of the jacket can be peeled back; it appeared that a seam orientation of ~45 degrees from the oncoming jet maximizes the potential for jacket opening. Another factor affecting the quality of debris generation data was the size of the jet nozzle relative to the insulation destruction pressure. If the target insulation had to be placed close to the nozzle to get the required destruction pressure, then the jet pressure became uneven along the length of the target; in fact, in some tests the target ends were likely located outside the influence of the jet. To test insulations with a higher destruction pressure, either larger nozzles or shorter targets are required. All of these considerations are factored into the evaluation of debris fractions.

ZOI debris fractions and insulation destruction pressures are interdependent; that is, the larger the ZOI, the smaller the fraction of the insulation within the ZOI that becomes small fine debris. Therefore, when the lower alternate pressure is used in the integration process, the resultant debris fraction will be less than that corresponding to the NEI-recommended destruction pressure.

The results and conclusions regarding relative conservatism of this confirmatory debris generation analyses are summarized in Table II-10 for the insulations examined. These results are relative to the NEI baseline guidance for the small-fine-debris-size category.

Table VI-10. Summary Comparison of Confirmatory and Baseline Potential Debris Volumes

Insulation	Confirmatory Research Result	Relative Conservatism of Baseline Guidance
Fibrous Insulations		
NUKON™	Baseline guidance results compare well with confirmatory results.	Baseline guidance for NUKON™ provides realistic results that are only slightly conservative.
Temp-Mat	Baseline results are approximately twice the confirmatory results (based on limited data).	Baseline guidance is conservative for Temp-Mat insulation.

Insulation	Confirmatory Research Result	Relative Conservatism of Baseline Guidance
K-wool	Baseline results are only about half that of the confirmatory results (based on limited data).	Baseline guidance is likely conservative for K-wool, despite the nonconservative comparison with confirmatory analysis. The poor nonconservative comparison is due to the extreme extrapolation of data required by the lack of data for pressures greater than the NEI destruction pressure. Still, conservatism cannot be proven with existing data.
RMI Insulations		
DARMET®	No confirmatory analysis for this insulation. Rather, a review of the debris generation data illustrated substantially less small fine debris than would be estimated using the baseline guidance methodology.	Baseline guidance is conservative for DARMET® insulation.
TPI	Baseline results account for only one-third of the confirmatory debris estimate, which includes the small quantities of debris generated at lower pressures but that are neglected when the baseline destruction pressure is used.	Baseline guidance is not conservative, but the quantities of this debris are relatively low; therefore, this nonconservative estimate is not a major issue.
DPSC Mirror®	Baseline results were almost 50 times that of the confirmatory result. The baseline minimum destruction pressure of 4 psi results is a very large ZOI volume, but the damage to the insulation is relatively minor at the lower pressures, thus the large differences in results.	Baseline guidance is conservative for Mirror® insulation.
Particulate Insulations		
Min-K	No confirmatory analysis for this insulation. Rather, the data from the single Min-K debris generation test were examined, i.e., approximately 2/3 of the insulation was turned into fine dust debris at a jet pressure of only 4 psi.	Baseline guidance is not conservative because the one test indicated that substantial damage would occur to Min-K insulation at significantly lower pressures than the destruction pressure of 4 psi and that the damage at 4 psi was extreme.
Calcium Silicate	Baseline results are approximately twice the confirmatory results, even when the lower jet pressure of 20 psi (recommended in NUREG/CR-6808) is considered instead of the baseline destruction pressure of 24 psi.	Baseline guidance appears to be conservative for calcium silicate insulation, but the debris generation data are not sufficient to determine the threshold jet pressure for generating small fine debris, i.e., the threshold destruction pressure could actually be less than the 20 psi alternate pressure used in the confirmatory analysis.

The following additional comments should be noted:

- The use of the alternate destruction pressure provides some quantification of the uncertainty associated with the selection of the destruction pressures. These uncertainties include the neglect of the tails of the debris damage curves and the uncertainty associated with the potential two-phase effect on debris generation relative to the available air-jet-generated data.

- A comparison of the NUKON™ results with the BWROG URG steam jet model illustrates that the neglect of the tails of the debris damage curve has a larger impact for PWRs than for BWRs (see Figure II-3).

- The NEI guidance recommendation that adapts the debris-size distribution for NUKON™ to other types of fibrous insulation that have a destruction pressure higher than that of NUKON™ has been partially supported (see Figure II-8), although it cannot be conclusively ensured.

- The ZOI for large debris generation in some cases does not correlate with the ZOI for small-fine-debris generation. A case in point is the analysis for TPI RMI, where most of the small fine debris would be generated inside jet pressures of 190 psi but large debris was generated (in the form of detached cassettes) at pressures as low as 4 psi. Therefore, rather larger quantities of large debris could be formed than were predicted using the baseline guidance ZOI sizes.

- It should be emphasized that the typical debris generation analyses were performed for insulations where the debris generation data were very limited. The data for the LDFG insulations (see Figure II-2) illustrate the potential variability in such data. Therefore, the limited debris generation data cause substantial uncertainty with debris generation estimations.

II.5 REFERENCES

[NUREG/CR-6762, Volume 3, 2002] C. J. Shaffer, D. V. Rao, and S. G. Ashbaugh, “GSI-191 Technical Assessment: Development of Debris-Generation Quantities in Support of the Parametric Evaluation,“ LA-UR-01-6640, NUREG/CR-6762, Volume 3, 2002.

[NUREG/CR-6369, 1999] D. V. Rao, C. Shaffer, B. Carpenter, D. Cremer, J. Brideau, G. Hecker, M. Padmanabhan, and P. Stacey, “Drywell Debris Transport Study: Experimental Work,“ SEA97-3501-A:15, NUREG/CR-6369, Volume 2, September 1999.

[NEDO-32686, Rev. 0, 1996] “Utility Resolution Guidance for ECCS Suction Strainer Blockage,“ BWROG, NEDO-32686, Rev. 0, November 1996. **not used in this section**

[SEA-95-970-01-A:2, 1996] Gilbert Zigler et al., “Experimental Investigation of Head Loss and Sedimentation Characteristics of Reflective Metallic Insulation Debris,“ draft letter report prepared for the US Nuclear Regulatory Commission, SEA No. 95-970-01-A:2, May 1996.

[N-REP-34320-10000-R00, 2001] Ontario Power Generation, “Jet Impact Tests—Preliminary Results and Their Applications,“ N-REP-34320-10000-R00, April 2001.

APPENDIX IV: DEBRIS TRANSPORT COMPARISON

The NEI GR baseline debris transport recommendations contain both conservative and nonconservative assumptions which were used to simplify the transport evaluation. To assess the effect of the nonconservative assumptions used in the baseline model, the baseline model was applied to the pressurized-water-reactor (PWR) volunteer plant, whereby those baseline results could be compared with the detailed debris transport evaluation performed for the volunteer plant. The comparison supported the review and acceptance of the NEI baseline evaluation methodology by illustrating that the baseline predicted conservative debris transport results for the volunteer plant. Insights gained from this comparison regarding debris entrapment in the inactive pool and the transport of large debris support staff imposed limitations on the acceptance of the baseline methodology.

Because the volunteer plant contains substantial quantities of both fibrous and reflective metal insulation (RMI), the baseline model was applied to both types of insulation debris. Detailed sump pool debris transport analyses were performed for the volunteer plant containment as documented in Appendix III. Detailed blowdown and washdown debris transport analyses were performed for the volunteer-plant containment documented in Appendix VI. Appendix IV (this appendix) compares the GR baseline analysis to the detailed analyses for the volunteer plant as documented in Appendices III and VI.

The comparison is based on the GR baseline two-group debris-size distributions, i.e., small fines and large-piece debris. The detailed analyses used a four-group distribution of fines, small pieces, large pieces, and intact pieces. The detailed four-group results were reduced to two groups by combining the fines and small-piece debris into the NEI small-fines group and combining the large-piece and the intact-piece groups into the NEI large-piece group. This approach was required to create a direct comparison.

The size distributions for both the NEI baseline results and the detailed analyses results were based on destruction pressures of 10 psi for the fibrous debris and 4 psi for the RMI debris. The respective size distributions were obtained from the research documented in Appendix II. The radii of the fibrous and RMI zone of influence (ZOI) for these pressures are 11.9 and 21.6 r/D, respectively (see Appendix I). In applying the baseline model to the volunteer plant, it was assumed that the containment was highly compartmentalized.

The baseline and detailed analyses results are compared by debris size in Tables IV.1 and IV.2 for fibrous and RMI debris, respectively. Table IV.3 compares the overall transport fractions, which combine the small fine debris and the large debris to obtain the total estimated screen accumulation. The respective debris-size distributions shown in Table IV.1 were used to calculate the overall transport results shown in Table IV.3. Note that the transport fractions in Tables IV.1 and IV.2 are pertinent only to the respective size categories.

Table IV.1. Baseline Comparison with Detailed Volunteer-Plant Fibrous Transport Results

Transport Phase	Debris Transport Fractions			
	Fine/Small Debris		Large-Piece Debris	
	Baseline	Detailed	Baseline	Detailed
Debris-Size Fraction	0.60	0.53	0.40	0.47
Blowdown Transport into Upward Levels	0.25	0.92	0	0.63
Blowdown Transport Directly to Sump Pool Floor	0.75	0.08	1	0.37
Washdown Transport from Upper Levels to Sump Pool	1	0.71	0	0.21
Total Debris Entering Pool	1	0.73	1	0.50
Entering Inactive Pool	0.14	0.03	N/A	0.07
Entering Active Sump Pool	0.86	0.70	1	0.43
Sump Pool Transport to Sump Screens	1	0.98	0	0.76
Fraction Accumulating on Sump Screens	0.86	0.69	0	0.33

Table IV.2. Baseline Comparison with Detailed Volunteer-Plant RMI Transport Results

Transport Phase	Debris Transport Fractions			
	Fine/Small Debris		Large-Piece Debris	
	Baseline	Detailed	Baseline	Detailed
Debris-Size Fraction	0.75	0.02	0.25	0.98
Blowdown Transport into Upward Levels	0.25	0.44	0	0.22
Blowdown Transport Directly to Sump Pool Floor	0.75	0.56	1	0.78
Washdown Transport from Upper Levels to Sump Pool	0	0.55	0	0.32
Total Debris Entering Pool	0.75	0.80	1	0.85
Entering Inactive Pool	0.11	0.15	N/A	0
Entering Active Sump Pool	0.64	0.65	1	0.85
Sump Pool Transport to Sump Screens	1	0.59	0	0.49
Fraction Accumulating on Sump Screens	0.64	0.39	0	0.42

Table IV.3. Comparison of Overall Baseline and Detailed Analysis Transport Fractions

Debris Type	Fraction of ZOI Insulation Debris Accumulated on Sump Screens	
	Baseline	Detailed
Fibrous Debris	0.52	0.52
RMI Debris	0.48	0.42

Substantial uncertainty exists in various aspects of the volunteer plant analyses that affect this comparison, which includes the following:

- Uncertainties in determining the debris generation size distributions.
- Uncertainties in specifying various aspects of the blowdown and washdown debris transport and deposition processes.
- Uncertainties in estimating the locations where debris enters the sump pool and when the debris enters with respect to the formation of the pool.

- Uncertainties in estimating the quantities of debris transported into the inactive pool regions.

- Uncertainties in estimating debris transport within an established sump pool.

The following points apply to the comparison of the fibrous debris transport:

1. The baseline recommendation for the debris-size distribution assumed 60% for the small fine debris, which is somewhat higher than the 53% determined from the integration of the air jet debris generation data (Appendix II). Although there is a potential that a two-phase steam/water jet could produce finer fibrous debris than a corresponding air jet, the baseline 60% small fines fraction for fibrous debris generated within the ZOI is accepted as conservative (note that the test data from the single available fibrous two-phase debris generation test is inconclusive in regards to this issue).

2. In the detailed analysis, most of the smaller fibrous debris was predicted to be deposited in the upper levels during blowdown debris transport, rather than directly on the sump floor as proposed in the baseline model. Because the transport of this upper-level debris to the sump pool by containment spray drainage (washdown) is delayed by a variable and indeterminate period of time, it must be postulated that relatively little of the debris reaches the sump floor in time to be entrained in the water flow filling the inactive pools (primarily the reactor cavity in the volunteer plant), which occurs relatively early in the accident sequence (<12 minutes). The detailed analyses predicted that at the end of the blowdown/washdown transport a significantly less amount of debris, compared to the baseline analyses, would enter the active sump pool

3. The baseline model sump pool transport was 100% for small fines and 0% for large-piece debris. The baseline model predicted more small fine debris accumulation on the sump screens than did the detailed analyses. However, the detailed analyses predicted substantial accumulation of large-piece debris on the screens, whereas the baseline predicted none.

4. The baseline and detailed analyses both predicted that approximately 52% of the fibrous debris generated within the ZOI would accumulate on the sump screens. Although this comparison does not explicitly demonstrate that the baseline methodology is conservative relative to the detailed volunteer plant evaluation, detail-specific conservatisms built into various aspects of the blowdown/washdown and pool debris transport analyses still support the overall conclusion that the baseline methodology is conservative with respect to its application to the volunteer plant.

The following points apply to the comparison of the RMI debris transport:

1. The baseline recommends using more small fine RMI debris than was determined from the integration of the air jet debris generation data (Appendix II). The primary reason for the large difference is the large increase in ZOI volume predicted by the ANSI/ANS-58.2-1988 standard when that standard is applied to jet pressures as low as 4 psi. That is, although damage extends to 4 psi, only a small amount of small fine debris is generated over much of the ZOI volume. Most of the ZOI debris is large-piece debris.

2. The detailed analyses predicted lesser quantities of RMI debris than fibrous debris would deposit in the upper levels of the containment, although it was substantially more than the baseline model recommendation of 25%. A primary reason for this result was that so little blowdown debris transport data exist for RMI debris and thus the blowdown analyses conservatively assumed a large fraction of debris depositing directly on the sump floor. Both the detailed and baseline analyses predicted that approximately the same amount of debris would enter the active sump pool at the end of the blowdown/washdown transport.

3. The baseline model sump pool transport was 100% for small fines and 0% for large-piece debris. The baseline model predicted more small fine debris accumulation on the sump screens than did the detailed analyses. However, the detailed analyses predicted substantial accumulation of large-piece debris on the screens, whereas the baseline predicted none.

4. The baseline method predicted slightly more RMI debris accumulation on the sump screens than did the detailed analyses, i.e., 48% as compared with 42% of the debris generated.

CONCLUSIONS NUMBER AS HEADER?

The application of the baseline methodology to the volunteer plant predicted approximately the same accumulation of fibrous debris and conservatively more RMI on the sump screen than did the detailed transport analyses. Although this comparison does not explicitly demonstrate that the baseline methodology is conservative relative to fibrous debris transport in the detailed volunteer plant evaluation, detail-specific conservatisms built into various aspects of the blowdown/washdown and pool debris transport analyses still support the overall conclusion that the baseline methodology is conservative with respect to its application to the volunteer plant. Even though the baseline and detailed evaluation arrived at the same fractions for sump screen debris accumulation, the intermediate steps disagreed. Due to the diversity among the PWR containment designs, this analysis does not conclusively demonstrate that the baseline methodology will be conservative for debris transport in all of the PWRs. In addition, substantial sources of uncertainty were noted in the detailed volunteer plant analyses.

Insights gained from this comparison regarding debris entrapment in the inactive pool and the transport of large debris support staff imposed limitations on the acceptance of the baseline methodology to prevent an outlier plant from demonstrating adequate NPSH margin using the baseline methodology where adequate NPSH margin might not exist in reality. The limitations resulted from the following two concerns that should be addressed before accepting baseline method results for plant-specific analyses.

First, if a plant baseline analysis estimates a relatively large fraction of the debris trapped in the inactive pools, as could be the case with a large reactor cavity volume and a shallow sump pool, then the baseline inactive pool fraction should be more limited than the current baseline model. Note that the detailed analyses reported herein predicted only approximately 3% of the small fibrous debris trapped in the inactive pool as compared with 14% using the baseline model. This comparison indicates for conservatism that the fraction of debris assumed to be trapped in the inactive pool should be limited to no more than ~15% unless a higher fraction is adequately supported by analyses or experimental data. The determination of a limiting faction is difficult based on the available research. Given this comparison where the baseline predicted sump screen accumulation results comparable to the detailed analyses and the volunteer plant

inactive pool fraction was 14%, it seems reasonable to assume an inactive pool fraction limitation of about 14% would maintain acceptable baseline results. A limiting inactive pool fraction of 15% was recommended..

Second, if the characteristic sump pool transport velocities are relatively fast, such that large transport fractions for large debris are indicated, then the baseline method should be modified to include the transport of large debris, as well as the transport of the small fine debris. In the volunteer plant, for example, approximately 98% of the large RMI ZOI (based on a destruction pressure of 4 psi) was predicted to be debris larger than about 6 in., of which about 42% would be transported to the sump screens. If the transport fraction for the large RMI was increased to ~50% from 42%, then the volunteer transport analysis results would have predicted more total RMI accumulation than the GR baseline recommendation predicted. The characteristic transport velocities must be compared with typical debris transport velocities to determine whether the baseline method should be modified to include the transport of large debris. Characteristic transport velocities can be sufficiently estimated using recirculation flow rates and nominal sump dimensions to determine if a potential exists that substantial portions of the large debris will transport. If substantial transport of large debris is reasonably possible and if such transport can alter the outcome of the NPSH margin evaluation, then analytical refinements are needed that evaluate large debris transport.

APPENDIX V: CONFIRMATORY HEAD-LOSS ANALYSES

Confirmatory research was performed to determine whether specific parameter assumptions made in the Nuclear Energy Institute (NEI) guidance report are conservative with respect to more realistic parameters. This research also provided additional insights into the estimation of head-loss parameters for the NUREG/CR-6224 head-loss correlation. Additional guidance is also provided for determining appropriate parameters for a mix of multiple fiber and particulate components.

V.1 FIBROUS DEBRIS HEAD-LOSS PARAMETERS

A comparison of specific surface areas (*Sv*) deduced from head-loss test data and the simple geometric correlation of four divided by the characteristic fiber diameter (4/d) is presented for NUKON™ and Kaowool™ insulation debris. The test data used in both of these deductions are available in the BWROG head-loss tests documented in Volume 1 of the BWROG Utility Resolution Guidance (URG).

V.1.1 NUKON™ Fibrous Debris

The URG has three head-loss tests that used only NUKON™ insulation debris and used a type of strainer that behaved similarly to that of a flat-plate screen (i.e., a truncated cone strainer). These tests were numbered 2, 4, and 5 and used 8, 8, and 16 lb of NUKON™, respectively, and no particulate. The flow velocities through the bed varied from ~0.15 to 0.75 ft/s, resulting in a total of 15 head-loss data points. A specific surface area was deduced for each data point using the NUREG/CR-6224 head-loss correlation and using an as-manufactured density of 2.4 lb/ft^3 and a fiberglass material density of 175 lb/ft^3 (NUREG/CR-6224 study recommendations). The resultant *Sv* values are compared in Figure V-1.

The comparison was based on the debris bed compression as determined by the NUREG/CR-6224 correlation (the ratio of the compressed thickness divided by the uncompressed thickness), which is directly affected by the flow pressure (i.e., flow velocity). The average value for *Sv* was ~170,600/ft. The nominal diameter for NUKON™ fibers has been specified as 7.1 µm, which translates into an *Sv* of 171,710/ft. The NUREG/CR-6224 study recommended an *Sv* of 171,420/ft. For NUKON™ insulation debris, the *Sv* determined using four divided by the fiber diameter is in excellent agreement with the experimentally deduced value.

The NEI guidance has recommended using a material density of 159 lb/ft^3 rather the NUREG/CR-6224 study value of 175 lb/ft^3. Confirmatory analysis using the NUREG/CR-6224 correlation confirmed that it is conservative to use 159 lb/ft^3 rather than 175 lb/ft^3, provided that the remaining head-loss parameters of 2.4 lb/ft^3 for the as-manufactured density and 171,000/ft for the specific surface area are maintained. The lower value for the material density estimates a slightly higher head loss than does the larger value.

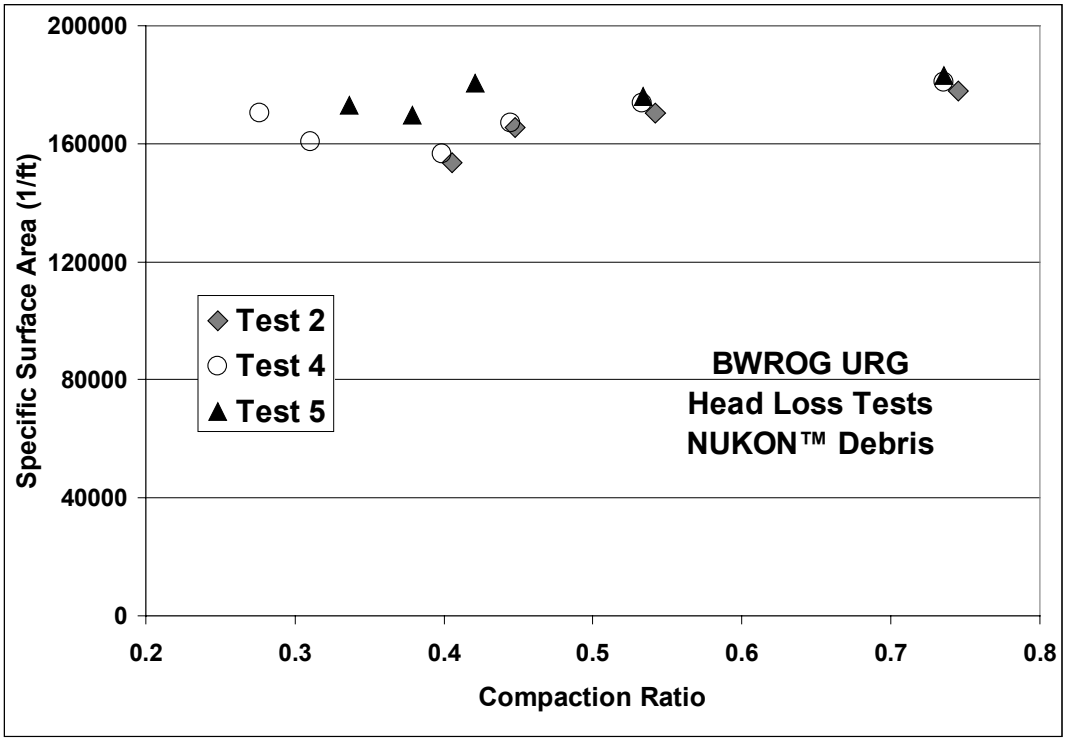

Figure 0V-1. NUKON™ Specific Surface Area.

Similarly, the NEI guidance recommended using 62.4-lb/ft^3 (1.0 g/cm^3) for material density of latent fibers to enhance transport (neutral buoyancy). The latent debris characteristics test results [LA-UR-04-3970, 2004a] that analyzed latent debris collected in the containments of several volunteer plants show that the latent debris fibers had material densities ranging from 1.3 to 1.9 g/cm^3. Again, confirmatory analyses verified that it is conservative from a head-loss prediction perspective to assume that the latent fiber material density is 1.0 g/cm^3 rather than 1.3 to 1.9 g/cm^3, provided that the remaining head-loss parameters are appropriately specified.

V.1.2 Kaowool™ Fibrous Debris

The URG has one valid head-loss test* that used Kaowool™ insulation debris and used a type of strainer that behaved similarly to that of a flat-plate screen (i.e., a truncated cone strainer). Test J13 initially had added 12 lb of Kaowool™, then later added 5 lb of iron oxide corrosion products (CPs), and then subsequently added another 5 lb of CP. The flow velocities through the bed varied from ~0.31 to 0.62 ft/s, resulting in a total of nine head-loss data points (three data points without particulate). A specific surface area was deduced for each data point using the NUREG/CR-6224 head-loss correlation, with the NUREG/CR-6224 study recommended parameters for the corrosion products used as input.† The recommended fiber material density for Kaowool™ is 160 lb/ft^3.

* Test J12 also used Kaowool, but the quantities of corrosion products so overwhelmed the debris bed that if all of the corrosion products had filtered from the flow, the granular bed, not counting the Kaowool, would have been nearly 2 in. thick. In any case, the head-loss contribution due to Kaowool was so overshadowed by the corrosion products that the test was not valid for determining the specific surface area for Kaowool.

† The NUREG/CR-6224-recommended parameters are 183,000/ft for the specific surface area, 324 lb/ft^3 for the particulate material density, and 65 lb/ft^3 for the granular packing-limit density.

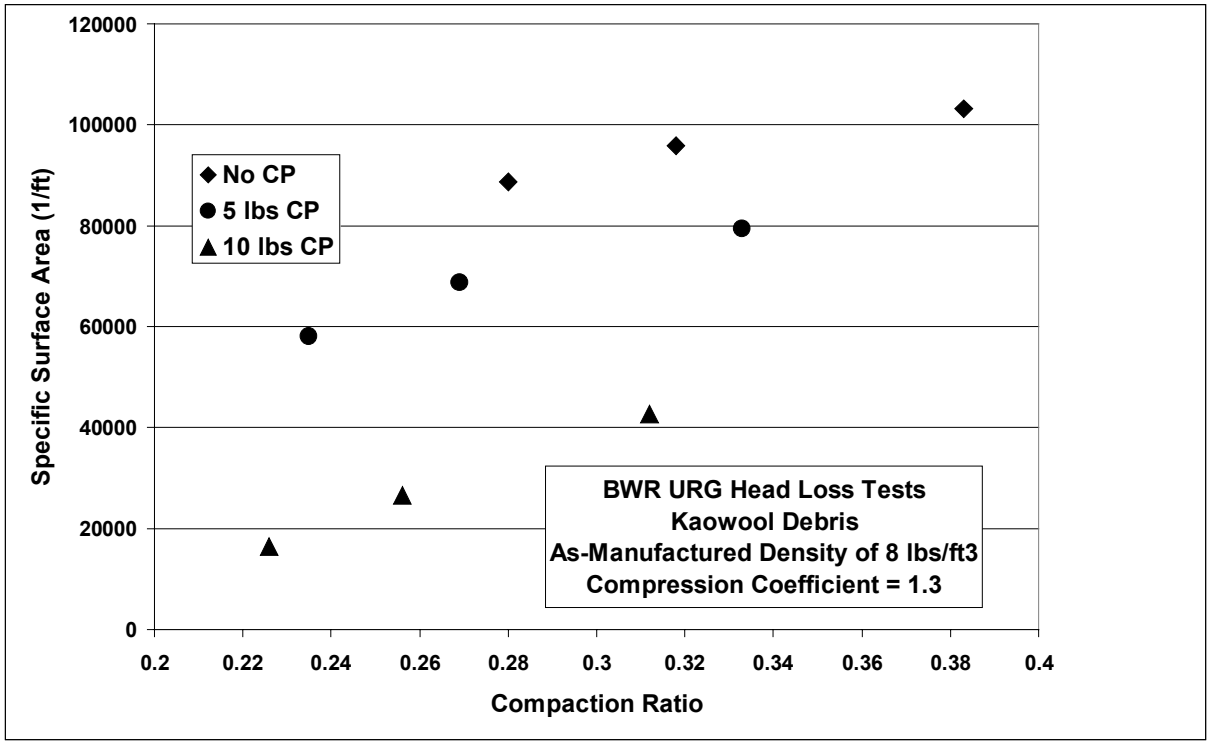

Figure V-2. Kaowool Specific Surface Area Assuming Base Parameters

The NEI guidance recommends an as-manufactured density of Kaowool™ ranging from 3 to 12 lb/ft^3, whereas the URG recommended a value of 8 lb/ft^3, apparently a midrange value. First, the *Sv* values were deduced from Test J13 data by assuming an as-manufactured density of 8 lb/ft^3 and the same bed compression correlation that was so successful for NUKON™. These resultant *Sv* values are compared in Figure V-2. The values of *Sv*, as shown, are very scattered, ranging from 16,000 to 103,000/ft. All in all, the NUREG/CR-6224 correlation does not work well with these input parameters. Noting that the as-manufactured density cited in the guidance report (GR) ranged from 3 to 12 lb/ft^3, it was subsequently determined that a smaller value of the density would reduce the scatter in the resultant *Sv* values. Further, it was discovered that stiffening the compression function also reduced the scatter. A second comparison of the deduced *Sv* values was developed assuming an as-manufactured density of 4 lb/ft^3 and a leading compression coefficient of 0.5 (rather than the standard 1.3). The results are shown in Figure V-3. The comparison in Figure V-3 has the deduced values in good agreement, with an average value of 165,500/ft.

The nominal diameter for Kaowool™ fibers has been specified as 2.7 to 3.0 μm in the NEI guidance, which translates into an *Sv* of 406,400 to 451,500/ft using the four-divided-by-the-diameter formula. Although using such high values for *Sv* is conservative, the simple formula is not even close to the experimentally deduced value of 165,500. The application of an *Sv* of 406,400/ft would substantially overpredict the results of Test J13.

The coefficient of the NUREG/CR-6224 compression correlation is an important issue. The standard coefficient of 1.3 was developed and validated essentially using NUKON™; therefore, the validation of other fibrous insulation must assess the validity of this value for the insulation

under consideration. It is noted that the baseline guidance in the GR considers this point by including the constant K (Equation 3.7.2-4 in Section 3.7.2.3.1.1 of the baseline guidance with a default value of 1 for K). For Kaowool™, a K = 0.385 and a Sv of 165,500/ft in the NUREG/CR-6224 correlation predicts URG Test J13 results reasonably well.

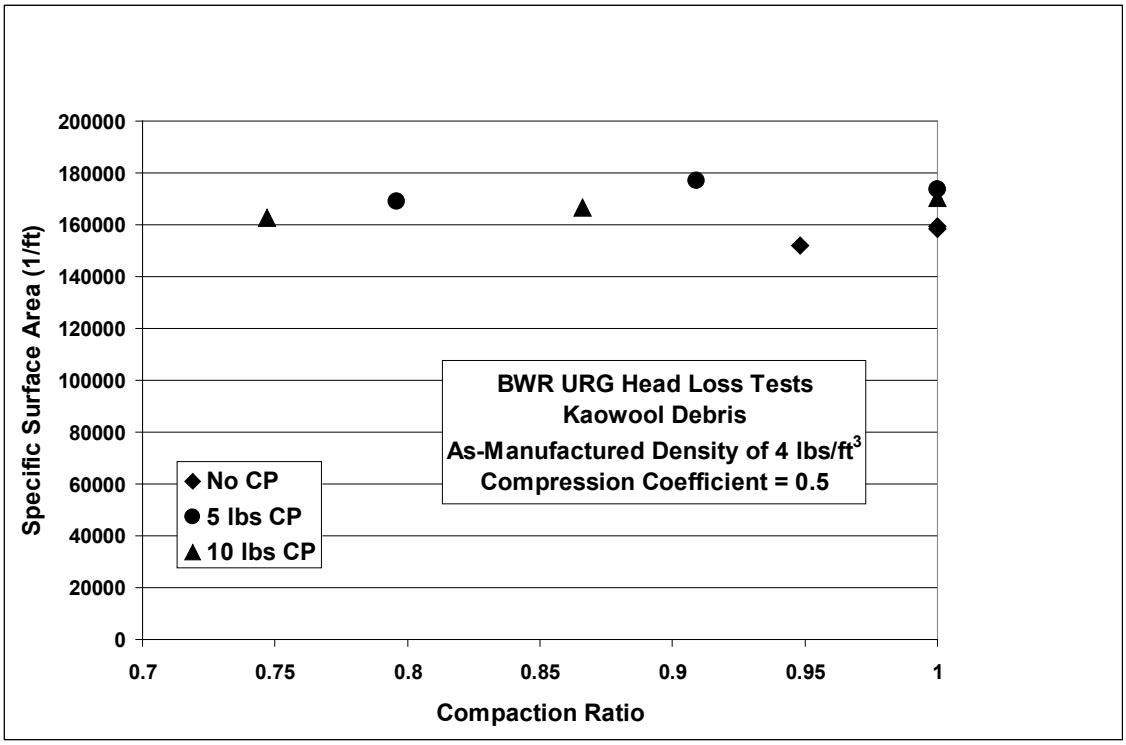

Figure V-3. Kaowool™ Specific Surface Area Using Modified Parameters.

V.1.3 Comparison of Fibrous Debris

The specific surface areas are compared in Figure V-4 for areas determined using the four-divided-by-the-fiber-diameter formula and the two experimentally deduced values presented herein for NUKON™ and Kaowool™. The following points are made:

1. The coefficient(s) for the compression correlation also have a role in the application of the NUREG/CR-6224 correlation to the various types of fibrous debris.

2. The 4/d formula was formerly validated using NUKON™, but not necessarily for other types of fibrous insulations.

3. The 4/d formula is not reliable and should not be applied indiscriminately. It should not be assumed that because this formula overpredicts Kaowool™ head losses that it will be conservative for untested types of fibrous debris. The only reliable method of determining the specific surface area of a particular insulation material is deduction from applicable test data.

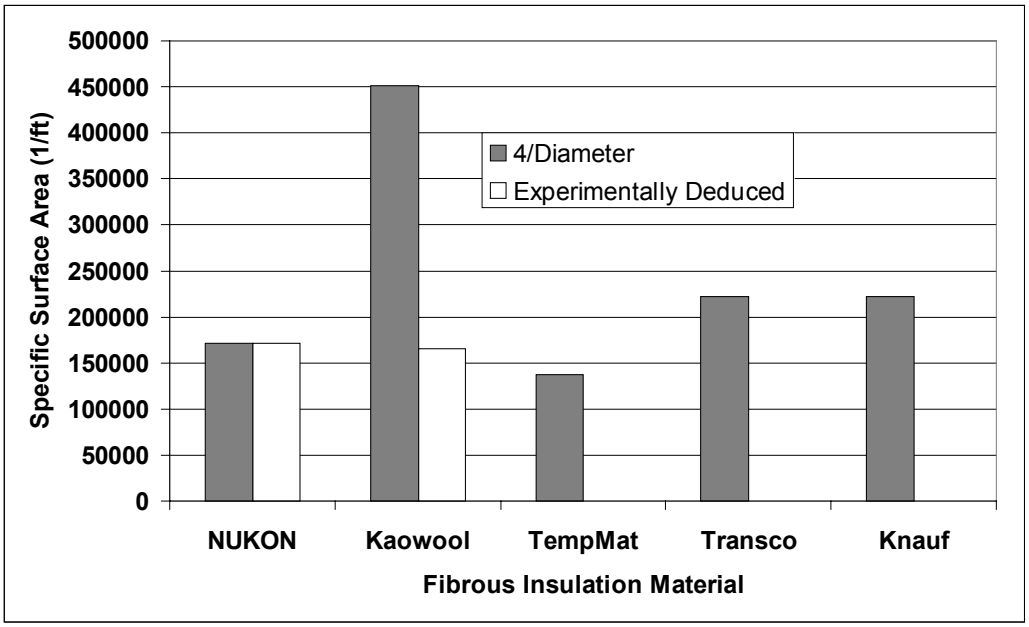

Figure 0-4. Comparison of Fibrous Insulation Specific Surface Areas.

V.2 PARTICULATE DEBRIS HEAD-LOSS PARAMETERS

In Section 3.7.2.3.1.1 of the GR, the NEI guidance recommends using the simple formula of six divided by the characteristic particle diameter to determine the specific surface areas for particulate debris. The following confirmatory analyses provide insights into this relationship and experimentally deduced values for particulate *Sv.*

V.2.1 Iron Oxide Corrosion Products

During the resolution of the BWR strainer blockage issue, the iron oxide CPs that accumulate in a boiling-water-reactor (BWR) suppression pool were the primary particulate in the head-loss calculations. The BWR sludge (CP) is characterized by the size distribution shown in Table V-1.

The NUREG/CR-6224 correlation recommends a specific surface area of 183,000/ft for head-loss estimates with CP, which has been validated by comparison with test data. Using the midrange diameters from Table V-1 to estimate the *Sv* for the CP distribution using the 6/d formula, the *Sv* estimate becomes 48,400/ft (almost a factor of four less than the NUREG/CR-6224 recommendation). Note that a factor-of-4 error in the *Sv* can result in a factor as large as 16 in error in the head loss at low flow velocities.

If the minimum value of the range is used (assuming a minimum particle size of 2 μm for the 0- to 5-μm size group), then an *Sv* of ~290,000/ft is calculated (~58% higher than the recommended validated area). The smaller particles have more effect on the particulate *Sv* than do the larger particles, which is why the midrange diameters are not a valid representation of the distribution. Using the smallest diameters of each group is conservative but can result in

large estimates of *Sv*. Further, these examples illustrate that it is difficult to determine where in a size range is an appropriate diameter for the *Sv* determination using 6/d.*

Table V-1. Size Distribution of BWR Suppression Pool Iron Oxide Corrosion Products†

Size Range (μm)	Percent by Number of Particles	Percent by Weight
0–5	81%	0.3%
5–10	14%	1.5%
10–75	5%	98.2%

An example of how the 6/d formula works over a particle-size grouping is illustrated in Figure V-5, where 6/d is plotted for particle diameters ranging from 5 to 75 μm (typical distribution grouping). If it is assumed that particles are uniformly distributed (by weight) across this size range (which is not necessarily a valid assumption), then the average 6/d corresponds to a diameter of 25.8 μm, whereas the midrange diameter is 40 μm. Because this simple arithmetic relationship arrives at differing conclusions, depending on the range specification, this method cannot be used reliably in a general sense, even if the uniform distribution assumption is valid.

In summary, the only reliable method of determining the *Sv* for a particulate, unless the particulate-size distribution is known in much greater detail than has been typically specified to date, is to deduce *Sv* from valid head-loss test data. It is conservative to use the lower diameter of each size group but this can lead to large estimates of the *Sv*. However, this method is valid when applicable head-loss data are lacking. Another difficulty is the determination of the smallest particles in the distribution. Although most particulates will have sub-micron particles in the distribution, fiber debris beds may not filter such small particles or certainly the efficiency of filtration could be rather low and is difficult to determine.

*Similar results were obtained when 6/d was applied to concrete dust head-loss test data during NRC-sponsored tests documented in LA-UR-04-1227.

†The NEI guidance (Table 4-3) and NUREG/CR-6224 (Table E-2) both have the percentages in the center column of this table listed as percentages by weight. However, the BWROG URG (Table 7) lists this column as percentages by the number of particles, as shown here. Because the data originated from the BWROG and the numbers only seem to make sense as the number of particles, it is assumed here that the URG is the correct source. Therefore, it is believed that the heading was mislabeled in NUREG/CR-6224 from which the NEI adapted the data for the guidance. In any case, it is conservative to assume that 81% of the particulate by weight is <5 microns because this assumption leads to very high specific-surface-area estimates.

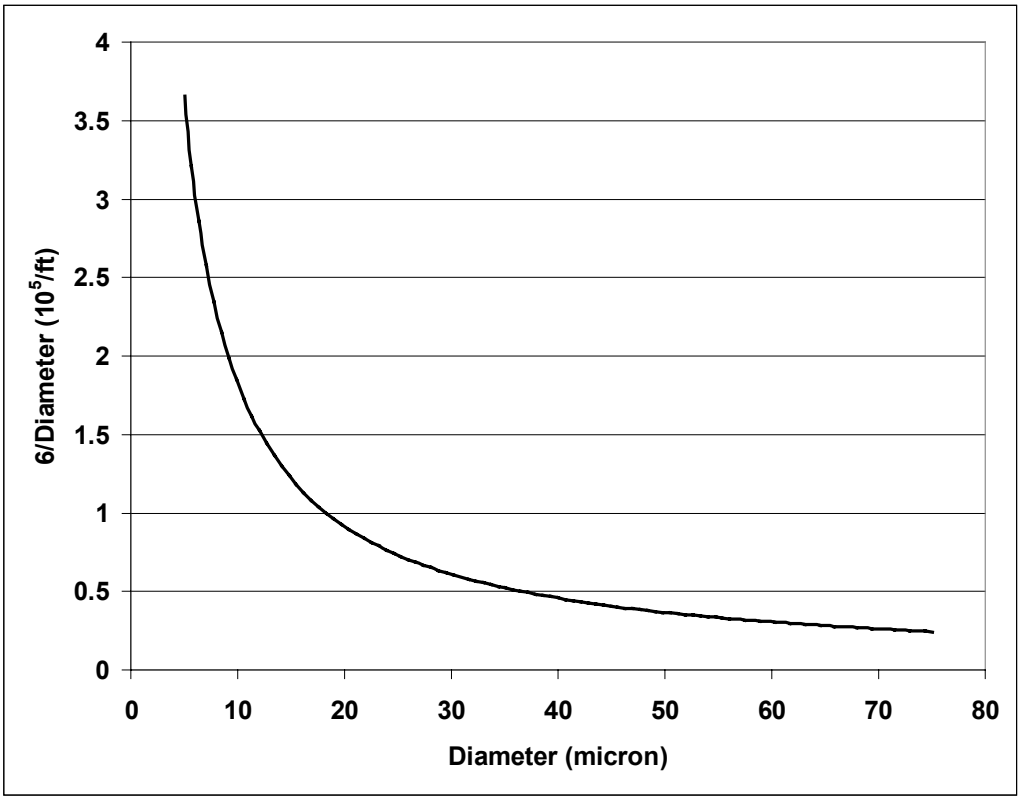

Figure V-5. Example of *Sv* Variance with Particle Diameter.

V.2.2 Latent Debris

The characteristics of latent debris collected from inside containments of several nuclear plants have been determined by Los Alamos National Laboratory (LANL) [LA-UR-04-3970, 2004a] . These characteristics included properties of material composition and hydraulic flow properties (e.g., specific gravities and characteristic dimensions). Based on these characteristic properties, surrogate latent particulate debris* was formulated for testing in the closed-circulation head-loss simulation loop operated by the Civil Engineering Department at the University of New Mexico (UNM).† Applying the NUREG/CR-6224 head-loss correlation to the test data for the surrogate latent debris resulted in parameter recommendations for the application of the correlation to plant latent debris. Those recommendations are summarized below, together with insights gained from the surrogate latent debris data reduction. The test apparatus and base test procedures are described in detail in the calcium silicate debris test report [LA-UR-04-1227, 2004b] .

The plant debris characteristics pertinent to the specification of a recipe to create a suitable latent particulate surrogate include the particulate specific gravity and the particulate-size distribution. The particulate-size distribution, shown in Table V-2, was used as a recipe for the

*A surrogate was required to provide the quantities of debris needed for head-loss testing. The latent debris collected in containment required the special handling associated with radioactive materials.

†NUKON™ insulation debris was selected to form the fiber bed to filter the surrogate particulate from the flow because of its well-established head-loss properties.

particulate. The surrogate particulate debris tested at UNM was constructed from common sand and soil (referred to as dirt) with the sand used for the two larger size groups and the dirt for the <75-µm-size group. The specific gravity of the latent debris characterized at LANL varied but is well represented as a specific gravity of 2.7, and both the sand and dirt used to formulate the surrogate were found to have a specific gravity near 2.7. The dirt had a clay component that tended to disintegrate, in part, in water, thereby adding substantial particulate <10 µm to accommodate the LANL finding that substantial very fine debris was collected in the filters. Both granular (thin-bed) and nongranular debris beds were tested.

Table V-2. Surrogate Particulate Size Distribution

Size Range (µm)	Fraction
500 to 2000	0.277
75 to 500	0.352
< 75	0.371

Tests were conducted using the individual size groupings for the 75- to 500-µm sand and the <75-µm dirt (without the other groups present) to determine specifically the head-loss characteristics of these individual size groupings; then the latent debris recipe was tested with all three size groups represented according to the recipe. The largest size group (500 µm to 2 mm) was not individually tested because of its relatively minor impact on the recipe head loss; its small specific surface area was estimated using the 6/d equation. For the other two size groups, the specific surface area was deduced from the head-loss data. The bulk densities of the three components were estimated by measuring the bulk volume in a calibrated beaker for a weighted mass of particulate. Given the particle specific gravity and the bulk densities, the granular debris bed porosities were estimated. The test results for the surrogate latent particulate debris are summarized in Table V-3.

Table V-3. Summary of Test Results

Particulate (µm)	Bulk Density (lbm/ft^3)	Limiting Granular Porosity	Limiting Granular Solidity	Specific Surface Area (ft^{-1})
500 to 2000 (Sand)	104	0.38	0.62	2000
75 to 500 (Sand)	99	0.41	0.59	10,800
<75 (Dirt)	39	0.77	0.23	285,000
Recipe	63 to 75	0.62 to 0.55	0.38 to 0.45	106,000

A range of numbers is shown for the bulk density and limiting granular porosity and solidity due to the uncertainty associated with filtration of the very fine dirt from the water flow, i.e., how much of the dirt introduced into the test loop actually resided in the debris bed. Test-loop water turbidity measurements clearly showed that significant, sometimes substantial quantities of the fine dirt were not filtered from the flow by the fibrous bed. If there is a minimum particle size for effective filtration, it is most certainly significantly <10 µm and likely less than a few microns. Table V-3 presents nominal estimates for the specific surface area for each component; however, there is significant uncertainty in determining these numbers. The primary uncertainty

associates with the less than 75 microns particulate was the filtration efficiency of the finer particles. Assessing the uncertainties in the turbidity resulted in the conclusion that between 30% and 45% of the particulate remained in solution, which corresponded to a range of about 250,000/ft to 340,000/ft in the specific surface area when the correlation was applied. For the two larger particulate size groups (75 to 500 microns and 500 to 2000 microns), the uncertainties were analytically estimated using the 6/diameter formula where the diameter was ranged from the smallest diameter particles up to 25% of the range. These estimated uncertainties are compared in Figure V-6.

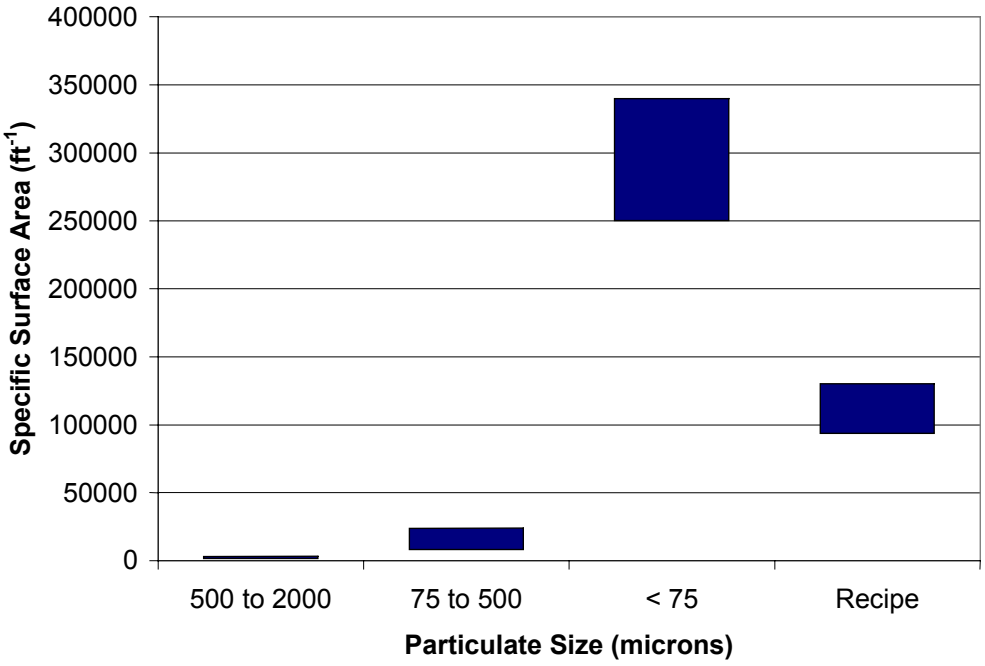

Figure V-6. Comparison of Component and Recipe Specific-Surface-Area Ranges.

Key points that can be deduced from the foregoing discussions relative to latent debris are the following:

1. The head loss through granular (thin-bed) debris is controlled by the limiting porosity (solidity), which depends on the composition of the debris. Solidity certainly is not a fixed number, as is indicated in the presentation of the NEI guidance as a solidity of 0.2. Handbooks on soils show many materials with limiting porosity <0.8, e.g., common sand is ~0.40 to 0.43 and was experimentally verified in the LANL tests.

2. The major contributors to the head loss are the increasingly smaller particles (<75 μm), as illustrated by the 6/d formula, until the particles become too small for filtration. However, it is difficult to determine some limiting particle diameter that will not filter.

3. It is difficult to formulate specific recommendations for the appropriate parameters to use in the NUREG/CR-6224 correlation for pressurized-water-reactor (PWR)-containment latent particulate because the latent debris composition will vary from plant to plant and because the latent debris transported to the sump screen will also be plant specific because of such differences as flow velocities. In addition, the uncertainties associated with whether the surrogate recipe suitably represents actual containment latent debris further compound the problem of developing recommended characteristics for latent debris. More important than specific recommendations are the methods for ascertaining appropriate head-loss parameters once the plant has assessed latent debris accumulation on the sump screen.

4. The surrogate latent particulate debris head-loss tests effectively demonstrate the necessity of characterizing the latent particulate so that appropriate parameters can be estimated. For example, if the entire mass of the latent debris is assumed to be deposited onto the sump screen, then a lower specific surface area, such as the recipe in these tests, can be applied. However, if transport analyses are used to limit the transport of latent particulate to only the fine particulate, then the appropriate specific surface area would be more like that of the fine dirt in these tests. The same consideration also applies to the limiting packing density.

5. It is recommended that plant latent debris estimates be separated into as many particle size groupings as reasonably possible and then that subsequent transport analysis be applied to each group to determine the particulate makeup on the sump screen.

6. Wherever possible, specific surface areas should be determined for each size group based on test data. When the areas must be estimated from the particle diameters, the appropriate diameter is clearly not the mean or average diameter of the size group but a diameter closer to the minimum diameter of the group. The minimum diameter should normally result in a conservative specific surface area.

7. The use of the simple geometric relationship of 6/d to estimate the specific surface areas for particulate is not reliable because the appropriate diameter within the range is not known. This point is illustrated in Table V-4, where values for *Sv* are estimated using both the mid-range and minimum diameters for each size group in the surrogate latent particulate recipe; these values are compared to the *Sv* deduced from the experimental head loss and the particle diameters that correspond to the experimental *Sv*. This minimum diameter in the size range estimates a conservative *Sv*; however, that number could be unacceptably large if the minimum size for the smallest particles is not well known. The use of mid-range diameters is unacceptable because this

approach excessively underpredicts *Sv* values for plant-specific evaluations. . If the specific surface areas corresponding to the minimum particle diameters in each size grouping range are unacceptable, then head loss test data is required to determine a specific surface area for the particulate size distribution in question.

8. The NEI guidance recommends the use of 100 lb/ft^3 for the material density of latent particulate, whereas LA-UR-04-3970 indicates a density of ~168 lb/ft^3 (specific gravity of ~2.7). The use of the lighter density of 100 lb/ft^3 is conservative relative to a heavier density of 168 lb/ft^3, for example, if the other head-loss parameters are appropriately specified.

Table V-4. Comparison of Specific Surface Area Estimation Methods

Particulate Size (μm)	Analysis			Experimental Sv	
	Mid-Range Diameter (μm)	Sv = 6/d Mid-Range Sv (ft^{-1})	Sv = 6/d Mid-Range Sv (ft^{-1})	Sv Deduced from Experimental Head-Loss Data (ft^{-1})	6/Sv Experiment (μm)
500 to 2000 (Sand)	1250	1460	3660	2000	914
75 to 500 (Sand)	287.5	6360	24,380	10,800	169
<75 (Dirt)	37.5	48,770	914,000*	285,000	6.4
Recipe	88.2	20,740	349,000	106,000	17.3

* Assuming a 2-μm minimum particle size.

V.3 FORMULAS FOR MIXING MULTIPLE FIBER AND PARTICULATE COMPONENTS

Most head-loss testing has been performed with a single type of fibrous debris, e.g., NUKON™, and particulates such as CPs. However, plant-specific analyses may well postulate debris beds containing more than one type of fiber and several types of particulate. The application of the NUREG/CR-6224 correlation requires the head-loss properties for the mixture to be estimated from the individual species properties.

V.3.1 Mixture of Specific Surface Areas

The equation for the mixture of the specific surface areas simply multiplies each area by the species volume and sums these products to get the total surface area, which is then divided by the total volume to get the mixture-average specific surface area. Such an equation was recommended in NUREG/CR-6371. Section 3.7.2.3.1.1 of the NEI guidance on the mixing equation* recommends using the square of the specific surface area rather than the linear

* The NEI guidance refers to NUREG/CR-6371 as the source of their recommendation; however, NUREG/CR-6371 recommends using the linear, not the square of the area in the mixing. The NEI source for the squaring equation has not been provided for review.

relationship The following equation for the mixing is set up to accommodate the linear (n = 1), the square (n = 2), or any other exponent. Performing example mixing evaluations demonstrated that using the square results in larger values for the mixture of specific surface areas than does using the linear relationship; therefore, it is conservative to use the square of the specific surface area in the mixing rather than the linear.

$$Sv_{Mixture} = \left[\frac{\sum_i \frac{m_i}{\rho_i} Sv_i^n}{\sum_i \frac{m_i}{\rho_i}} \right]^{\frac{1}{n}} \quad ,$$

where

Sv = the specific surface area for component *i* or for the mixture,

m_i = the mass of component *I*,

ρ_i = the material (solid) density of the particles in component *I*, and

n = the weighting exponent.

For the surrogate latent particulate debris, mixing the three constituents to get the recipe test result seemed to work best using an n = 4/3 (assuming that ~40% of the fine dirt did not filter from the flow). Because of the substantial uncertainties associated with head-loss predictions, it is prudent to include a safety factor; therefore, the NEI recommendation of using the square of the specific surface area in the mixing equation is a good recommendation.

V.3.2 Mixture Densities

The equation for the mixture of densities (bulk, material, or granular) simply adds all of the species masses and then divides by the total of the species volumes as

$$\rho_{Mixture} = \frac{\sum_i m_i}{\sum_i \frac{m_i}{\rho_i}} \quad ,$$

where

ρ_i = the density of the particles in component *I* and

m_i = the mass of component *i*.

This density mixing equation can be reduced to the following, even simpler form:

$$\frac{1}{\rho_{Mixture}} = \sum_i \frac{f_i}{\rho_i} \quad ,$$

where

f_i = the mass fraction of component *i*.

V.4 REFERENCES FOR APPENDIX V

[NEDO-32686-A, 1998] GE Nuclear Energy, “Utility Resolution Guide for ECCS Suction Strainer Blockage,” prepared by the BWR Owners’ Group, NEDO-32686-A, October 1998.**not referenced in this section**

[NUREG/CR-6224, 1995] NUREG/CR-6224, “Parametric Study of the Potential for BWR ECCS Strainer Blockage due to LOCA Generated Debris,“ October 1995.

[NUREG/CR-6371, 1996] C. Shaffer, C., W. Bernahl, J. Brideau, and D. V. Rao, BLOCKAGE 2.5 Reference Manual, NUREG/CR-6371, US Nuclear Regulatory Commission, December 1996.

[LA-UR-04-3970, 2004a] Mei Ding, Amr Abdel-Fattah, Stewart Fischer, Bruce Letellier, Kerry Howe, Janet Garcia, and Clint Shaffer, "Characterization of Latent Debris from Pressurized-Water-Reactor Containment Buildings," Los Alamos National Laboratory report LA-UR-04-3970 (June 2004).

[LA-UR-04-1227, 2004b] C. J. Shaffer, M. T. Leonard, B. C. Letellier, J. D. Madrid, A. K. Maji, K. Howe, A. Ghosh, and J. Garcia, "GSI-191: Experimental Studies of Loss-of-Coolant-Accident-Generated Debris Accumulation and Head Loss with Emphasis on the Effects of Calcium Silicate Insulation," Los Alamos National Laboratory report LA-UR-04-1227 (April 2004).

This page is intentionally blank.

APPENDIX VI: DETAILED BLOWDOWN/WASHDOWN TRANSPORT ANALYSIS FOR PRESSURIZED-WATER-REACTOR VOLUNTEER PLANT

VI.1 INTRODUCTION

In the event of a loss-of-coolant accident (LOCA) within the containment of a pressurized-water reactor (PWR), piping thermal insulation and other materials in the vicinity of the break will be dislodged by break-jet impingement. A fraction of this fragmented and dislodged insulation and other materials, such as chips of paint, paint particulates, and concrete dust, will be transported to the containment floor by the steam/water flows induced by the break and by the containment sprays (CSs). Some of this debris eventually will be transported to and will accumulate on the recirculation sump suction screens. Debris accumulation on the sump screen may challenge the sump's ability to provide adequate, long-term cooling water to the emergency core-cooling system (ECCS) and to the CS pumps. The Generic Safety Issue (GSI)-191 study titled "Assessment of Debris Accumulation on PWR Sump Performance" addresses the issue of debris generation, transport, and accumulation on the PWR sump screen and its subsequent impact on ECCS performance. The purpose of the GSI-191 study is to determine whether debris accumulation in containment following a postulated LOCA would prevent or impede the performance of the ECCS. Los Alamos National Laboratory (LANL) has been supporting the United States (US) Nuclear Regulatory Commission (NRC) in the resolution of GSI-191.

Analytical studies were performed and small-scale experimental programs [NUREG/CR-6772, 2002, NUREG/CR-6773, 2002] were conducted to support the resolution of GSI-191. A parametric evaluation of the US PWR plants demonstrated that potential sump-screen blockage was a plausible concern for operating PWRs [NUREG/CR-6762, Vol. 2, 2002]. As part of the GSI-191 study, a US PWR plant was volunteered and selected for a detailed analysis to develop and demonstrate a methodology for estimating the debris-transport fractions within PWR containments using plant-specific data. This report documents the blowdown and washdown transport portion of the study, describes the methodology, and provides an estimate for the transport of debris from its points of origin to the sump pool. The transport analysis consisted of (1) blowdown debris transport, where the effluences from a high-energy pipe break would destroy insulation near the break and then transport that debris throughout the containment; and (2) washdown debris transport caused by the operation of the CSs. Along the debris-transport pathways, substantial quantities of debris came into contact with containment structures and equipment where that debris could be retained, thereby preventing further transport. The blowdown/washdown debris-transport analysis provides the source term for the subsequent sump-pool debris-transport analysis.

The volunteer plant has a large, dry, cylindrical containment with a hemispherical dome constructed of steel-lined reinforced concrete and having a free volume of ~3 million ft^3. The nuclear steam supply system is a Westinghouse reactor with four steam generators (SGs). Each of the SGs is housed in a separate compartment that vents upward into the dome. Approximately two-thirds of the free space within the containment is located in the upper dome region, which is relatively free of equipment. The lower part of the containment is compartmentalized. The internal structures are supported independently so that a circumferential gap exists between the internal structures and the steel containment liner. Numerous pathways, including the circumferential gap, interconnect the lower compartments. The CS system has spray train headers at four different levels; however, ~70% of the spray nozzles are located in the upper dome. Some spaces in the lower levels are not sprayed by the spray system; therefore, areas of significant size exist where debris washdown by the sprays

would not occur. The sprays activate when the containment pressure exceeds 18.2 psig. If the sprays do not activate, debris washdown likely would be minimal. The insulation composition for the volunteer plant is ~13% fiberglass, 86% reflective metal insulation (RMI), and 1% Min-K insulation. For the purposes of this study, it was assumed that the fiberglass insulation was one of the low-density fiberglass (LDFG) types. For plant-specific analyses, these transport results for fibrous debris may have to be adjusted to compensate if the fiberglass insulation makeup is determined to be significantly different.

The effluences from a high-energy pipe break not only would destroy insulation near the break but also would transport that debris throughout the containment (i.e., blowdown debris transport). Substantial amounts of this airborne* debris would come into contact with containment structures and equipment and would be deposited onto these surfaces. As depressurization flows slow, debris would settle gravitationally onto equipment and floors. If pressurization of the containment were to occur, the CSs would activate to suppress pressurization. These sprays would tend to wash out remaining airborne debris (except in areas not covered by the sprays), and the impact of these sprays onto surfaces and the subsequent drainage of the accumulated water would wash deposited debris downward toward the sump pool (i.e., washdown debris transport). In addition, CSs could degrade certain types of insulation debris further through the process of erosion, thereby creating even more of the fine transportable debris.

An assessment of the likelihood of blocking the recirculation sump screens requires an estimate of the debris transport from the containment to the sump pool.† The debris transport within the sump pool is analyzed separately from this analysis, but the sump pool analysis requires the quantities of debris and the entry locations and timing as input to that analysis. An objective of this analysis was to develop and demonstrate an effective methodology for estimating the transport of debris from the debris point of origin in the containment down to the sump pool, thereby providing the source term to the sump-pool debris-transport analysis. Applying the methodology to the volunteer plant generated plausible debris-transport fractions for that plant.

The analyses herein considered only one break location: a LOCA located in one of the SG compartments, which is a probable location for that plant because most of the primary system piping is located in these compartments.

Neither the debris-size distributions nor the overall transport fractions in this report are valid for plant-specific evaluations because these fractions were calculated using LOCA-generated debris-size distributions that did not account properly for PWR jet characteristics. Boiling-water-reactor (BWR) jet characteristics were substituted for PWR jet characteristics because the PWR jet analyses had not yet been performed. When the PWR jet characteristics do become available, the overall transport fractions can be recalculated easily using PWR LOCA-generated debris-size characteristics.

The basic concepts of this methodology are applicable to the assessment of the debris transport within other PWR plants, as well; however, that application depends on the plant-specific aspects of each plant. The complexity of a plant-specific methodology could vary significantly from one plant to the next.

---

*The terms “airborne“ and “airflow“ are used loosely with regard to gas flows, which actually consist of both air and steam.

†The simplest and most conservative assessment would be to assume 100% transport to the sump pool.

VI.2 DEBRIS-TRANSPORT PHENOMENOLOGY

The transport of debris within a PWR would be influenced both by the spectrum of physical processes and phenomena and by the features of a particular containment design. Because of the violent nature of flows following a LOCA, insulation destruction and subsequent debris transport are rather chaotic processes. For example, a piece of debris could be deposited directly near the sump screen or it could take a much more tortuous path, first going to the dome and then being washed back down to the sump by the sprays. Conversely, a piece of debris could be trapped in any number of locations. Aspects of debris-transport analysis include the characterization of the accident, the design and configuration of the plant, the generation of debris by the break flows, and both air- and water-borne debris dynamics.

Long-term recirculation cooling must operate according to the range of possible accident scenarios. A comprehensive debris-transport study should consider an appropriate selection of these scenarios, as well as all engineered safety features and plant-operating procedures. The maximum debris transport to the screen likely will be determined by a small subset of accident scenarios, but this scenario subset should be determined systematically. Many important debris-transport parameters will be dependent on the accident scenarios. These parameters include the timing of specific phases of the accident (i.e., blowdown, injection, and recirculation phases) and pumping flow rates. The blowdown phase refers to primary-system depressurization. The injection phase corresponds to ECCS injection into the primary system, a process that subsequently establishes the sump pool. The recirculation phase refers to long-term ECCS recirculation.

Many features in nuclear-power-plant containments significantly affect the transport of insulation debris. The dominant break flows will move from the break location toward the pressure suppression system (i.e., the suppression pool in BWR plants and the upper regions of the compartment in PWR plants). Structures such as gratings are placed in the paths of these dominant flows and likely would capture substantial quantities of debris. The lower-compartment geometry—such as the open floor area, ledges, structures, and obstacles—defines the shape and depth of the sump pool and is important in determining the potential for debris to settle in the pool. Furthermore, the relative locations of the sump, LOCA break, and drainage paths from the upper regions to the sump pool are important in determining pool turbulence, which in turn determines whether debris can settle in the pool.

Transport of debris is strongly dependent on the characteristics of the debris that has formed. These characteristics include the types of debris (insulation type, coatings, dust, etc.) and the size distribution and form of the debris. Each type of debris has its own set of physical properties, such as densities, specific surface areas, buoyancy (including dry, wet, or partially wet), and settling velocities in water. Several distinct types of insulation are used in PWR plants [NUREG/CR-6762, Vol. 2, 2002]. The size and form of the debris, in turn, depends on the method of debris formation (e.g., jet impingement, erosion, aging, and latent accumulation). The size and form of the debris affect whether the debris passes through a screen, as well as the transport of the debris to the screen. For example, fibrous debris may consist of individual fibers or of large sections of an insulation blanket and all sizes within these two extremes.

The complete range of thermal-hydraulic processes affects the transport of insulation debris, and the containment thermal-hydraulic response to a LOCA includes most forms of thermal-hydraulic processes. Debris transport is affected by a full spectrum of physical processes, including particle deposition and resuspension for airborne transport and both settling and resuspension within calm and turbulent water pools for both buoyant and nonbuoyant debris.

The dominant debris-capture mechanism in a rapidly moving flow likely would be inertial capture; however, in slower flows, the dominant process likely would be gravitational settling. Much of the debris deposited onto structures likely would be washed off by the CSs or possibly by condensate drainage. Other debris on structures could be subject to erosion.

A panel of experts was convened to identify and rank the important phenomena, processes, and systems in regard to PWR debris transport [LA-UR-99-3371, 1999]. The insights gained from the work of this panel were factored into the analysis methodology. Additionally, all of the experimental and analytical research performed to resolve the BWR strainer-blockage issue was accessed for this analysis [LA-UR-01-1595, 2001; NUREG/CR-6369-1, 1999; NUREG/CR-6369-2, 1999; NUREG/CR-6369-3, 1999]. A summary was published on the base of knowledge for the effect of debris on PWR ECC sump performance [NUREG/CR-6808, 2003].

VI.3 METHODOLOGY

VI.3.1 Overall Description

Transport of LOCA-generated debris from its point of origin to the PWR sump pool is a complex process involving many physical processes and complex plant-specific geometry. To evaluate the blowdown and washdown debris transport within the drywell of a BWR plant, the NRC developed a methodology that accomplished the objectives of the drywell-debris-transport study (DDTS) [NUREG/CR-6369-1, 1999; NUREG/CR-6369-2, 1999; NUREG/CR-6369-3, 1999]. The methodology used herein was based on the BWR methodology.

The BWR methodology separated the overall transport problem into many smaller problems that were either amenable to the solution or that could be judged conservatively. The breakdown of the problem was organized using logic charts that were similar to well-known event-tree analyses. For some solution steps, sufficient data were available to solve that step reasonably. For other steps, insufficient data were available; therefore, the solution had to be found using engineering judgment that was applied after the available knowledge base was reviewed. Judgments were tempered to the desired level of conservatism called for in that particular analysis (sometimes assuming the worst case for a particular step). The result of each specific analysis was a transport fraction, defined as the fraction of insulation contained within the pipe-break destructive zone of influence (ZOI) that subsequently was damaged or destroyed by a LOCA and was eventually transported to the suppression pool. Certainly, the degree of refinement that is feasible depends on available resources and time restraints. Also, the conservatism in the estimates for each step in the divided problem may be compounded when the final transport fraction is quantified.

The PWR debris-transport methodology necessarily will differ from the BWR transport methodology because of differences in plant designs. These differences include the basic transport pathways, dominant capture mechanisms, and the timing of the accident sequence events. The dominant transport pathway for a PWR is different from the dominant pathway for a BWR. In a BWR, where pressure suppression would be due to steam condensation in the suppression pool, the debris initially would be transported directly to the suppression pool, where the ECCS strainers operate. In PWR containments, which are designed to suppress pressurization by channeling break effluences* to the relatively large free volume of PWR containments, debris likely would be blown away from the sump area initially. Because one-half

* In an ice-condenser plant, the break effluences would be channeled through the ice banks to condense steam.

to three-quarters of the containment free volume typically is located in the upper regions of the containment that includes the dome, it is justified to assume that a significant fraction of the small debris is blown directly into the upper regions, where the debris will settle onto floor surfaces or structures. Although debris blown into the upper regions then could be washed back down to the compartment sump area by the CSs, the washdown pathway can be tortuous and could certainly result in substantial debris entrapment.

The dominant debris-capture locations are different in a PWR than in a BWR. In many typical PWRs, the likely dominant locations are the upper regions of the containment, the ice condensers in an ice-condenser plant, the refueling pool, an outer annulus pool, and the sump pool. In the volunteer-plant containments, dominant locations for debris capture may not exist; rather, the debris likely would be blown throughout the entire containment. Gratings in a PWR could play a substantially different role versus the gratings played in the BWR methodology because the debris likely would be blown up through a grating as opposed to down through a grating. Debris trapped underneath a grating would be less likely to remain there than debris trapped on top of a grating.

Debris transport during the washdown phase would be caused by the water drainages of break recirculation overflow, the CSs, and condensate. The most important of these drainages would be the drainage of the activated CSs because the sprays usually cover a majority of the containment free volume, whereas the break overflow would wash only surfaces directly below the break. In a PWR, the break overflow could impinge on piping and equipment before reaching the containment sump floor, thereby washing debris from these surfaces, as well as potentially dispersing the flow. In a BWR, the break overflow for a majority of postulated breaks would pass down through at least one grating, where the flows would erode larger debris trapped on the gratings directly below the break—a situation less likely in a PWR. Although condensate drainage could transport debris from surfaces, the quantities of debris transported would likely be much less than the quantities transported by spray drainage.

The following methodology was designed specifically to analyze debris transport within the volunteer-plant containments; however, it is also directly applicable to several other containment designs, and it can be modified to tailor the methodology to any other PWR design. The best method for a particular plant will depend on the complexity of the containment design. If the containment has definitive upper and lower compartments that are separated by relatively few and narrow pathways, the analysis may be used to track debris transports in a manner similar to the DDTS analysis. Using an ice-condenser plant as an example, the containments were designed specifically to channel break flow through the ice banks to the dome region. This generally means that the connecting flow pathways between the lower and upper containments include the ice banks, small air-circulation return pathways, (needed to establish post-blowdown air circulation through the ice banks), and refueling-pool drains. Debris capture through the ice banks could be substantial. In addition, a large fraction of the small and fine debris would be blown into the dome region, where substantial quantities could be retained, even with the CSs operating.

The analysis here would focus on debris capture in the ice banks during blowdown and on debris retention in the upper compartment during the spray washdown process to identify debris transported from the lower containment and not likely to return there. Some plants would have a flooded outer annulus in which debris deposited in that pool would be less likely to transport from that pool to the sump pool. A conservative estimate of the maximum debris quantities that would be expected to transport to the sump pool can be made by subtracting masses of debris retained at various locations from the generation totals.

The design of the volunteer-plant containments is more complex than an ice-condenser design, from a debris-transport point of view; that is, the lower and upper regions of the containment are less well defined and are connected by several different pathways, thereby making it difficult to determine the motion of air and steam flows and the transport of debris. Certainly, system-level codes such as MELCOR can model the progression of break flows throughout the containment; however, the input model for the volunteer plant would have to be rather detailed to follow the flows through all of the lower levels in the containment. The modeling detail must include all of the levels and rooms and separate sprayed areas from non-sprayed areas. The model would need to simulate all of the connecting flow pathways, such as stairwells, equipment hatches, and doorways. A detailed thermal-hydraulics analysis was not performed for the volunteer-plant analysis.

The transport and deposition of insulation debris cannot be simulated realistically using a thermal-hydraulics computer code that incorporates aerosol transport models. The primary mode of debris capture during the violent primary-system depressurization is inertial capture. The available models for inertial capture are based on data taken for rather simple geometries (e.g., a bend in a pipe). Inertial capture in the complex geometry of containments cannot be modeled reasonably using current codes. However, inertial capture can be determined in specific parts of the containment. For example, at the volunteer plant, the personnel access doors between an SG compartment and the sump annulus have at least one 90° bend. A LOCA, particularly a large LOCA, in an SG compartment would result in depressurization flows that would carry insulation debris through these doors with the flow. As the flow underwent the sharp bend, some types of debris would be deposited by inertia on the wall at the bend. The tests conducted at the Colorado Engineering Experiment Station, Inc. (CEESI) demonstrated an average inertial capture fraction for fibrous debris of 17% at such a bend if the surface were wetted, and analysis has shown that surfaces within the containment likely would build a filmy layer of condensation rapidly. Because the CSs do not impinge on these wall surfaces, the debris would remain attached to those surfaces. In this situation, small amounts of debris can be removed from the equation, thereby lowering the transport fraction. Perhaps many of these types of definable captures can add up to a significant reduction in the transport fraction. Again, the size of that reduction would depend somewhat on both the geometry/conditions and the depth of the analysis.

The basic idea of the mechanics of this methodology is to look for such reductions systematically. The demonstration of this methodology in this volunteer-plant analysis assumed a large LOCA occurred inside SG compartment number 1 (SG1) of the containment. Figure IX-1 illustrates this methodology in the general sense. The idea is first to estimate the blowdown dispersal of the debris until all of the debris is associated with some surface area. Then the likelihood of debris remaining on each of these surfaces during washdown is estimated or judged. For example, debris deposited onto a surface that has been impacted by the CSs is much more likely to transport than debris deposited onto surfaces that have been wetted only by condensate.

As with the DDTS, the debris for transport must first be categorized according to type and size according to transport properties so that the transport of each type of debris can be analyzed independently. All insulation located within the break-region ZOI is assumed to be damaged to some extent. These categories and their properties are the subject of Section VI.3.2.

The containment free volume in the volunteer plant was subdivided into many regions based on geometry and the locations of the CSs. The volume region containing the postulated LOCA was

analyzed separately and first. For SG1, a MELCOR simulation of only the break compartment was used to determine the distribution of flows exiting that compartment (i.e., the fraction of flow going upward into the dome as opposed to the fraction entering the lower levels through personnel access doors). Debris capture within SG1 was based on such considerations as flows through gratings and flows making sharp bends (see Section VI.3.3.1). In each region, debris capture would deposit debris onto the “floor” or “other” surfaces, based on surface areas and judgment regarding whether debris was deposited by settling or by another mechanism. Floor surfaces were treated separately because these surfaces would collect and drain spray water differently from vertical surfaces, for example, and because debris that gravitationally settles would deposit onto horizontal surfaces. These surfaces were divided further according to their exposure to spray and condensate moisture. All surfaces would collect condensate. The sprays would impact some surfaces directly, and others simply would be washed by the process of spray drainage. Debris entrained by spray-drainage water could become captured a second time as the drainage fell from one level to another.

Because the chart illustrated in Figure IX-1 would become unreasonably large if it were developed for the entire volunteer-plant containment, another approach was used. The process was handled using an equation-format model (described in Figure IX-1), with the input entered into data arrays.

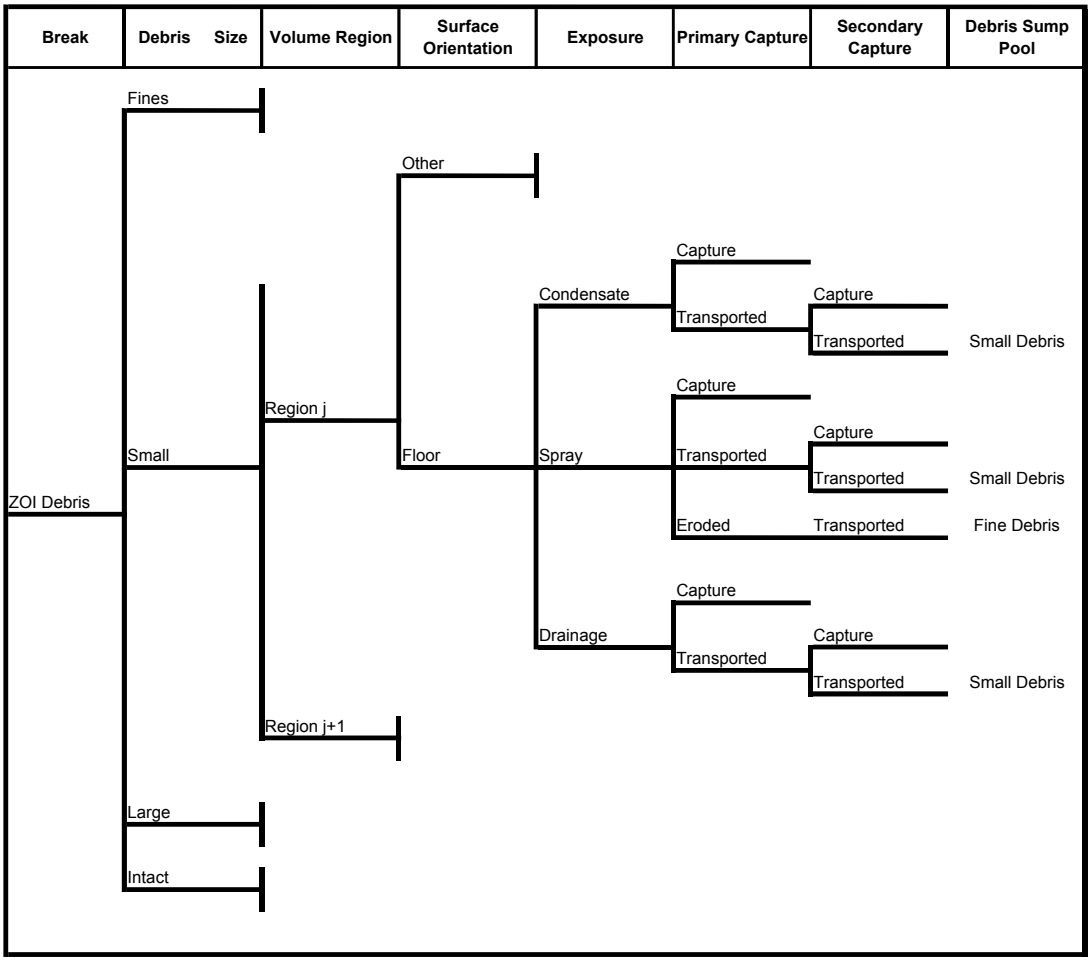

Figure IX-1. Example of a Section of a Debris-Transport Chart.

VI.3.2 Debris-Size Categorization

The types of insulation used inside the volunteer-plant containments include fiberglass insulation,* RMI, and stainless-steel-encapsulated Min-K insulation at ~13.4%, 85.7%, and 0.9%, respectively [NUREG/CR-6762, Vol. 2, 2002]. Although a majority of the insulation within these containments is RMI, the fibrous insulation more likely would cause blockage of the sump. First of all, the RMI debris would transport less easily than the fibrous debris (i.e., it takes a faster flow of water to move RMI debris than it does for fibrous debris). In addition, it takes substantially more RMI debris on the sump screens to block the flow effectively through the screens than it does for fibrous debris. Although the Min-K debris, in combination with the fibrous debris, could create substantial head losses on the screen, the inventory of the Min-K in the containments is relatively low. Therefore, the primary focus in this analysis was on the transport of fibrous debris, with the transport of RMI and Min-K estimated more crudely.

The difficulties associated with determining debris-size distributions to represent the LOCA-generated debris are (1) the limited debris-generation data and (2) the need to determine the characteristics of the LOCA jet (i.e., the size of the ZOI and volumes within specific pressure isobars). The limitations in the debris-generation data must be handled by skewing the integration of size fractions conservatively over the ZOI toward the smaller debris sizes; the more limited the data, the more conservative the integration. The determination of the jet characteristics for a PWR jet is a relatively straightforward analysis; but those characteristics unfortunately were not yet available for use in this report. Because, debris-size distributions are necessary to determine estimates for the overall transport of debris to the sump pool, assumptions were made to provide distributions that were suitable to illustrate the transport methodology. Therefore:

Neither the debris-size distributions nor the overall transport fractions in this report are valid for plant-specific evaluations.

However, the transport fractions for specific debris-size classes are considered to be valid for the volunteer plant.

VI.3.2.1 Fibrous Insulation Debris-Size Categorization

All insulation located within the break-region ZOI is assumed to be damaged to some extent. The damage could range from slight damage (insulation erosion occurring through a rip in the blanket cover) that leaves the blanket attached to its piping to the total destruction of a blanket (with its insulation reduced to small or very fine debris). For the purposes of this analysis, all of the insulation within the ZOI was considered to be debris. The fibrous debris was categorized into one of four categories based on transport properties so that the transport of each type of debris could be analyzed independently. These categories and their properties are shown in Table IX-1.

The primary difference between the two smaller and two larger categories was whether the debris was likely to pass through a grating that is typical of those found in nuclear power plants. This criterion also was used in the DDTS analysis. Thus, fines and small pieces pass through gratings but large and intact pieces do not. The fines and small pieces are much more transportable than the large debris. The fines were then distinguished from the small pieces

*The type (or types) of fiberglass insulation used in the volunteer-plant containments has yet to be determined. This analysis assumes that the fiberglass is LDFG.

because the fines would tend to remain in suspension in the sump pool, even under relatively quiescent conditions, whereas the small pieces would tend to sink. Furthermore, the fines tended to transport slightly more as an aerosol in the containment-air/steam flows and were slower to settle than the small pieces when airflow turbulence decreased. The CEESI tests illustrated that when an LDFG blanket was completely destroyed, 15% to 25% of the insulation was in the form of very fine debris (i.e., debris too fine to collect readily by hand).

The distinguishing difference between the large and intact debris was whether the blanket covering was still protecting the fibrous insulation. The primary reason for this distinction was whether the CSs could further erode the insulation material.

Table IX-1. Debris-Size Categories and Their Capture and Retention Properties

Fraction Variable	Size	Description	Airborne Behavior	Waterborne Behavior	Debris-Capture Mechanisms	Requirements for Crediting Retention
D_F	Fines	Individual fibers or small groups of fibers.	Readily moves with airflows and slow to settle out of air, even after completion of blowdown.	Easily remains suspended in water, even relatively quiescent water.	Inertial impaction Diffusiophoresis Diffusion Gravitational settling Spray washout	Must be deposited onto surface that is not subsequently subjected to CSs or to spray drainage. Natural-circulation airflow likely will transport residual airborne debris into a sprayed region. Retention in quiescent pools without significant flow through the pool may be possible.
D_S	Small Pieces	Pieces of debris that easily pass through gratings.	Readily moves with depressurization airflows and tends to settle out when airflows slow.	Readily sinks in hot water, then transports along the floor when flow velocities and pool turbulence are sufficient. Subject to subsequent erosion by flow water and by turbulent pool agitation.	Inertial impaction Gravitational settling Spray washout	Must be deposited onto surface that is not subsequently subjected to high rates of CSs or to substantial drainage of spray water. Retention in quiescent pools (e.g., reactor cavity). Subject to subsequent erosion.
D_L	Large Pieces	Pieces of debris that do not easily pass through gratings.	Transports with dynamic depressurization flows but generally is stopped by gratings.	Readily sinks in hot water and can transport along the floor at faster flow velocities. Subject to subsequent erosion by flow water and by turbulent pool agitation.	Trapped by structures (e.g., gratings) Gravitational settling	Must be either firmly captured by structure or on a floor where spray drainage and/or pool flow velocities are not sufficient to move the object. Subject to subsequent erosion.

Fraction Variable	Size	Description	Airborne Behavior	Waterborne Behavior	Debris-Capture Mechanisms	Requirements for Crediting Retention
D_I	Intact	Damaged but relatively intact pillows.	Transports with dynamic depressurization flows, stopped by a grating, or may even remain attached to its piping.	Readily sinks in hot water and can transport along the floor at faster flow velocities. Assumed to be still encased in its cover, thereby not subject to significant subsequent erosion by flow water and by turbulent pool agitation.	Trapped by structures (e.g., gratings) Gravitational settling Not detached from piping	Must be either firmly captured by structure or on a floor where spray drainage and/or pool flow velocities are not sufficient to move the object. Intact debris subsequently would not erode because of its encasement.

The volume (or mass) distribution, D_i, of the four categories of insulation debris was estimated first. This estimate assumed that the fibrous insulation within the ZOI was uniformly distributed and that the distribution must add up to one, as

$$\sum_{i=1}^{N_{types}} D_i = 1 \quad ,$$

where

D_i = the fraction of total debris that is type *i*.

The volume of each category of debris is simply the distribution fraction multiplied by the total volume of insulation within the ZOI. In debris-transport analysis, volumes of fibrous debris have been used interchangeably with mass on the basis that the density is that of the undamaged (as fabricated) insulation. Certainly the density would be altered by the destruction of the insulation and again when the debris became water saturated. For example, the physical volume of debris on the screen must include the actual density of the debris on the screen as

$$V_i = D_i V_{ZOI} \quad ,$$

where

V_i = the volume of debris of type *i* and
V_{ZOI} = the total volume of insulation contained within the ZOI.

The estimation of the debris-size distribution must be based on experimental data. When sufficient data are available, the following analytical model illustrates how the fraction of fine and small debris can be estimated from that data. Using the spherical ZOI destruction model, the fraction of the ZOI insulation that becomes type-*i* debris is given by the following integration:

$$F_i = \frac{3}{r_{ZOI}^3} \int_0^{r_{ZOI}} g_i(r)\, r^2\, dr \quad ,$$

where

F_i = the fraction of debris of type *I* ;
$g_i(r)$ = the radial destruction distribution for debris of type *I* ;
r = the radius from the break in the spherical ZOI model; and
r_{ZOI} = the outer radius of the ZOI.

Typical test data provide an estimate of the damage to insulation samples at selected distances from the test jet nozzle (i.e., the size distribution of the resultant debris). The jet pressure at the target is determined from test pressure measurements, suitable analytical models, or both. Thus, the size distribution as a function of the jet pressure is obtained. The volume associated with a particular level of destruction is determined by estimating the volume within a particular

pressure isobar within the jet [i.e., any insulation located within this pressure isobar would be damaged to the extent (or greater) associated with that pressure]. The isobar volumes then are converted to the equivalent spherical volumes; thus, the debris-size distribution is associated with the spherical radius (i.e., $g_i(r)$). The distribution would be specific to a particular kind of insulation, jacketing, jacketing seam orientation, and banding.

To demonstrate the transport methodology completely, it was assumed that the fibrous insulation used in the volunteer-plant containments was LDFG insulation, for which significant data are available to predict the LOCA-generated size distribution. The most extensive debris-generation data for LDFG insulation are the data from the BWR Owners' Group (BWROG) air-jet impact tests (AJITs) [NEDO-32686, 1996]. These data, combined with the jet characteristics of a PWR LOCA, could result in a realistic LOCA size distribution; however, the PWR jet characteristics were not available at the time of this writing.

The development of a suitable size distribution for the purposes of demonstrating this methodology follows. For fibrous debris, the BWROG correlated the fraction of the original insulation that became fine debris with the distance from the jet nozzle and then crudely estimated the ZOI destruction fractions for specific types of insulation. The fine debris in the BWROG analysis correlates with the combined fine and small debris of Table IX-1.

For the NUKON™ insulation debris—both jacketed and unjacketed insulation—the BWROG recommended in its Utility Resolution Guidance (URG) the assumption that 23% of the insulation within the ZOI be considered in the strainer head-loss evaluations during the resolution of the BWR strainer blockage issue. Applying this recommendation to this analysis means that 23% of the ZOI would be distributed between the fine and small debris and that the remaining 77% would be distributed between the large and intact debris. The NRC reviewed the BWROG recommendations and documented its findings in a safety evaluation report (SER) [NRC-SER-URG, 1998]. Although the NRC had some reservations regarding the BWROG's method for determining the debris fractions, the NRC believed the debris fractions to be conservative primarily because the blanket seams were arranged in the AJITs to maximize the destruction of the blankets.

Whereas the BWROG's recommendations were based on AJITs, more recent testing using two-phase jet impact testing indicated the need for somewhat higher small-debris fractions than did the AJIT data (refer to the staff evaluation of GR, Section 3.4.2.2 in this report, for the evaluation of the two-phase jet concern). Ontario Power Generation (OPG) of Canada conducted these debris-generation tests [OPG, 2001]. A comparison of the AJIT and the OPG tests was discussed in a report [NUREG/CR-6762, Vol. 3, 2002] that was supporting the PWR parametric evaluation [NUREG/CR-6762, Vol. 1, 2002]. This comparison illustrated the potential for more small debris to be generated by a two-phase jet than was supported by the AJIT data. For the parametric evaluation, the qualitative conclusion of comparing these two sets of test data was that the small debris fraction should be increased from the BWROG's recommendation. An engineering judgment was used to increase the recommended destruction fraction for small debris from 23% to 33%. The remaining 67% of the insulation would be assumed to be large debris either exposed or enclosed in its covering material.

For this analysis, the small-debris fraction of 33% that was used in the parametric evaluation was split to accommodate the fine- and small-debris categories of this analysis. The analysis of the AJIT testing performed at CEESI to support the DDTS determined that whenever entire blankets were completely destroyed, 15% to 25% of the insulation was too fine to collect by

hand.* Complete destruction here means that nearly all of the insulation was either fine or small pieces. In any case, the 15% to 25% of the blanket (an average of 20%) can be considered fine debris for the purposes of this analysis. For this analysis, it was assumed that 20% of the 33%-small-debris fraction was fine debris (i.e., $0.2 \times 0.33 = 0.066$). Therefore, 7% of the ZOI insulation was estimated to be destroyed into fine debris, leaving 26% for the small-piece debris.

In a similar manner, the parametric evaluation of the 67%-large-debris fraction was split in this analysis to accommodate the large and intact debris categories. In DDTS analysis, based on the AJIT data, 40% of the blanket insulation was assumed to remain covered. The DDTS assumption of 40% was accepted for the covered (intact) debris fraction for this analysis. However, that number had to be adjusted downward to account for the increase in the small-debris fraction from 23% to 33% (i.e., $0.67/0.77 \times 0.4 = 0.35$). Therefore, 35% of the ZOI insulation was considered to be intact debris, leaving 32% for the exposed large-piece debris. The debris category distribution for fibrous debris assumed in this analysis is summarized in Table IX-2.

Table IX-2. Fibrous-Debris-Category Distribution

Category	Category Percentage
Fines	7%
Small Pieces	26%
Large Pieces	32%
Intact	35%

VI.3.2.2 RMI Insulation Debris-Size Categorization

In the volunteer-plant containments, the RMI insulation is made of stainless steel. TPI manufactured the insulation around the reactor vessel. Diamond Power Specialty Company (DPSC) manufactured all of the other RMI inside the containments and marketed it as DPSC MIRROR™ insulation. Furthermore, the insulation panels generally are held in place simply by buckling the panels together (i.e., an absence of bands on most panels). Because the reactor vessel insulation is shielded from a postulated jet impingement for the most part, LOCA-generated RMI debris would consist primarily of the DPSC type. The threshold jet-impingement pressure required to damage DPSC MIRROR™ insulation with standard bands was estimated by the BWROG [NEDO-32686, 1996] and accepted by the NRC [NRC-SER-URG, 1998] as 4 psi; these data should be applicable to the volunteer-plant RMI. Therefore, some debris could be formed from any insulation subjected to a differential of 4 psi or greater, but the extent of damage would depend on the magnitude of the pressure. Insulation that is closer to the break would be destroyed completely and form small pieces of debris, whereas insulation farther from the break may remain nearly intact. A size distribution is needed for the transport analysis. Data from two experimental programs provide limited information on the extent of destruction that would occur in this type of RMI insulation. These programs were (1) the Siemens Karlstein tests [SEA-95-970-01-A:2, 1996], and (2) the BWROG AJIT [NEDO-32686, 1996].

* This debris either was blown through the fine-mesh screen at the end of the test chamber and lost from the facility or was deposited onto surfaces inside the chamber in such a dispersed manner that it could be collected only by hosing down the walls and structures.

Swedish Nuclear Utilities conducted metallic insulation jet impact tests at the Siemens AG Power Generation Group (KWU) test facility in Karlstein am Main, Germany (1994 and 1995 **can't find these in references**). During this test program, the US NRC conducted a single RMI debris-generation test to obtain debris-generation data and debris samples that are representative of RMI used in US plants. The NRC test sample was provided by the DPSC. The NRC-sponsored test was performed with a high-pressure blast of two-phase water/steam flow from a pressurized vessel connected to a target mount by a blowdown line with a double-rupture disk. The target was mounted directly on a device designed to simulate a double-ended guillotine break (DEGB) such that the discharge impinged the inner surface of the RMI target as it would an insulation cassette surrounding a postulated pipe break. Most of the RMI debris was recovered and analyzed with respect to size distribution. The overall size distribution for the total recovered debris mass is shown in Figure IX-2, and a photograph of the recovered RMI debris is shown in Figure IX-3. This debris sample is likely typical of debris formed from the RMI cassettes nearest the break.

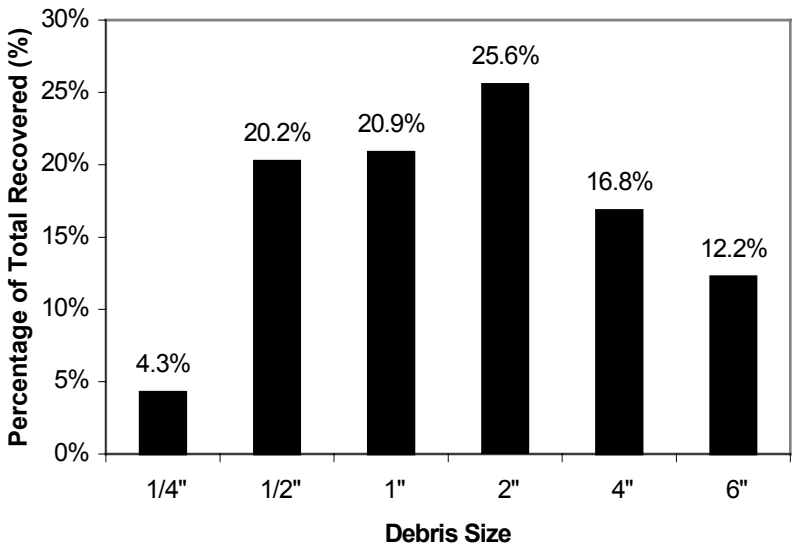

Figure IX-2. Size Distribution of Recovered RMI Debris.

Figure IX-3. RMI Debris Observed in Siemens Steam-Jet Impact Tests.

The BWROG-sponsored tests conducted at CEESI examined the failure characteristics of various types of insulation materials when subjected to jet impingement forces. CEESI has compressed-air facilities that provided choked nozzle airflow. This airflow was directed at insulation samples mounted inside a test chamber that did not pressurize significantly but retained most of the insulation debris for subsequent analysis. The variety of insulation materials tested included samples of the stainless-steel DPSC MIRROR™ insulation. The test samples were mounted at various distances from the nozzle, thereby subjecting similar samples to varying damage pressures. In this manner, the test data were used to estimate the threshold pressure required to damage this type of insulation. The data also provided information regarding the size distribution of the resulting debris. The formation of debris was dependent on the separation of the outer sheath, which in turn depended on the type, number, and placement of the supporting bands. The data used herein were for stainless-steel DPSC MIRROR™ cassettes mounted either with standard bands or without bands; therefore, these data are conservative with respect to data for cassettes mounted with even stronger banding. The recorded debris-generation data separated the quantities of debris into several distinct size groupings. For this transport analysis, the debris was grouped into three size groups: (1) debris generally smaller than 2 in. in size, (2) debris larger than 2 in. but smaller than 6 in., and (3) all RMI pieces larger than 6 in. (including both debris and relatively intact insulation cassettes). Figure IX-4 shows the fractions of the collected debris for the two finer groups as a function of the damage pressure on the cassette; all other insulation either remained relatively intact or formed debris larger than ~6 in.

The BWROG data describe the damage to stainless-steel DPSC MIRROR™ insulation (standard banding) when subjected to jet pressures of up to 120 psi. The NRC-sponsored Siemens test demonstrates the complete destruction of stainless-steel DPSC MIRROR™ insulation when impacted by the highest jet pressure near the break. A gap exists in the data between 120 psi and the higher pressure near the jet. The damage to the RMI within the ZOI was estimated using the spherical equivalent volume method in conjunction with BWR-specific data (i.e., volumes with specific pressure isobars). The BWROG analysis that was provided to the utilities [NEDO-32686, 1996] was used to convert jet isobar volumes to equivalent spherical volumes. Furthermore, the outer radius of the equivalent sphere was assumed to be 12D (i.e., 12 times the diameter of the pipe break), which corresponds to an insulation destruction pressure of 4 psi for a BWR radial offset DEGB. **The resultant size distribution can demonstrate the overall transport methodology fully but is not suitable for PWR plant-**

specific analyses. The BWROG data were applied when the impact pressure was <120 psi; the Siemens data were conservatively applied when the impact pressure was >130 psi (insulation totally destroyed), and a linear extrapolation was applied between 120 and 130 psi. The data shown in Figure IX-2 indicates that when the insulation is totally destroyed, ~70% of the debris would be <~2 in. in size and the remaining 30% would be between 2 and 6 in. in size.

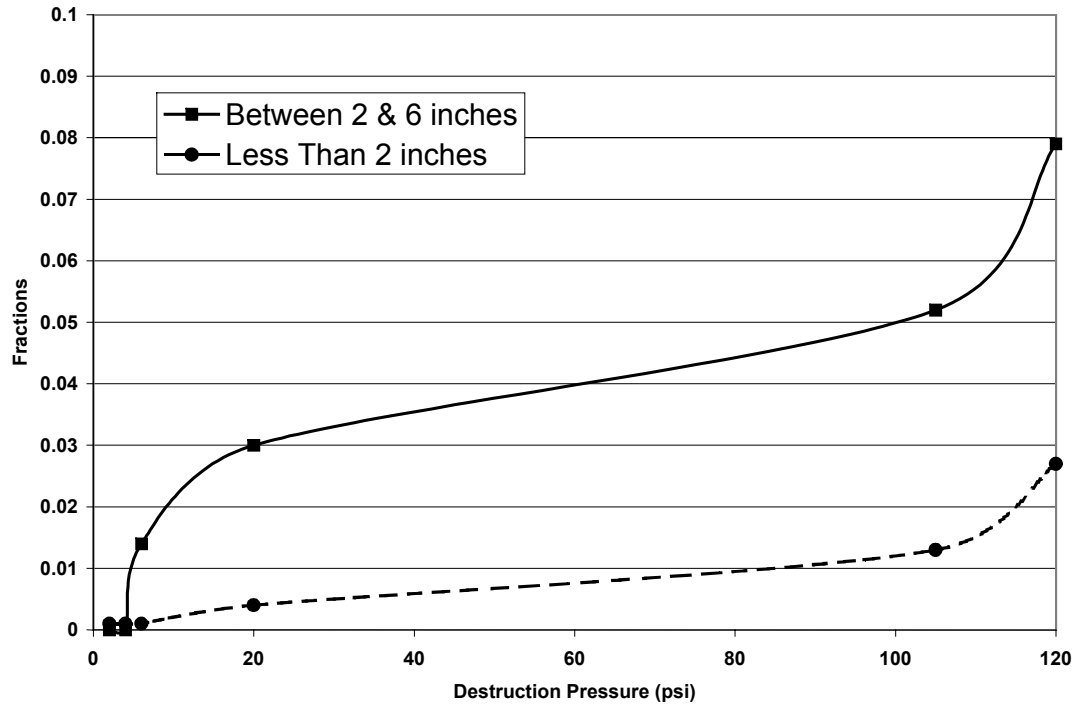

Figure IX-4. Relative Damage of Stainless-Steel DPSC MIRROR™ Insulation.

Because of variability and uncertainty in debris-generation estimates, as well as the use of BWR-specific jet characteristics, it is prudent to enhance the fractions for the finer groups of debris, noting that the smaller debris would transport more easily than would the larger debris. One uncertainty is the fact that the BWROG data were generated using an air jet, whereas the postulated accident would involve a two-phase steam/water jet; the comparison of two-phase and air test data has indicated that a two-phase jet could generate finer debris than could an air jet. To make the debris-generation estimates more conservative to compensate for variability and uncertainty in the estimates, the fractions for the two fines size groups were increased by 50%. The spherical volume damage estimates with and without the 50% increase are shown in Table IX-3.

Table IX-3. RMI Debris Category Distribution

Category	Category Percentage	
	Integration Result	Conservative Estimate
<2 in.	14%	21%
Between 2 and 6 in.	8%	12%
>6 in.	78%	67%

VI.3.2.3 Min-K Insulation Debris-Size Categorization

In locations where insulation thickness was a specific concern, such as pipe-whip-restraint locations, fully encapsulated Min-K insulation was used instead of the usual RMI insulation. Containment-wide, ~0.9% of the insulation is Min-K. Although the potential quantities of Min-K debris would be substantially smaller than corresponding quantities of fibrous or RMI debris, a small amount of Min-K particulate debris could contribute more significantly than RMI debris to sump-screen head loss. In particular, Min-K debris dust would contribute to the particulate load in the debris bed when combined with the fibrous debris on the screens. Min-K is a thermo-ceramic insulation (also referred to as a particulate insulation) that is made of microporous material. The particulate insulations include calcium silicate, asbestos, Unibestos, Microtherm, and gypsum board. Test data have demonstrated that microporous particulate, combined with fibrous debris, creates a debris bed that can cause relatively high head losses across that bed. This head loss is over and above the corresponding head loss associated with more ordinary particulate, such as corrosion products. The most notable of the particulate insulation types has been calcium silicate.

Limited debris-generation data exist for the microporous insulations, and most of the available data were obtained for calcium silicate. No debris-generation data were available for Min-K insulation. The primary source of calcium silicate debris-generation data are test data from tests conducted by the OPG [NUREG/CR-6762, Vol. 3, 2002]. These tests involved impacting aluminum-jacketed calcium silicate insulation targets with a two-phase water/steam jet. The size distribution data are shown in Figure IX-5.

Even if it is assumed that Min-K behaves similarly to calcium silicate with regard to debris generation, the OPG data cover only a limited range of damage pressures. Integrating the damage over the spherical ZOI requires a conservative extrapolation to a full range of pressures. The ZOI for Min-K corresponds to a destruction pressure of 4 psi, based on the BWROG guidance to utilities. At high pressures, the conservative extrapolation should assume that complete destruction of the insulation occurs (i.e., all of the insulation is pulverized to dust). At lower pressures, the damage fractions of the lowest pressures tested would be extended out to the ZOI boundary. This crude conservative extrapolation indicates that about half of the insulation should be considered dust. In addition to the conservative extrapolation, the debris-generation fraction is conservative with respect to the jacket seam angle relative to the jet. The seams in the test data shown in Figure IX-5 were oriented toward maximum damage. In reality, the seams within the ZOI likely would be distributed more randomly with respect to the jet; therefore, many of the jackets would provide more protection for the Min-K than is indicated by the OPG data. On the other hand, applying data for calcium silicate to Min-K insulation introduces substantial uncertainty.

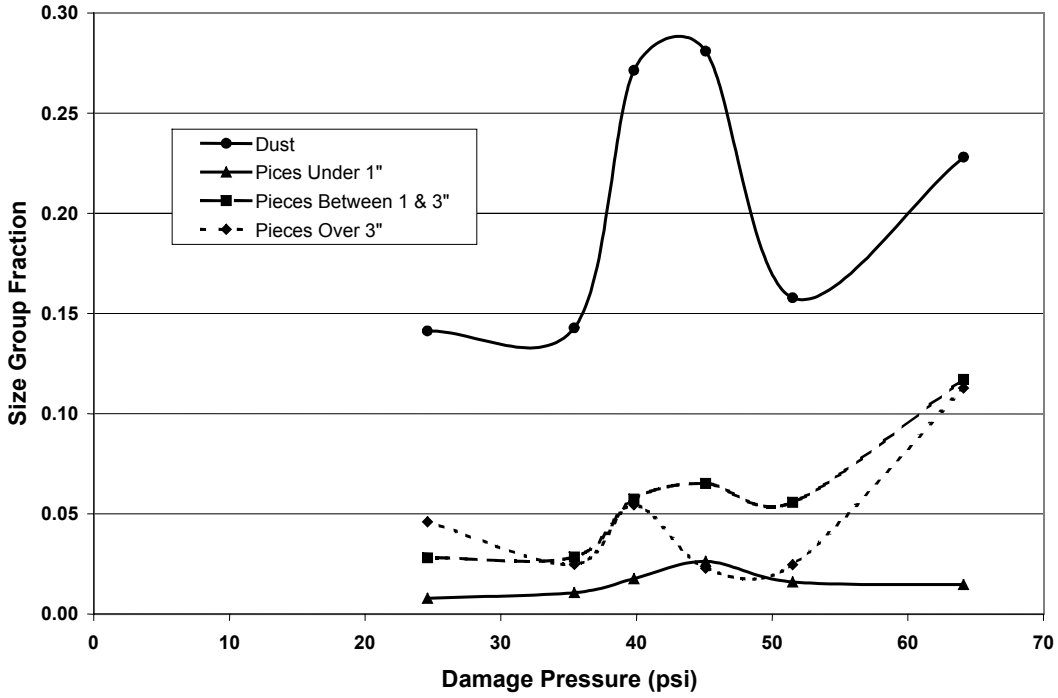

Figure IX-5. Debris-Size Distributions for OPG Calcium Silicate Tests.

Another source of uncertainty is the location of the minimal quantities of Min-K insulation with respect to the break. A key assumption of the ZOI integration is a uniform distribution of insulation within the ZOI. However, with so little Min-K insulation inside the volunteer-plant containments, all damaged Min-K insulation could be located preferentially near or far from the break. Therefore, all Min-K insulation could be destroyed totally or only slightly damaged. Another source of uncertainty that has not been assessed experimentally is the subsequent erosion of the Min-K debris by the CSs. In light of these uncertainties, it is conservative and prudent to assume that all of the Min-K insulation inside a ZOI would be pulverized to dust.

VI.3.3 Blowdown Debris Transport

The break region, SG1, would be the source of all insulation debris and would be subject to the most violent of the containment flows, and the primary debris capture mechanism in this region would be inertial capture. For these reasons, the transport of debris within the region of the pipe break likely should be solved separately from that of the rest of the containment. The methodology is described for fibrous-debris transport but also was applied to RMI debris in a similar manner.

VI.3.3.1 Break-Region Dispersion and Capture

The first step in determining the dispersal of debris near the debris-generation source was to determine the distribution of the break flow from the region—specifically, the fractions of the flow directed to the dome versus other locations. This determination was accomplished using the containment thermal-hydraulics code MELCOR. The containment was designed to force reactor-coolant-system (RCS) break effluents upward through the open tops of the SG

compartments and into the dome. Figure IX-6 shows the nodalization diagram for the break-region MELCOR calculation.

The LOCA-generated debris that was not captured within the region of the break would be carried away from the break region by the break flows. The primary capture mechanism near the break would be inertial capture or entrapment by a structure such as a grating. The break-region flow that occurred immediately after the initiation of the break would be much too violent to allow debris simply to settle to the floor of the region.

The inertial capture of fine and small debris occurs when a flow changes directions, such as flows through the doorways from the SG compartments into the sump-level annular space. These flows must make at least one 90° bend through these doorways, and these surfaces would be wetted by steam condensation as well as by the liquid portion of the break effluence. Debris-transport experiments conducted at CEESI [NUREG/CR-6369-2, 1999] demonstrated an average capture fraction of 17% for fine debris and small debris that make a 90° bend at a wetted surface. Other bends in the flow would occur as the break effluents interacted with equipment and walls.

The platform gratings within the SG compartments would capture substantial debris, even though the gratings do not extend across the entire compartment. The CEESI debris-transport tests demonstrated that an average of 28% of the fine and small debris was captured when the airflow passed through the first wetted grating that it encountered and that an average of 24% was captured at the second grating. By definition, the large and intact debris would be trapped completely by a grating. In addition, equipment such as beams and pipes was shown to capture fine and small debris. In the CEESI tests, the structural maze in the test section captured an average of 9% of the debris passing through the maze.

To evaluate the transport and capture within the break region, the evaluation must be separated into many smaller problems that are amenable to resolution. This separation can be accomplished using a logic-chart approach that is similar to the approach developed for the resolution of the BWR-strainer-blockage issue [NUREG/CR-6369-1, 1999]. The chart for a LOCA in the volunteer-plant SG1 is shown in Figure IX-7 and is based on the MELCOR nodalization diagram in Figure IX-6. This chart tracks the progress of small debris from the pipe break (Volume V12) until the debris is assumed to be captured or is transported beyond the compartment. Because SGs 1 and 4 are joined at two locations, the compartments were combined into one model (i.e., a LOCA in SG1 will discharge to the containment through SG4 as well).

The questions across the top of the chart, shown in Figure IX-7, alternate among volume capture, flow split, and junction capture as the debris-transport process progresses through the nodalization scheme. The nodalization scheme was constructed to place the gratings at junction boundaries. The first chart question (header) after the initiator asks how much debris would be captured in Volume V12, where the LOCA was postulated to occur. The evaluation of this question involves simply estimating the fraction of small debris that was deposited by inertia near the pipe break; the remainder of the debris would be assumed to transport beyond this volume. The next question in the chart concerns a flow split (i.e., the distribution of the break flow going upward or downward from the break). The flow split is actually a debris split (i.e., how much debris goes in each direction). For fine- and small-piece debris, it is reasonable to assume that the debris split is approximated by the flow split. For large and intact-piece debris, the debris split may differ from the flow split, depending on the geometry. The third question concerns the amount of the debris captured at the flow junction between two volumes. The two

junctions in the third question represent gratings that extend partly across the compartment at two levels. The fourth question starts the cycle over again for the next set of volumes in the sequence.

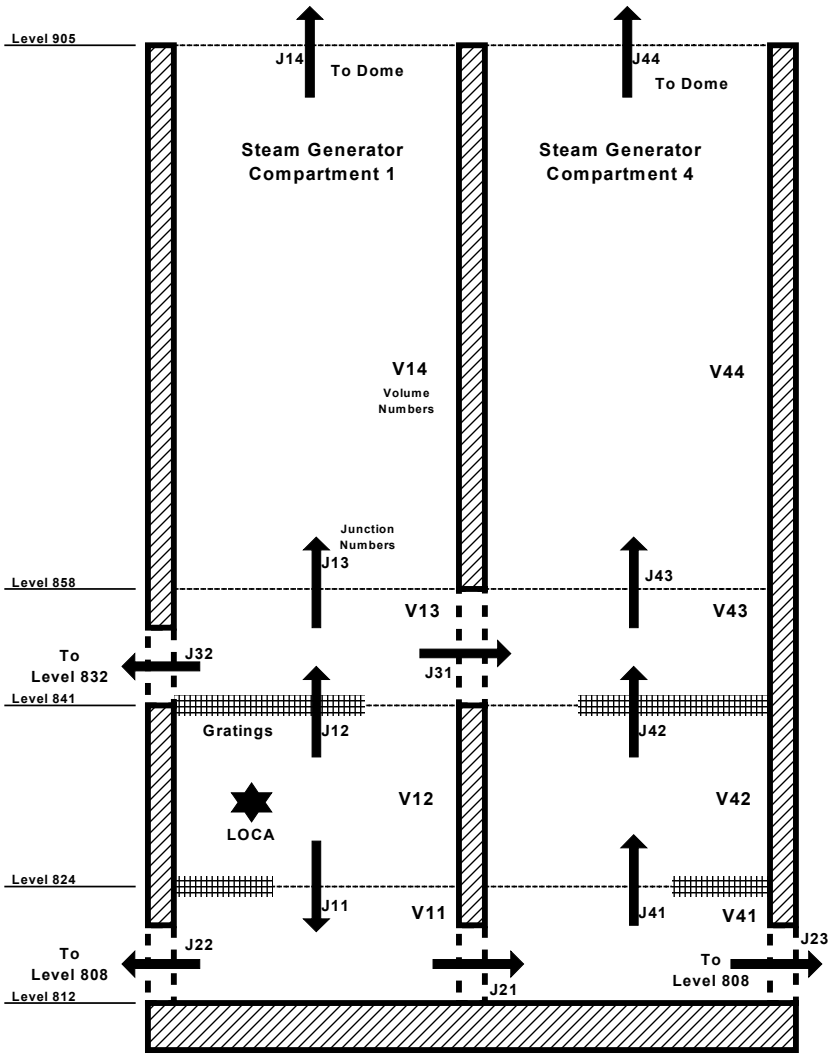

Figure IX-6. Break-Region Nodalization.

Once the distributions are inserted into the chart and the results are quantified, the results will indicate the distribution of captured debris within the compartments, as well as the debris transport from the compartments. The chart also will indicate where the debris that is transported from the SG compartments goes (e.g., to the dome or to the lower levels through access doorways).

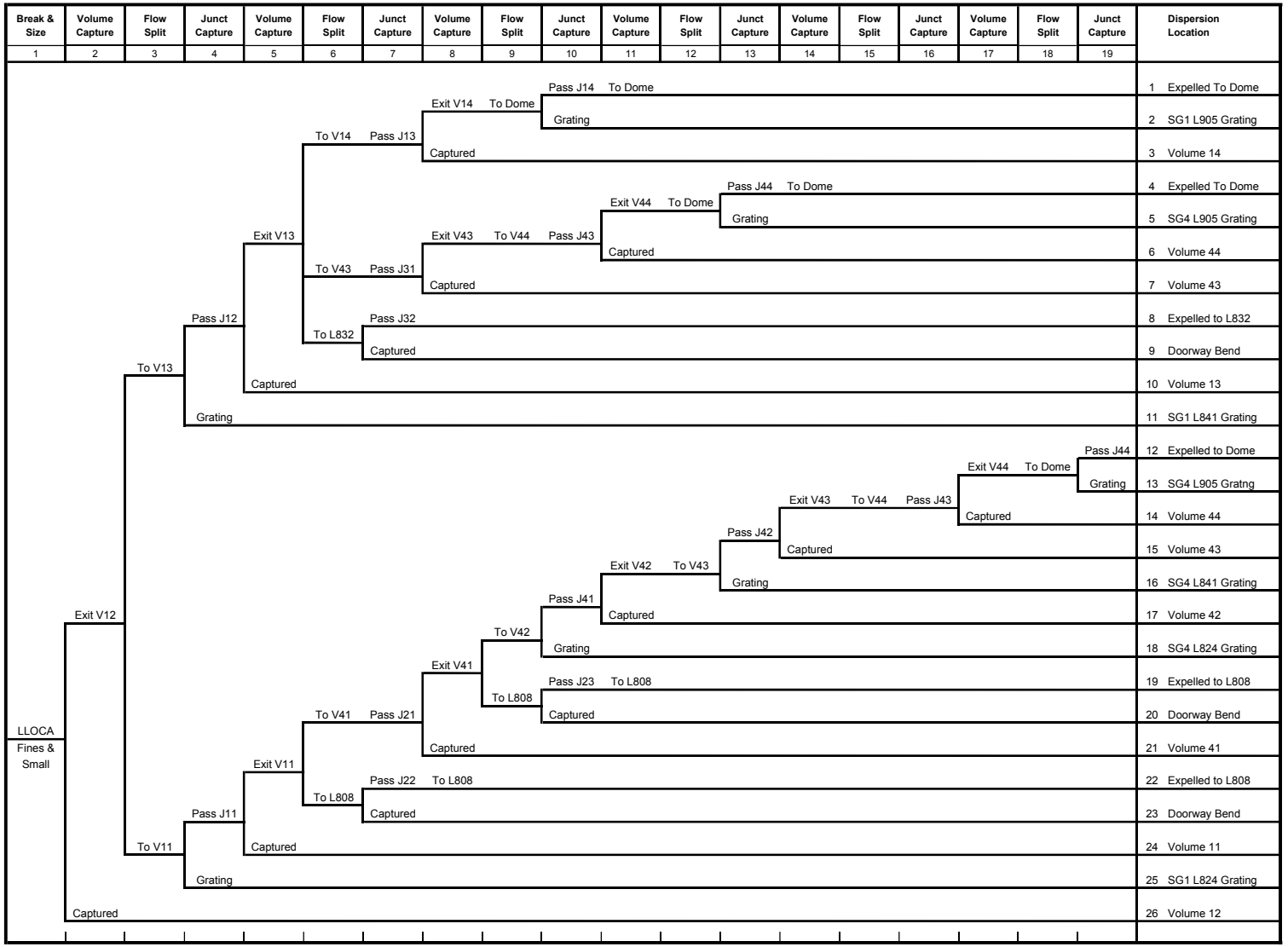

Figure IX-7. Chart for the Structure of Break-Region Debris-Transport.

VI.3.3.2 Dispersion and Capture throughout the Containment

The debris dispersion model used to evaluate debris transport within the volunteer-plant containments estimated dispersion throughout the containment first by free volume and then by surface orientation within a volume region. Dispersion distributions were based first on actual volumes and areas and then were adjusted using weighting factors that were based on engineering judgment.

VI.3.3.2.1 Dispersion by Region

As the containment pressurizes following a LOCA, break flows carrying debris would enter all free volume within the containment. Larger debris would tend to settle out of the break flows as the flow slowed down after leaving the break region. However, the fine and smaller debris more likely would remain entrained so that fine and small debris would be distributed more uniformly throughout the containment. Certainly, the distribution would not be completely uniform because of debris being captured along the way, which is the reason for the weighting factors.

First, the containment free volume was subdivided into volume regions. This subdivision was based on geometry (i.e., floor levels and walls) and on the location of CSs. Specifically, areas where deposited debris likely would not be entrained by the CSs were separated from areas that were impacted by the sprays. Some areas that were not actually sprayed still could be washed by the drainage of spray water as the water worked its way down through the containment structures. Areas where debris could be deposited without subsequently being washed downward by the sprays and the spray drainage could reduce the estimated transport fractions.

The total free volume of the containment is the sum of the free volumes for all of the volume regions. The volunteer-plant containment free volume was subdivided into a total of 24 volume regions (J = 24) as

$$V_{cont} = \sum_{j=1}^{J} Vc_j \quad ,$$

where

V_{cont} = the total free volume of the containment;
Vc_j = the free volume in containment region *j*; and
J = the number of volume regions.

The following equations define the dispersion model;

$$V_{i,j} = F_{i,j}\ D_i\ V_{ZOI} \quad ,$$

where

$V_{i,j}$ = the volume of debris-type *i* located in region *j*;
$F_{i,j}$ = the fraction of debris-type *i* deposited in region *j* during blowdown;

D_i = the fraction of total debris-type *i*; and

V_{ZOI} = the total volume of insulation contained within the ZOI.

For fibrous debris, the numbering system is *i* = 1, 2, 3, and 4 for fines, small pieces, large pieces, and intact debris, respectively.

The volume dispersion distribution must add up to one, as

$$\sum_{j=1}^{J} F_{i,j} = 1 \text{ (for each } i\text{)} \quad .$$

The break region was designated as Region 1 (i.e., *j* = 1 and $F_{i,1} = F_{i,break}$), and the methodology for the break-region dispersion fraction was provided in Section VI.3.3.1. The remaining distribution fractions were estimated using the following volume and engineering judgment weighted distribution:

$$F'_{i,j(j\neq 1)} = (1 - F'_{i,break}) \frac{wc_{i,j}\, Vc_j}{\sum_{j=2}^{J} wc_{i,j}\, Vc_j} \quad ,$$

where

$wc_{i,j}$ = the weighting factor based on engineering judgment.

If all of the $wc_{i,j}$ were set to one, then the distribution would be simply a volume-weighted distribution.

For large and intact pieces, many of these weighting values $wc_{i,j}$ were set to zero to reflect the fact that large and intact debris likely would not transport into many of the lower-level volume regions. It is anticipated that most of the large and intact debris would reside in the break-region volume, sump-pool volume, containment-dome volume, or refueling area.

The substantial quantities of debris transported into the dome subsequently would tend to either fall out of the atmosphere or be washed out by the CSs. About half of this debris would be deposited onto the Level 905 floors that are associated with the dome. However, the other half would fall below this level, thereby entering other volume regions. The volume distribution function $F'_{i,j}$ is modified as follows to account for debris fallout between regions:

$$F_{i,j} = F'_{i,j} + T_j\, F'_{i,2} \quad ,$$

where

T_j = the fraction of debris (type independent) located in the dome that subsequently falls or washes to region *j*.

The values of T_j are based on the opening areas into regions below the dome (e.g., the cross-sectional area of the SG compartments divided by the total cross-sectional area of the containment provides the values for debris that is falling into an SG compartment). The value for a region receiving no debris from dome fallout would be zero. Note that the dome volume region was designated Region 2; therefore, the value for region 2 (i.e., T_2) must be negative to remove debris from Region 2:

$$T_2 = -\sum_{j=1}^{J} T_{j(j\neq 2)} \quad .$$

VI.3.3.2.2 Dispersion by Surface Orientation and Exposure

Once the debris was dispersed to a volume region, it was assumed to have been deposited within that region. Some residual fine debris could remain airborne in regions that are not impacted by the sprays; however, the total quantity of this residual airborne debris was not expected to be significant.

The surface area within each volume region was subdivided into six subsections. These subsections reflect both the differing surface orientations and their exposure to moisture. The floors were separated from all of the other surfaces because the floors would receive the gravitationally settled debris and the other surfaces could be flooded partially by spray drainage. The spray water would not accumulate on the other surfaces, which include the walls, ceilings, and equipment.

Three surface exposures or moisture conditions were considered in the analysis: surfaces wetted directly by the CSs, surfaces not directly sprayed but washed by spray drainage (most likely floor surfaces), and surfaces wetted only by steam condensation. All surfaces likely would be wetted by condensation. The surface exposure determined how likely debris that was deposited onto that particular surface subsequently would be transported by the flow of water.

These areas were described by the following three-dimensional array:

$A_{j,k,l}$ = area for volume region *j*, orientation *k*, and exposure *l*.

All of the area within a particular volume region then would be

$$A_j = \sum_{k=1}^{2} \sum_{l=1}^{3} A_{j,k,l} \quad .$$

The numbering system is *k* = 1 and 2 for “floor“ and “other“ surfaces, respectively, and *l* = 1, 2, and 3, for condensate, spray, and drainage exposures, respectively.

The surface-area distribution fractions were estimated using the following area and engineering judgment weighted distribution:

$$f_{i,j,k,l} = \frac{w_{i,j,k,l}\ A_{j,k,l}}{\sum_{k=1}^{2}\sum_{l=1}^{3} w_{i,j,k,l}\ A_{j,k,l}} \quad ,$$

where

$f_{i,j,k,l}$ = the fraction of debris-type *i* deposited within volume region *j* that was deposited onto surface *k*, *l*; and

$w_{i,j,k,l}$ = the weighting factor based on engineering judgment for debris-type *i* deposited within volume region *j* that was deposited onto surface *k*, *l*.

An equivalent expression for $f_{i,j,k,l}$ is

$$f_{i,j,k,l} = \frac{w_{i,j,k,l}\ g_{j,k,l}}{\sum_{k=1}^{2}\sum_{l=1}^{3} w_{i,j,k,l}\ g_{j,k,l}} \quad ,$$

where

$$g_{j,k,l} = \frac{A_{j,k,l}}{A_j} \quad .$$

The fractions summed within a particular volume region and for a particular debris type must add up to one:

$$\sum_{k=1}^{2}\sum_{l=1}^{3} f_{i,j,k,l} = 1 \quad .$$

If all of the $w_{i,j,k,l}$ were set to one, then the distribution would be simply an area-weighted distribution. If all the $w_{i,j,k,l}$ were set to zero for *k* = 2 (“other“ surfaces), then all of the debris would be deposited on the floor, as likely would be the case for the large and intact debris. It is anticipated that most of the large and intact debris would reside on the floors in the break-region volume, sump pool volume, containment dome volume, or refueling area. In the SG compartment, much of the large debris stopped on the underside of a grating could fall back down after the depressurization flows subsided.

The volume of debris on a particular surface is expressed by

$$V_{i,j,k,l} = f_{i,j,k,l}\ F_{i,j}\ D_i\ V_{ZOI} \quad .$$

VI.3.4 Washdown Debris Transport

Debris that is deposited throughout the containment subsequently would be subject to potential washdown by the CSs, the drainage of the spray water to the sump pool, and (to a lesser extent) the drainage of condensate. Debris on surfaces that would be hit directly by CS would

be much more likely to transport with the flow of water than would debris on a surface that is wetted merely by condensation. The transport of debris entrained in spray water drainage is less easy to characterize. If the drainage flows were substantial and rapidly moving, the debris likely would transport with the water. However, at some locations, the drainage flow could slow and be shallow enough for the debris to remain in place. As drainage water dropped from one level to another, as it would through the floor drains, the impact of the water on the next lower level could splatter sufficiently to transport debris beyond the main flow of the drainage, thereby essentially capturing the debris a second time. In addition, the flow of water could erode the debris further, generating more of the very fine debris. These considerations must be factored into the analysis. The washdown processes are illustrated schematically in Figure IX-8.

The drainage of spray water from the location of the spray heads down to the sump pool was evaluated. This evaluation, reported in Appendix A **Appendix I?**, provided insights for the transport analysis, such as identifying areas that were not impacted by the CSs, the water drainage pathways, likely locations for drainage water to pool, and locations where drainage water plummets from one level to the next.

VI.3.4.1 Debris Erosion during Washdown

Experiments conducted in support of the DDTS analysis demonstrated that insulation debris could be eroded further by the flow of water. The primary concern of the DDTS analysis was LDFG debris that was deposited directly below the pipe break and therefore was inundated by the break overflow. Debris erosion in this case was substantial (i.e., ~9%/h at full flow). Debris erosion due to the impact of the sprays and spray drainage flows was certainly possible but was found to be much less significant. The DDTS study concluded that <1% of the LDFG was eroded because of the CSs. Debris erosion occurring because of condensation and condensate flow was neglected. Debris with its insulation still in its cover was not expected to erode further. For RMI debris, erosion was not a consideration. However, for a microporous insulation such as calcium silicate or Min-K, the washdown erosion has not been determined; it would be expected to be substantial and could potentially erode this type of debris completely into fine silt.

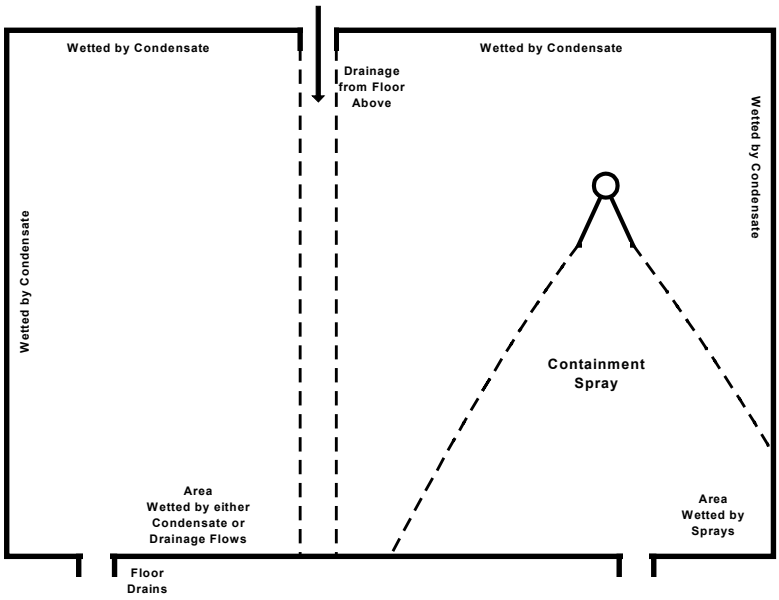

Figure IX-8. Schematic of Debris-Washdown Processes.

Because the byproduct of the erosion process is more of the very fine and easily transportable debris, the process must be evaluated. All erosion products were assumed to transport to the sump pool. Recall that this debris would remain suspended in the sump pool until filtered from the flow at the sump screens. Therefore, even a small amount of erosion could contribute significantly toward the likelihood of screen blockage.

The only erosion process evaluated herein was the erosion of debris that was impacted directly by the CSs. Erosion caused by break overflow was deferred to the degeneration of debris due to sump pool turbulence associated with the plummeting of the break flow into the pool. This assumption neglects the erosion of any large debris that is deposited on top of the lower grating in SG1 and impacted directly by the break overflow; however, this quantity of debris was not considered to be substantial. Most of the debris that is located directly below the break likely would be pushed away from the break and into the sump pool. Note that the floors of the SG compartments are 4 ft above the floor of the sump pool. At switchover, the SG floor would not be flooded but that at the maximum pool height, that pool would have a depth of 0.7 ft in the SG compartment.

The assumed fractions of fibrous debris that were eroded are summarized in Table IX-4. It was assumed that condensate drainage would not cause further erosion of debris and that intact or covered debris would not erode further. Erosion does not apply to fine debris because that debris is already fine. About 1% of the small- and large-piece debris that was directly impacted by the sprays was considered to have eroded. This amount of erosion was considered to be conservative because the DDTS concluded that the erosion was <1%. No erosion of the intact debris was assumed because the canvas cover likely would protect the insulation.

Table IX-4. Total Erosion Fractions for Fibrous Debris

Exposure	Fines	Small	Large	Intact
Condensate	N/A	0	0	0
Sprays	N/A	1%	1%	0

To estimate the volume of debris that was eroded, the volume of debris that was impacted by the sprays first must be estimated. The latter estimate can be made using the data arrays that were already established in this methodology. These volumes for small and large debris, respectively, are estimated using the following two equations:

$$Vspr_2 = \sum_{j=1}^{J} \sum_{k=1}^{2} f_{2,j,k,2} \; F_{2,j} \; D_2 \; V_{ZOI}$$

and

$$Vspr_3 = \sum_{j=1}^{J} \sum_{k=1}^{2} f_{3,j,k,2} \; F_{3,j} \; D_3 \; V_{ZOI} \quad .$$

The volumes that are eroded (E_2 and E_3 for small and large debris, respectively) are simply 1% of the debris volumes impacted by the sprays, given as

$$E_2 = e_{spr} Vspr_2$$

and

$$E_3 = e_{spr} Vspr_3 \quad ,$$

where the spray erosion fraction e_{spr} is 0.01.

VI.3.4.2 Capture Retention during Washdown

The retention of debris during washdown must be estimated for the debris deposited on each surface (i.e., the fraction of debris that remains on each surface). These estimates, based on experimental data and engineering judgment, were assigned somewhat generically. For surfaces that would be washed only by condensate drainage, nearly all deposited fine and small debris likely would remain there. The DDTS assumed that only 1% of the fibrous debris would be washed away in the more realistic central estimate of that study (a value of 10% was assumed for the upper-bound estimate). When the 1% assumption was applied, all of the surfaces that drained only condensate would have a retention fraction of 0.99 with respect to fibrous debris.

For surfaces that were hit directly by sprays, the DDTS assumed 50% and 100% for the central- and upper-bound estimates for small fibrous debris. Large and intact debris likely would not be washed down to the sump pool (retention fractions of 1). For surfaces that were not sprayed directly but subsequently drain accumulated spray water, such as floors close to spray areas, the retention fractions were much less clear. These fractions likely would vary with location and drainage flow rates and therefore must be area location specific, with more retention for small pieces than for fine debris.

The retention fraction for a specific volume region is expressed as

$$R_{i,j} = \sum_{k=1}^{2} \sum_{l=1}^{3} f_{i,j,k,l} \; r_{i,j,k,l} \quad ,$$

where

$R_{i,j}$ = the fraction of debris-type *i* retained in region *j*; and

$r_{i,j,k,l}$ = the fraction of debris-type *i* retained, on surface *k*, *l*, in region *j*.

These volume region retention fractions $R_{i,j}$ do not account for the quantities that are eroded from the captured pieces of debris. To complete the erosion model, the volumes of eroded debris that came from debris that remained captured versus debris that transported to the sump pool were estimated. Therefore, the debris that remained captured during the washdown process is estimated using the following two equations for small- and large-piece debris, respectively:

$$Rspr_2 = \sum_{j=1}^{J} \sum_{k=1}^{2} r_{2,j,k,2}\ f_{2,j,k,2}\ F_{2,j}\ D_2\ V_{ZOI}$$

and

$$Rspr_3 = \sum_{j=1}^{J} \sum_{k=1}^{2} r_{3,j,k,2}\ f_{3,j,k,2}\ F_{3,j}\ D_3\ V_{ZOI} \quad .$$

Therefore, the volumes of eroded debris associated with the debris that remained captured are expressed as

$$ER_2 = e_{spr} Rspr_2$$

and

$$ER_3 = e_{spr} Rspr_3 \quad .$$

Debris transported from its original volume region still could be captured at a lower elevation. This secondary capture was neglected in this analysis.

VI.3.5 Debris Volumes Introduced to the Sump Pool

The primary result of the blowdown/washdown transport analysis is the volume that is transported to the sump pool by debris category. The volumes of debris transported to the pool are given by

$$V_{i,pool} = \left[1 - \sum_{j=1}^{J} R_{i,j} F_{i,j} \right] D_i\ V_{ZOI} + Ve_i \quad ,$$

where

$V_{i,pool}$ = the volume of debris-type *i* transported to the sump pool and
Ve_i = the volumes of eroded debris transferring from small- and large-debris categories to the fine-debris category.

The erosion translation array is given by

$$Ve_i = \begin{bmatrix} +(E_2 + E_3) \\ -(E_2 - ER_2) \\ -(E_3 - ER_3) \\ 0 \end{bmatrix} \quad .$$

This array adds the eroded product ($E_2 + E_3$) to the fine-debris category and subtracts the eroded volume from the noncaptured small- and large-debris categories ($E_i - ER_i$).

The total debris that transports to the pool is

$$V_{pool} = \sum_{i=1}^{4} V_{i,pool} \quad .$$

This model does not track debris transport in sufficient detail to determine where the debris would enter the sump pool. It was assumed simply that the debris would be mixed uniformly with flows entering the pool.

VI.3.6 Transport Fractions

The overall debris-transport fraction now can be estimated as

$$TF_{ZOI} = \frac{V_{pool}}{V_{ZOI}} \quad ,$$

where

TF_{ZOI} = the fraction of insulation that is located in the ZOI and subsequently is transported to the sump pool.

The transport fractions for each individual debris category can be estimated as

$$TF_i = \frac{V_{i,pool}}{D_i V_{ZOI}} \quad ,$$

where

TF_i = the fraction of debris-type *i* that is generated within the ZOI and subsequently is transported to the sump pool.

Note that the translation of erosion products from the small- and large-debris categories to the fine-debris category has been incorporated into the transport fractions.

VI.4 DEBRIS-TRANSPORT ANALYSIS

When the methodology presented in Section VI.3 was used, plausible estimates were developed for the transport of insulation debris within the volunteer-plant containments. Because of the complexity of the analysis and the limited available data, substantial uncertainty exists in these estimates. Engineering judgment that was used to fill gaps in the data was tempered conservatively. Despite the uncertainty, the transport analysis illustrated trends, as well as plausible estimates of the fractions of the debris that was generated and subsequently could transport to the sump pool.

VI.4.1 Fibrous Insulation Debris Transport

As discussed in Section VI.3.2, the insulation that is used in the volunteer-plant containments consists of fibrous, RMI, and Min-K insulation at ~13.4%, 85.7%, and 0.9%, respectively. The

majority of the available debris-transport data was obtained for LDFG insulation debris, specifically experimental data taken for the DDTS [NUREG/CR-6369-2, 1999]. Although a majority of the insulation within these containments is RMI, the fibrous insulation debris, in combination with particulate, is expected to be a larger challenge to the operation of the recirculation sump screens. Therefore, the debris transport for the fibrous debris was analyzed first. Even with the available transport data for LDFG debris, the transport analysis required the application of conservatively tempered engineering judgment.

VI.4.1.1 Fibrous Blowdown Debris Transport

The first consideration in performing the dispersion estimate for the fibrous blowdown insulation debris was the dispersion and deposition within the break region (assumed to be a break in SG1), where deposition likely resulted from inertial impaction. The dispersion through the remainder of the containment was subsequently estimated.

VI.4.1.1.1 Break-Region Blowdown Debris Deposition

The effluences from the break would carry insulation debris with the flows into the upper-containment dome through the large opening at the top of the SG compartment and into lower compartments through the compartment access doorways. Along the way, substantial portions of that debris likely would be inertially deposited or otherwise entrapped onto structures. In general, the break-region flow immediately after the initiation of the break would be much too violent to allow debris simply to settle to the floor of the region.

VI.4.1.1.1.1 Characterize Break Flows within Break Region

The thermal-hydraulic MELCOR code was used to determine the distribution of the break effluents from the SG compartment. When a break in SG1 was postulated, it was determined that most of the break effluent would be directed upward toward the large upper dome. Because of the large openings connecting SG1 to SG4, the venting to the dome would occur through both SG compartments. Effluents venting into lower-level compartments (surrounding the two SGs) by way of open access doorways would flow at much lower rates than the upward flows to the dome. The nodalization of the two SG compartments is shown in Figure IX-6, where the break was postulated to occur in Volume V12. Break effluents that are typical of three break sizes were assumed: large-break (LB) LOCA, medium-break (MB) LOCA, and small-break (SB) LOCA. The results of the MELCOR simulations are summarized in Table IX-5, where the distributions from a particular control volume are shown by the connecting junction. For example, given an LB LOCA scenario, ~80% of the flow from Volume V12, where the break was postulated, went upward through Junction J12, with the remainder going downward through Junction J11. Note that the flow splits were somewhat transient and that the results in Table IX-5 are reasonable approximations of the transients over the time where most debris transport would occur. LB LOCA and MB LOCA flows were reasonably steady over the transport period, but SB LOCA flows were not steady because of transition into natural circulation after ~6 s.

Inertial debris deposition is dependent on the flow velocities transporting the debris. The MELCOR calculations predicted transient flow velocities for each flow junction and each size of break. The general ranges of these velocities are provided in Table IX-6. The velocities are in the general range as the test velocities for which the debris-capture data were measured in the DDTS.

Table IX-5. Break Effluent Flow Splits

Break Size	Flows Exiting Volume V_i through Junction J_j								
	V12		V11		V41		V13		
	J11	J12	J21	J22	J23	J41	J13	J31	J32
LB LOCA	20%	80%	70%	30%	5%	95%	62%	33%	5%
MB LOCA	20%	80%	70%	30%	14%	86%	62%	33%	5%
SB LOCA	15%	85%	80%	20%	30%	70%	66%	28%	6%

Table IX-6. Characteristic Velocities in SG1

Postulated Break Size	Characteristic Velocities	
	m/s	ft/s
LB LOCA	25–200	80–660
MB LOCA	5–45	15–150
SB LOCA	1–8	5–25

VI.4.1.1.1.2 Debris-Transport Distributions from Volumes

The very fine debris would transport more like an aerosol in that the particles would disperse within the flow and follow the flow. Portions of this debris would be deposited onto structures along the transport pathways, primarily because of inertial deposition at bends in the flow. However, with larger debris, the tendency would be greater for the debris not to follow the flow through sharp bends in the flow and larger debris would more likely be trapped by a structure such as a grating. In addition, gravitational settling as the flow velocities slow would be more effective for larger debris than smaller debris. For example, following an LB LOCA in an SG compartment, a large, nearly intact insulation pillow could travel upward with the main flow to the containment dome unless an obstacle, such as a grating, impeded that pillow. However, this pillow would be much less likely to follow the flow through a connecting doorway to the next SG compartment.

Assumptions based on engineering judgments that were tempered by experimental observations were required to reach a solution. The assumptions provide a reasonable crude approximation of debris transport from a volume when there is a split in the flow. These assumptions are the following.

- The fine and small fibrous debris would be well dispersed within the flow and would transport uniformly with the flow; therefore, the debris-transport junction distributions for fines and small debris are the same as the junction flow distributions in Table IX-5.

- Large and intact debris would not make the turn to exit SG1 at Level 832 (Junctions J31 and J32). In addition to the turn, most of this debris that was moving toward these exits would be stopped by the gratings that cover ~45% of the cross-sectional area of the compartment that is nearest those exits.

- Large and intact debris entering SG4 at the floor level (Level 812) would be much less likely to follow the flow through the 90° bend and subsequently transport upward through SG4. Debris entering Volume V41 that is not captured in Volume V41 would exit by

either Junction V23 or V41. For large and intact debris, the flow fractions for Junction V41 were reduced by one-half and two-thirds, respectively (engineering judgment).

Applying these assumptions to the transport of the large and intact debris through the node junctions resulted in the junction transport distributions that are shown in Table IX-7 and Table IX-8.

Table IX-7. Large-Debris-Transport Junction Distributions

Break	V12		V11		V41		V13		
	J11	J12	J21	J22	J23	J41	J13	J31	J32
LB LOCA	20%	80%	70%	30%	52%	48%	100%	0%	0%
MB LOCA	20%	80%	70%	30%	57%	43%	100%	0%	0%
SB LOCA	15%	85%	80%	20%	65%	35%	100%	0%	0%

Table IX-8. Intact-Debris-Transport Junction Distributions

Break	V12		V11		V41		V13		
	J11	J12	J21	J22	J23	J41	J13	J31	J32
LB LOCA	20%	80%	70%	30%	68%	32%	100%	0%	0%
MB LOCA	20%	80%	70%	30%	71%	29%	100%	0%	0%
SB LOCA	15%	85%	80%	20%	77%	23%	100%	0%	0%

VI.4.1.1.1.3 Capture Fractions at Junctions

Debris-transport data from the Army Research Laboratory (ARL) and the CEESI tests that were conducted to support the DDTS [NUREG/CR-6369-2, 1999] provide average capture fractions for LDFG debris that is passing though typical gratings and around typical structures, such as piping and beams, and for debris making a 90° bend. These structures and the bend were wetted during the tests; the data do not apply to dry structures. These data are assumed to apply in general to the volunteer-plant containments because it is expected that the containment surface would be wetted rapidly by steam condensation,* as well as liquid break effluent, and because the range of predicted flow velocities (Table IX-6) are in general agreement with the flow velocities of the tests. The flow velocities ranged from 25 to 150 ft/s for the ARL tests and from 35 to 60 ft/s for the CEESI tests. The debris capture was most applicable to MB LOCAs and perhaps least applicable to SB LOCAs.

Fine and small fibrous debris could be captured inertially onto wetted surfaces whenever the break flow changed direction, such as flows through the doorways from the SG compartments into the sump-level annular space. These flows must make at least one 90° bend through those entrances. Debris-transport experiments that were conducted at CEESI demonstrated an average capture fraction of 17% for fine and small debris that were making a 90° bend. These surfaces would be wetted because of steam condensation and the liquid portion of the break effluence. Other flow bends likely would occur within the violent three-dimensional flows near the break. The platform gratings within the SG compartments would capture substantial amounts of debris, even though the gratings do not extend across the entire compartment. The

*Based on analyses performed for the DDTS [NUREG/CR-6369-3, 1999].

CEESI debris-transport tests demonstrated that an average of 28% of the fine and small LDFG debris was captured when the airflow passed through the first wetted grating encountered and that an average of 24% was captured at the second grating. The large and intact debris, by definition, would be trapped completely by a grating. In addition, equipment (such as beams and pipes) was shown to capture fine and small debris. In the CEESI tests, the structural maze in the test section captured an average of 9% of the debris passing through the maze.

Grating Capture: In the volunteer plant, partial gratings exist at three levels in each of the SG compartments. The gratings extend out over ~22%, 45%, and 15% of the SG cross-sectional area at plant elevations 824, 841, and 905 ft, respectively.* If it is assumed that 28% of small and fine fibrous debris and 100% of the large and intact debris are captured from the flow by a grating as the flow passes through the grating, the capture fractions for model junctions that contain a grating are provided in Table IX-9.

Table IX-9. Grating Capture Fractions at Model Junctions

Grating Level	Model Junctions	Fine and Small Debris		Large and Intact Debris	
		Unit Area Capture Fraction	Junction Capture Fraction	Unit Area Capture Fraction	Junction Capture Fraction
Level 905	J14 and J44	0.28	0.04	1.0	0.15
Level 841	J12 and J42	0.28	0.13	1.0	0.45
Level 824	J11 and J 41	0.28	0.06	1.0	0.22

Doorway Capture: Depressurization flows also would exit the SGs by way of the SG access doorways at Levels 808 and 832. Flows traveling through these pathways would carry debris directly into the lower levels of the containment; in fact, some of the debris likely would be deposited near the recirculation sumps. Because these doorways were designed with at least one 90° bend, debris would be deposited inertially onto wetted surfaces at each bend in the flow. Furthermore, because the CSs would not impact these vertical surfaces, the debris likely would remain on the surfaces once it was captured there. The CEESI data showed an average of 17% debris capture at its 90° bend for debris that was small enough to already have passed through a grating (i.e., fines and small debris). It was assumed that 17% of fine and small debris that was transported from the SG break region through the Level 808 and Level 832 doorways to the bulk containment would be captured at a bend (one bend assumed). No comparable data exist for the large and intact debris; however, the larger debris would be much less likely to stick to a wall once it impacted inertially against the wall. Because of a lack of appropriate data, it was assumed conservatively that no large or intact debris would be captured at these doorways.

*These fractions were estimated from plant drawings.

VI.4.1.1.1.4 Capture Fractions within Volumes

As illustrated in Figure IX-7, debris would be captured on structures within the model nodes, as well as the node junctions. As the break effluents flowed around and through the structural and equipment congestion within the SG compartment, debris would be driven inertially onto surfaces where some portion of it would remain captured. The structures include the pumps; SGs; and associated piping, beams, equipment stands, cabling, etc. The chaotic nature of the flows as the break jet is deflected off structures and wall surfaces could create a multitude of bends in the flow that could deposit debris inertially onto wall surfaces and irregular wall features. In the CEESI tests, ~9% of the fine and small debris was deposited onto wetted structures as the debris passed through a test structural assembly and 17% was captured onto a wetted surface at a sharp 90° bend in flow. Estimates of the amounts of debris captured within a node volume were based on this CEESI test data and on conservatively tempered engineering judgment. It is likely conservative to capture more debris within the SG than to transport the debris throughout the containment because washdown within the SG should be relatively greater than some other areas of the containment and because debris washed off the SG structures can go directly to the sump pool.

Applying a number of engineering judgments in conjunction with the CEESI data resulted in estimates for the capture of debris within each volume of the break-region debris-transport model. These estimates, along with the associated assumptions, are provided in Table IX-10.

Table IX-10. Fractions of Debris Captured within Each Volume

SG1					**SG4**			
Volume	**Fines and Small Pieces**	**Large Pieces**	**Intact Pieces**		**Volume**	**Fines and Small Pieces**	**Large Pieces**	**Intact Pieces**
V14	1% (A)	2% (A)	5% (A)		V44	1% (A)	2% (A)	5% (A)
V13	1% (A)	2% (A)	5% (A)		V43	1% (A)	2% (A)	5% (A)
V12	14% (C)	30% (E)	50% (F)		V42	9% (B)	15% (E)	30% (G)
V11	26% (D)	40% (E)	80% (H)		V41	14% (C)	25% (E)	80% (H)

Assumptions
A. Volumes contain minimal structures and no significant flow bends; therefore, a minimal amount of capture occurs. It is somewhat more likely that large debris would be captured than small debris and more likely that intact debris would be captured than large debris.
B. Structures are equivalent to one CEESI structural test assembly (9%), and no significant flow bends exist.
C. Structures are equivalent to one CEESI structural test assembly (9%), and significant flow bending that is less than a sharp 90° bend exists (5%).
D. Structures are equivalent to one CEESI structural test assembly (9%), and significant flow bending that is equivalent to a sharp 90° bend exists (17%).
E. Large debris is more likely to be captured than small debris, and 50% more large debris is captured than small debris.
F. Intact debris is much more likely to snag on equipment than the large debris. In addition, some insulation within the ZOI likely could remain attached to piping.
G. Intact debris is much more likely to snag on equipment than the large debris.

H. The congestion of equipment and cables near the floor is expected to trap most of the intact debris as the flow makes a 90° bend near the floor. Intact debris is less likely to follow the distribution of flow than is smaller debris.

VI.4.1.1.1.5 Break-Region Debris-Transport Quantification

The logic chart shown in Figure IX-7 and discussed in Section VI.3.3.1 was used to quantify the various flow splits and capture and to estimate the debris deposition within and from SG1. These charts divide the evaluation into many smaller problems that are amenable to resolution—an approach that was adapted from the resolution of the BWR strainer-blockage issue [NUREG/CR-6369-1, 1999]. This chart tracks the progress either of small debris from the pipe break (Volume V12) until the debris is assumed to be captured or until the debris is transported beyond the compartment. Charts were quantified for each of the three LOCA sizes (i.e., small, medium, and large) and for three classifications of fibrous debris (i.e., fines and small pieces, large pieces, and intact pieces). Note that there was no basis to treat the fines and small pieces differently. The data that were used to quantify the charts are discussed in Sections VI.4.1.1.1.1 through VI.4.1.1.1.4. As an example, the chart for the transport of fines and small debris following an LB LOCA is shown in Figure IX-9.

The overall results of the break-region quantification are shown in Table IX-11. The results for the three break sizes were averaged into a single set of results. This was done because the differences among the three size groups were substantially less than the substantial uncertainties associated with these analyses. The charts also provided information regarding the distribution of debris captured with the SGs, as well as the debris driven from the SGs.

Table IX-11. Distribution of Debris Captured and Exiting Break Region

Location	Debris Category		
	Fines and Small Pieces	Large Pieces	Intact Pieces
Captured within SGs 1 and 4	0.36	0.70	0.82
Expelled to Dome	0.58	0.26	0.17
Expelled to Level 832	0.03	0	0
Expelled to Level 808	0.03	0.04	0.01

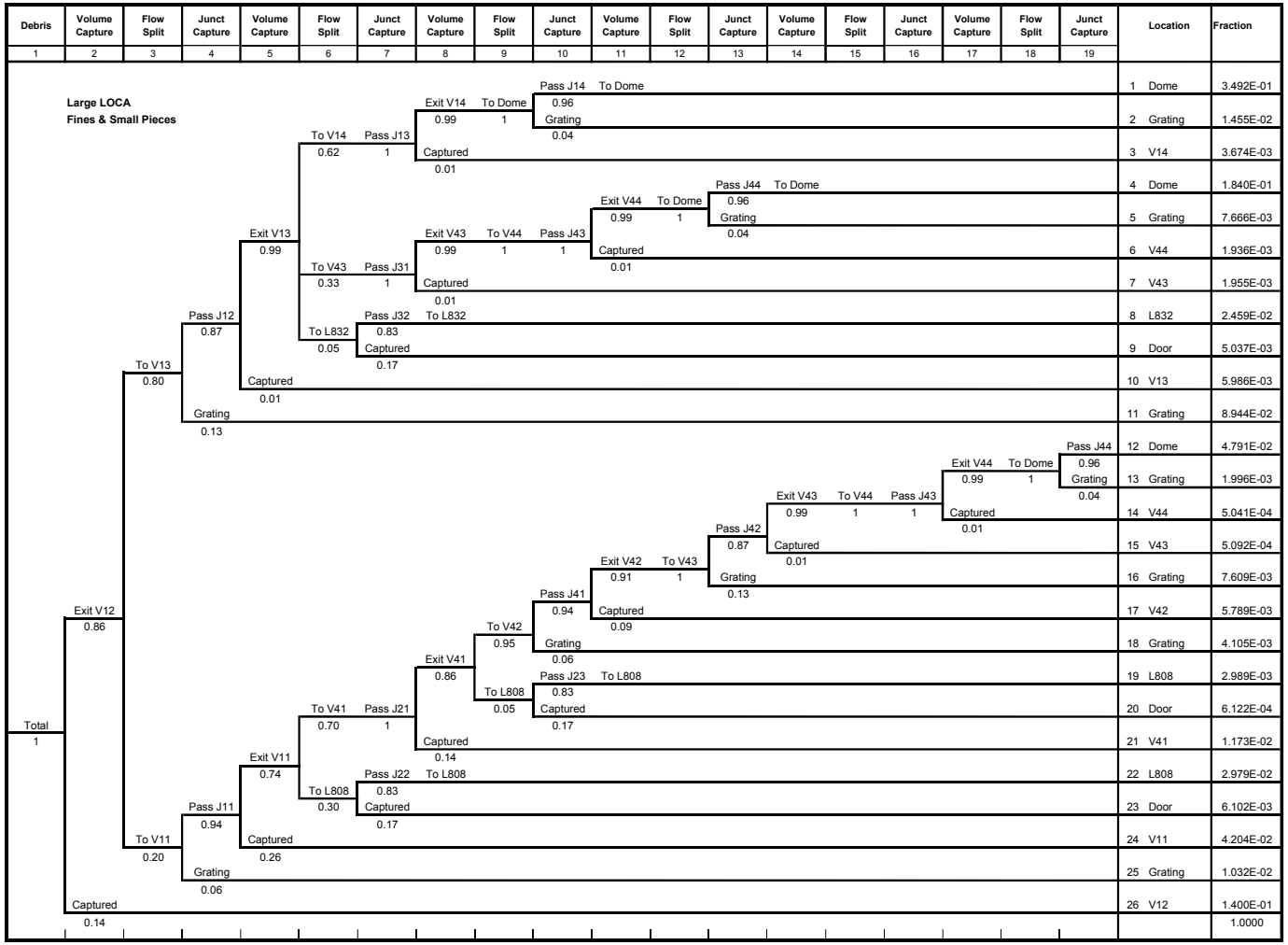

Figure IX-9. Break-Region LB LOCA Transport Chart for Fines and Small Debris.

VI.4.1.1.2 Dispersion throughout Remainder of Containment

The debris dispersion model that was presented in Section VI.3.3.2 was used to evaluate debris transport within the volunteer-plant containments by estimating dispersion throughout the containment first by free volume and then by surface orientation within a volume region.

VI.4.1.1.2.1 Dispersion by Volume Region

The containment free volume was subdivided into volume regions that were based on geometry, such as floor levels and walls, and on the location of CSs. Specifically, areas where deposited debris likely would not be washed down by the CSs were separated from areas that were impacted by the sprays. The volunteer-plant free volume was subdivided into 24 distinct regions of free volume, as shown in Table IX-12. The volumes of each region were estimated from plant drawings.

Table IX-12. Subdivision of Containment Free Volume

No.	Volume Region	Volume (ft^3)	Volume Fraction Vc_j
1	SG1&4	76600	0.02570
2	Dome - Above 905.75-ft	1992060	0.66848
3	L873 - MS	39300	0.01319
4	Head Lay-Down - L871.5	17120	0.00574
5	Below Head Platform	5750	0.00193
6	Refueling A	45340	0.01521
7	Refueling B	53860	0.01807
8	Refueling C	48660	0.01633
9	Refueling D	47960	0.01609
10	SG2&3	76600	0.02570
11	Pressurizer	11250	0.00378
12	L860 Annulus - Section 1	34100	0.01144
13	L860 Annulus - Section 2	54580	0.01832
14	L860 Annulus - Section 3	94310	0.03165
15	L851 - FW	25800	0.00866
16	Accumulator Section	31500	0.01057
17	L832 Annulus - Section 1	37250	0.01250
18	L832 Annulus - Section 2	33940	0.01139
19	L832 Annulus - Section 3	69890	0.02345
20	L808 Annulus - Section 1	61650	0.02069
21	L808 Annulus - Section 2	30830	0.01035
22	L808 Annulus - Section 3	61650	0.02069
23	Reactor Cavity	25000	0.00839
24	Equipment Room L808	5000	0.00168
	Containment Total	2980000	1.00000

Key aspects of the region subdivision follow. The first region, designated SG1 and 4, is the SG compartment 1 where the break was postulated and its connected neighboring SG compartment, SG4. Debris dispersion and deposition in these SG compartments was predicted

in Section VI.4.1.1.1. The second region represents the free volume above the highest floor (i.e., the dome region), which is approximately two-thirds of the entire containment free volume. As shown in Figure IX-10, the lower floor levels were subdivided azimuthally into three sectors to better distinguish the areas with CSs from areas without the sprays. The refueling pool area was subdivided into four regions to reflect the three different pools and the reactor-vessel (RV) head area [i.e., (A) storage pool for RV upper internals, (B) RV area, (C) storage pool for RV lower internals, and (D) pool for fuel transfer and storage].

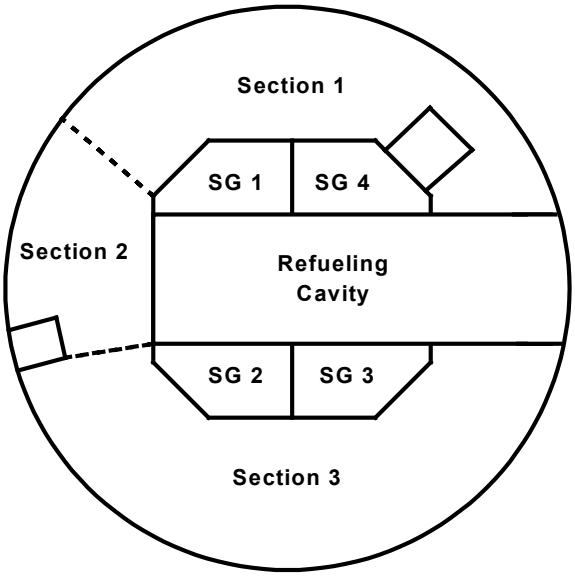

Figure IX-10. Volume Region Sector Model

Debris, particularly the larger debris, would not distribute uniformly throughout the free volume. The methodology presented in Section VI.3.3.2.1 applies weighting factors ($wc_{i,j}$) to the free-volume distribution to estimate the distribution of debris throughout the containment (i.e., the distribution of the debris among the 24 volume regions) by debris type. The very fine debris likely would transport somewhat uniformly with the depressurization flows, which would penetrate all free space within the containment as the containment pressurized. The transient nature of debris generation would also introduce nonuniformities into the dispersion of the fine debris. Because no rationale was found to weight the distribution of the fine and small debris away from that of a uniform free-volume distribution outside the break region, all weighting factors were assumed to be one for fine and small fibrous debris.

For the largest debris, specifically the large-piece and intact-piece classifications, the debris that is ejected from the SG compartments into the dome region likely would fall back to the floors and structures of the higher levels. The settling of debris that was ejected into the dome atmosphere was proportioned onto the upper floors according to the distribution of floor area (e.g., the cross-sectional area of a SG compartment divided by the cross-sectional area of the overall containment determined the fraction of settling debris that would fall into that compartment). The largest debris likely would not enter lower compartment volumes, except for debris ejected into the sump-level annulus via personnel access doorways. The assumed weighting factors for the large and intact debris were specified to preference the deposition of larger debris onto the uppermost floors and into the sump-level annulus. The large-piece debris

was assumed to transport somewhat more easily than the intact-piece debris. The assumed weighting factors and the dome fallout fractions are shown in Table IX-13.

Table IX-13. Volume Region Weighting Factors

No.	Volume Region	Dome Fallout Fraction T_j	Volume Weighting Factors			
			Fines $wc_{1,j}$	Small Pieces $wc_{2,j}$	Large Pieces $wc_{3,j}$	Intact Pieces $wc_{4,j}$
1	SG1&4	0.0951	1	1	1	1
2	Dome - Above 905.75-ft	0	1	1	1	1
3	L873 - MS	0.0555	1	1	0.5	0.3
4	Head Lay-Down - L871.5	0.0349	1	1	0.8	0.5
5	Below Head Platform	0	1	1	0.3	0
6	Refueling A	0.0495	1	1	0.8	0.5
7	Refueling B	0.0579	1	1	0.8	0.5
8	Refueling C	0.0505	1	1	0.8	0.5
9	Refueling D	0.0596	1	1	0.8	0.5
10	SG2&3	0.0978	1	1	0.5	0.3
11	Pressurizer	0	1	1	0	0
12	L860 Annulus - Section 1	0.0092	1	1	0.3	0
13	L860 Annulus - Section 2	0.0052	1	1	0.3	0
14	L860 Annulus - Section 3	0.0241	1	1	0.3	0
15	L851 - FW	0	1	1	0	0
16	Accumulator Section	0.0060	1	1	0.8	0.5
17	L832 Annulus - Section 1	0	1	1	0	0
18	L832 Annulus - Section 2	0	1	1	0	0
19	L832 Annulus - Section 3	0	1	1	0	0
20	L808 Annulus - Section 1	0	1	1	1	1
21	L808 Annulus - Section 2	0	1	1	1	1
22	L808 Annulus - Section 3	0	1	1	0.3	0
23	Reactor Cavity	0	1	1	0	0
24	Equipment Room L808	0	1	1	0	0
	Total	0.5453				

The results of the blowdown distribution by groups of volume regions are illustrated in Figure IX-11. In this estimate, the largest portion of the debris was deposited inside the SG compartments, where the break was postulated because of inertial deposition that occurred as the fast-moving flows drove the debris into and through equipment and structures. This was particularly true for the larger debris, which could not pass through the gratings. The upper-level floors (871-, 873-, and 905-ft levels) received substantial debris falling or settling out of the dome atmosphere. The regions above the refueling pools received debris that was driven into those volumes, as well as debris falling or settling from the dome atmosphere; this comment also applies to the opposite SG compartments, SGs 2 and 3. The pressurizer compartment received only small amounts of fine and small debris and no larger debris because the compartment has a roof that prevents debris from falling into the compartment and is relatively small. The lower levels receive relatively small quantities of mostly large-piece debris because

of their remoteness from the dome. Most of the debris entering Levels 832 and 808 was debris that was expelled from the SG compartments by way of the personnel access doorways; therefore, this debris would likely be located near those doors.

CSs would impact most of the deposited debris; these surface areas include the four SG compartments, the upper floor surfaces, and the refueling area. Regions that were not impacted by the sprays included the pressurizer compartment and certain portions of the lower levels. This observation suggests that a large fraction of the more transportable debris would transport to the sump pool.

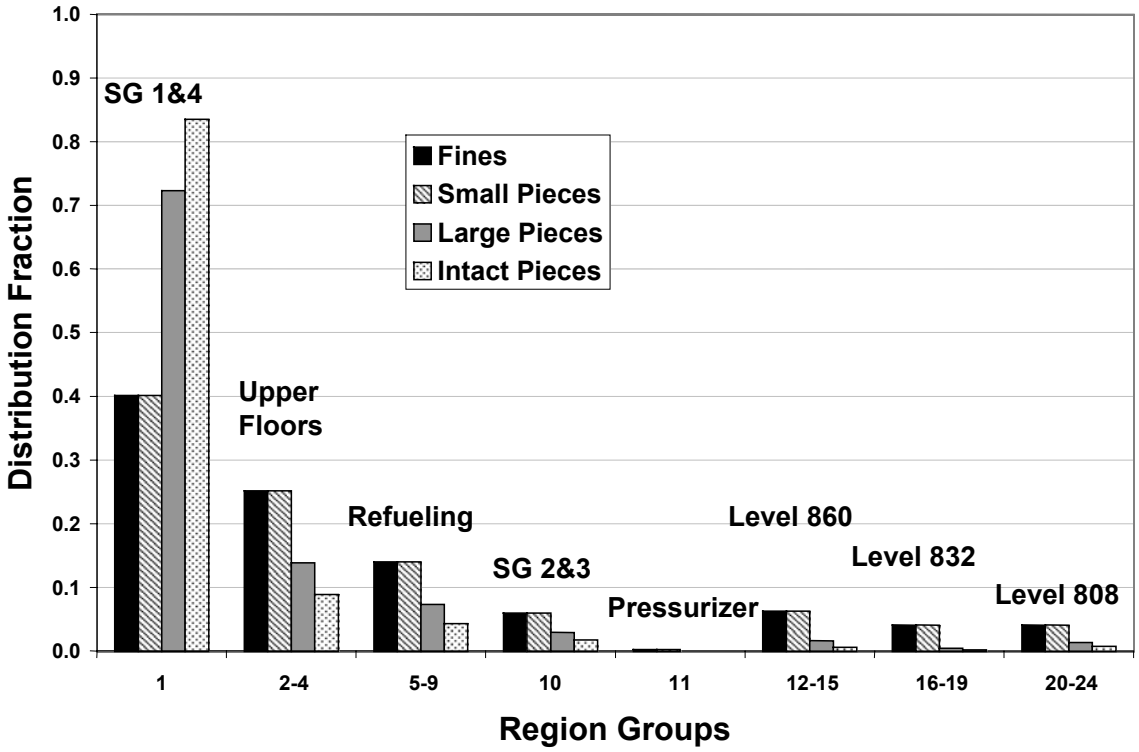

Figure IX-11. Blowdown Distribution by Region Groups.

VI.4.1.1.2.2 Dispersion by Surface Orientation and Surface Wetness

Once the debris dispersion prediction placed each type of debris within the 24 volume regions, the debris was dispersed further by surface area classification, i.e., orientation and exposure to moisture. The surface orientation was either “floor area“ or “other“ area; the distinction was that gravitational settling preferentially deposited debris onto the floor. The surface exposure to moisture included surfaces that were impacted directly by the CSs, surfaces subjected to spray drainage but not sprayed directly, and the remaining surfaces, which would be wetted by condensation. In this manner, the surface area within each volume region was subdivided into six surface groupings. This subdivision was based on both engineering drawings and engineering judgment. The drawings provided basic geometric information such as floor areas;

however, engineering judgment, in addition to drawings, was required to estimate fractions of surfaces that were sprayed directly or covered by spray drainage. The estimated area distribution fractions are shown in Table IX-14.

The floor fraction is an estimate of the total surface area that would receive gravitationally settling debris. This estimate includes upward-facing equipment, as well as the floor (the equipment and piping was assumed to have the same floor fraction as the wall, floor, and ceiling surfaces). The condensate, spray, and drainage fractions represent the fraction of each orientation with this type of exposure. With these fractions, the surface areas and area ratios (i.e., $A_{j,k,l}$ and $g_{j,k,l}$) are determined. For example, the floor fraction for a given region multiplied by the spray $g_{j,k,l}$) are fractions for that region's floor multiplied by the total surface area of the region yields the floor surface area that was sprayed directly by the sprays.

Table IX-14. Regional Areas Fractions

No.	Volume Region	Floor Fraction	Floor Surface Area			Other Surface Area		
			Condensate Fraction	Spray Fraction	Drainage Fraction	Condensate Fraction	Spray Fraction	Drainage Fraction
1	SG1&4	0.07	0	1	0	0.1	0.5	0.4
2	Dome - Above 905.75-ft	0.09	0	1	0	0	1	0
3	L873 - MS	0.17	0.2	0.6	0.2	0.9	0.1	0
4	Head Lay-Down - L871.5	0.61	0	1	0	0	0	1
5	Below Head Platform	0.30	0.6	0.1	0.3	0	0	1
6	Refueling A	0.37	0	1	0	0	0	1
7	Refueling B	0.41	0	1	0	0	0	1
8	Refueling C	0.55	0	1	0	0	0	1
9	Refueling D	0.68	0	1	0	0	0	1
10	SG2&3	0.07	0	1	0	0.1	0.5	0.4
11	Pressurizer	0.04	1	0	0	1	0	0
12	L860 Annulus - Section 1	0.10	0.9	0.1	0	1	0	0
13	L860 Annulus - Section 2	0.19	0.1	0.6	0.3	0.6	0.1	0.3
14	L860 Annulus - Section 3	0.19	0.1	0.6	0.3	0.6	0.1	0.3
15	L851 - FW	0.19	0.8	0	0.2	1	0	0
16	Accumulator Section	0.13	0	0.5	0.5	0.5	0	0.5
17	L832 Annulus - Section 1	0.18	0.9	0	0.1	0.7	0	0.3
18	L832 Annulus - Section 2	0.15	0.4	0	0.6	0.6	0	0.4
19	L832 Annulus - Section 3	0.17	0.3	0.5	0.2	0.6	0	0.4
20	L808 Annulus - Section 1	0.18	0	0	1	0.7	0.3	0
21	L808 Annulus - Section 2	0.18	0	0	1	0.7	0.3	0
22	L808 Annulus - Section 3	0.19	0	0	1	0.7	0.3	0
23	Reactor Cavity	0.13	0	0	1	1	0	0
24	Equipment Room L808	0.21	0	0	1	1	0	0

Next, the area weighting factors ($w_{i,j,k,l}$) were estimated, which preference debris toward one surface over another. The dominant preferential debris deposition (and the only preference that can be estimated realistically) is gravitational debris that settles to the floor surfaces. The weighting factors for the non-floor surfaces ($k = 2$) were set first to 1 (i.e, $w_{i,j,2,l} = 1$), and then the weighting factors for the floor surfaces within each volume region were estimated for each debris type such that the weighting factors preferentially forced debris deposition onto the floor surfaces. The floor weighting factor estimates used the following equation, where the weighting factor is a function of two physical variables that can be estimated more readily. These variables are the fraction of the surface area that is floor area (a geometric determination) and the fraction

of the debris that is deposited onto the floor (an engineering judgment and computational determination):

$$w_{floor} = \left(\frac{d_{floor}}{1-d_{floor}}\right)\left(\frac{1-g_{floor}}{g_{floor}}\right) \quad ,$$

where

w_{floor} = the weighting factor for debris deposited onto the floor inside a volume;

d_{floor} = the fraction of the debris deposited within a volume that was on the floor; and

g_{floor} = the fraction of the volume surface area that is floor area.

The determination of the floor-area fraction (g_{floor}) is a straightforward estimate of the floor area divided by the total surface area in a volume region (listed in Table IX-14). In actuality, the surface-area estimate includes the areas associated with equipment and piping because debris can settle onto equipment and piping, as well as onto floors. To reduce the complexity of the area estimates, it was assumed that the area fractions for the equipment and piping were the same as the area fractions for the wall, ceiling, and floor surfaces. Because of this assumption and other geometrical assumptions, these area fractions have an inherent uncertainty associated with the estimates; however, this uncertainty should be significantly smaller than some of the other transport uncertainties.

Debris deposition processes other than gravitational settling, such as diffusiophoresis (condensation-driven deposition), do not depend on surface orientation for these processes; the weighting factors all would be set to 1. Driven debris could be deposited inertially onto any surface or could snag on an obstacle. Heavy, inertially deposited debris subsequently may fall to the floor, but substantially smaller debris likely would remain pasted onto the surface. Even heavy debris can remain on a nonhorizontal surface if the piece were physically snagged. Vertically moving debris eventually would settle onto a surface that is sufficiently horizontal to retain the debris. The fraction of debris deposition onto the floor is highly dependent on the size of the debris.

The estimate of the fraction of the debris that was deposited onto the floor depended greatly on conservative judgments; therefore, the fraction introduced substantial uncertainty into the transport estimates. The engineering judgments accounted for the geometry of the region under consideration, including the relative structural congestion. It was conservative to place the debris on the floor as opposed to other surfaces because more of the debris that was deposited on the floor would be subjected to spray washdown on the floor than on other surfaces. For the SG compartments where the pipe break was postulated (SGs 1 and 4), debris deposition data from the logic charts were used to estimate debris on the floor of these compartments. This estimate included larger debris that was trapped on the underside of gratings and that would likely fall back once the depressurization flow subsided. It was assumed that debris that fell or settled from the dome atmosphere into lower-level regions would fall or settle onto a floor surface.

A typical judgment estimate for fractions of debris that had been driven into an enclosure and that would subsequently settle to the floor was 0.4, 0.7, 0.99, and 0.99 of the fines, small pieces, large pieces, and intact pieces, respectively. For fine debris, the floor deposition fraction was

two to three times the floor area fraction, thereby allowing a substantial settling of the very fine debris, even though diffusion processes would deposit the fine debris onto any surface. The floor fraction for small-piece debris was substantially higher than for the fine debris. Large and intact debris would fall to a horizontal surface unless it snagged on an obstacle. The floor fraction was set to 0.99 to place the large debris on the floor; however, some pieces could have snagged on an obstacle before reaching the floor.

For the far-side SG compartments (SGs 2 and 3) and the pressurizer compartment, the floor-debris deposition fractions acknowledged that the debris would have to travel downward in the compartment and through a variety of structures, including gratings, before reaching the floor; the fractions were reduced for these compartments. For instance, the gratings would catch much of the large debris before it could reach the floor. For open regions, such as the refueling pool regions, where a small amount of equipment and piping is located and the region is not enclosed completely by walls, the floor-debris fractions were increased substantially.

Once the weighting factors were estimated, the final deposition of the debris was determined both as a function of the region and by the surface orientation and its exposure to moisture. Figure IX-12 and Figure IX-13 illustrate the dispersion patterns in the containment according to surface orientation and surface wetness.

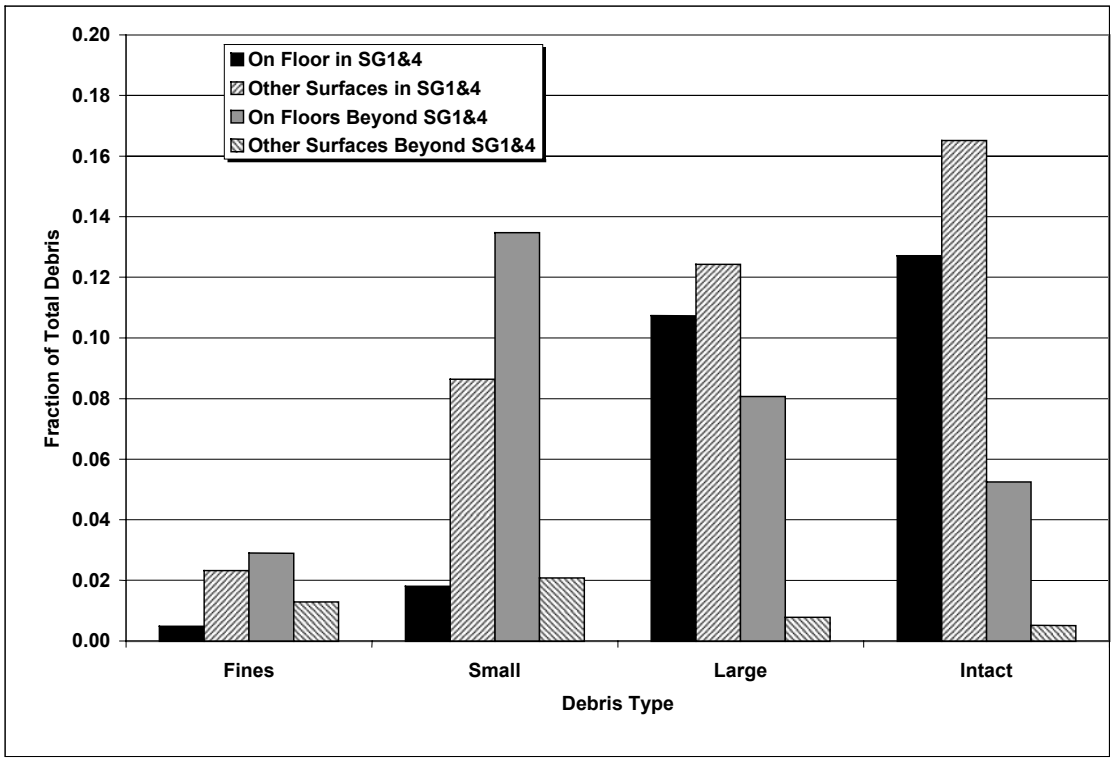

Figure IX-12. Blowdown Debris Dispersion by Surface Orientation.

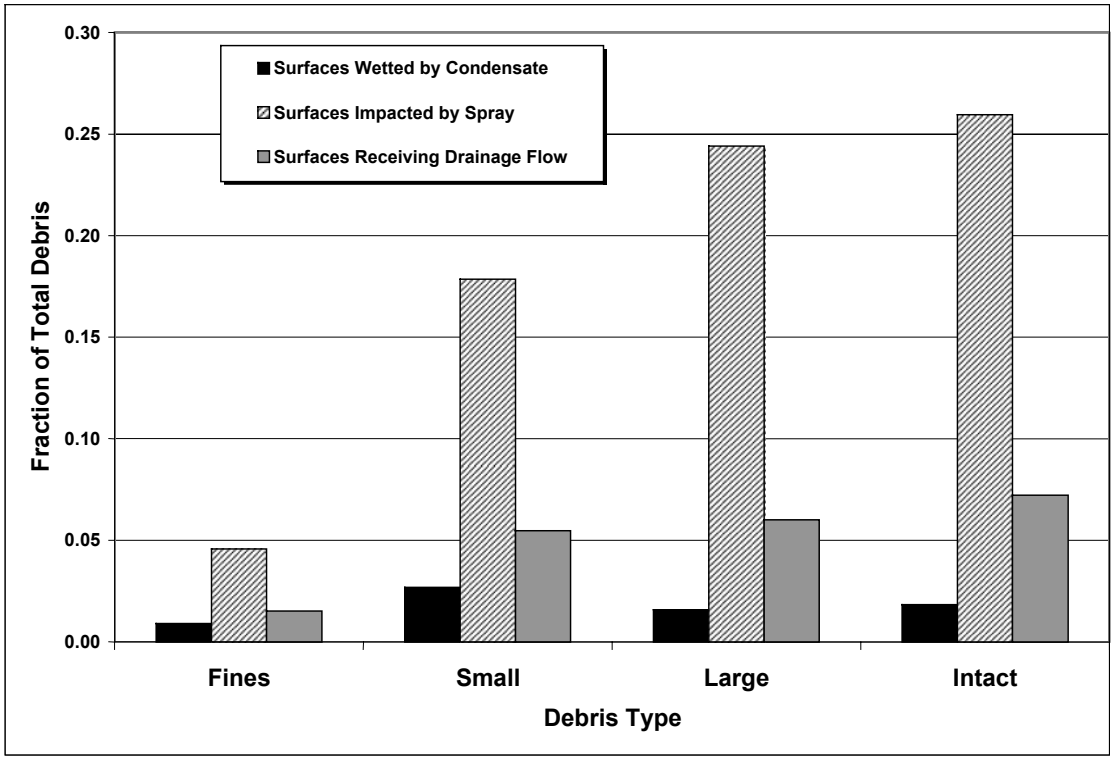

Figure IX-13. Blowdown Debris Dispersion by Surface Wetting.

In Figure IX-12, all of the LOCA-generated debris is distributed fractionally according to surface orientation (floor surfaces or other surfaces), whether the debris was captured within the break region (SGs 1 and 4), and debris type. This distribution reflects the debris-generation size distribution of Table IX-2 and the break-region capture fractions of Table IX-11. For the fines and small-piece debris, the largest fractions corresponded to floor surfaces outside or beyond the break region; debris preferentially settled onto the floors. Most of the debris that was captured within the break region was located on other structures that correspond to equipment, piping, and gratings within those SG compartments. For the larger debris, the majority of the debris was trapped within the break region by the congestion of structures. Nearly half of this debris either was deposited onto the floor of the break region or was assumed to fall to the floor after the break flows subsided. Most large debris that was ejected from the break region was predicted to fall out onto floor surfaces; therefore, small amounts of large debris were found on other structures outside of the break region.

In Figure IX-13, all of the LOCA-generated debris is distributed fractionally according to the surface wetting condition (condensate, sprayed, or spray drainage) and by debris type. Only relatively small quantities of debris were predicted to reside at locations where the debris would not be washed downward by the CSs or by the spray drainage. Conservatively speaking, the sprays falling from the upper dome would wash a majority of the surfaces within the SG compartments, as well as all of the upper floor surfaces and the refueling pool areas.

Although there is a relatively high degree of uncertainty with these blowdown transport results, the trends generally make sense. Because so little debris is protected from the CSs, these trends indicate a relatively high transport of debris to the sump pool.

VI.4.1.2 Fibrous Washdown Debris Transport

The CSs and condensation of steam throughout the containment and subsequent drainage to the sump pool would entrain substantial debris that was deposited onto the various surfaces and would transport the debris to the sump pool. In addition, these processes would degrade the fibrous insulation debris to some extent further, thereby creating more of the very fine, readily transportable debris.

VI.4.1.2.1 Surface Retention of Deposited Debris

The fraction of debris that stays on a specific surface, as opposed to being washed away, is referred to as the retention fraction. The fraction transported from a specific surface would then be 1 minus the retention fraction. Estimates of the retention fractions were essentially engineering judgments that were based on experience with small-scale testing during the DDTS. These experiments did not examine specifically the flow requirement needed to remove a piece of debris from a specified type of surface. Most of these tests dealt with either debris generation or airborne debris transport. One set of tests examined the erosion that was associated with fibrous debris inundated by water flow. During the conduct of these tests, experience with the handling of the debris provided some understanding regarding the ease or difficulty of forcing a piece of debris to move. These findings are summarized in Table IX-15. The estimated transport and corresponding retention fractions are shown in Table IX-16 and Table IX-17, respectively.

Debris transport due to condensate drainage would be expected to affect only the smaller debris. As condensation builds on a surface, it forms a thin film that subsequently drains and typically forms small rivulets of flow. This flow usually would move around significantly sized pieces of debris. Individual fibers could be entrained in the flow, or the fiber simply could be pushed to the sides of the rivulets. Some fine and small-piece debris certainly would transport, but the quantities of small debris transporting were estimated to be a small portion of the total. The DDTS's central estimate (realistic yet conservative) assumed that 1% of small debris transported (the extreme upper bound was 10%) but no large debris. The DDTS did not separate fines from small pieces. For this estimate, increasing the 1% to 2% for small-piece debris and increasing the 1% to 5% for the fines increased the level of conservatism. The larger debris was assumed not to transport because of condensate runoff.

Table IX-15. Fibrous-Debris Washdown Transport Trends

Debris Type	Surfaces Wetted by Condensate	Surfaces Either Sprayed or Receiving Drainage Flow	
		Without Intervening Floor Drains	With Intervening Floor Drains
Fines	Minority Transport	Nearly Complete Transport	
Small Pieces	Minority Transport	Majority Transport	
Large Pieces	No Significant Transport	Medium Transport	No Significant Transport
Intact Pieces	No Significant Transport	Minority Transport	No Significant Transport

Table IX-16. Estimated Fibrous-Debris Washdown Transport Percentages

Debris Type	Surfaces Wetted by Condensate	Surfaces Either Sprayed or Receiving Drainage Flow	
		Without Intervening Floor Drains	With Intervening Floor Drains
Fines	5%	99%	
Small Pieces	2%	70%	
Large Pieces	0%	50%	0%
Intact Pieces	0%	20%	0%

Table IX-17. Estimated Fibrous-Debris Washdown Retention Fractions

Debris Type	Surfaces Wetted by Condensate	Surfaces Either Sprayed or Receiving Drainage Flow	
		Without Intervening Floor Drains	With Intervening Floor Drains
Fines	0.95	0.01	
Small Pieces	0.98	0.3	
Large Pieces	1	0.5	1
Intact Pieces	1	0.8	1

Whenever fine and small-piece debris would be subjected to the substantial flows of the impacting CSs or the subsequent drainage of the sprays, the flow likely would entrain nearly all of the fine debris and a majority of the small debris. Test experience indicates that the CSs would wash fines from surfaces easily and carry those fines with the drainage to the sump pool. However, some of this fine debris would be pushed into relatively protected spots, corners, crevices, etc., where the debris would remain. Surfaces that were impacted directly by sprays and drained surfaces were grouped together for washdown transport because of the lack of information that was required to treat these two surface types differently. It was assumed that 99% of the fines would be transported from surfaces that were impacted by the sprays or drainage and that the other 1% experienced something less than total transport.

CSs also would wash substantial small-piece debris off structures, walls, and floors. The DDTS's central estimate was 50% (realistic yet conservative), with an extreme upper bound of 100%. Substantial quantities of debris likely would become trapped at locations that were protected from full spray flow due to the complex arrangements of containment equipment, piping, etc. It was assumed that 70% of the small debris would transport from surfaces that were impacted directly either by the CSs or by the subsequent drainage. This assumption adds additional conservatism to the DDTS's central estimate without becoming excessively conservative.

The 70% estimate was supported further by a simple floor-water drainage calculation, in which a uniform spray was applied to a floor area at a rate of flow corresponding to the containment-dome spray Trains A and B. A floor-area estimate indicates that ~800 ft^2 would be drained by each floor drain. A plant calculation estimated that the floor-water hold-up depth would be ~1.5 in. The separate-effect characterization of debris transport in water tests [NUREG/CR-6772, 2002] shows that a turbulent flow velocity as low as ~0.06 ft/s can cause a small piece of debris to tumble or slide along the floor. If circular drainage geometry is assumed, the transport estimate indicates that 30% to 40% of the floor area would not have sufficient flow velocity to

transport small-piece debris. This calculation did not consider the effect of structures on the transport, which would create locations for debris entrapment. Therefore, the 70% estimate is a reasonable number for small-debris transport by the CSs.

For the large and intact pieces of debris, the surfaces were split into two additional categories based on whether the transport of the debris would encounter floor drain holes that would prevent further transport. A typical floor drain is ~6 1/2 in. in diameter and has a coarse grating that would stop any debris that is larger than ~3 in. square. A few floor drains have a relatively fine mesh screen over the hole. Floor surfaces are sloped to channel water to the drains. Large debris deposited onto the upper floors likely would have to pass through more than one of these floor drains to reach the sump. Large debris settling into the refueling pools would also have to pass through drains to reach the sump, some of which have a screen cover. The two largest of the refueling drains are nominal 6-in. drains without any cover or grating and are open during normal operation. Although a piece of large debris could pass through this 6-in. drain, the amount of debris would not be enough to treat these drains separately. It was assumed that these drains would stop further transport of large and intact debris.

Conversely, large and intact debris that is deposited at locations such as the SG compartments would not encounter any drain holes as the debris transports toward the sump pool. CSs would wash substantial quantities of large-piece debris off structures, walls, and floors. A portion of the large debris would be trapped on top of gratings and would not transport. Other large pieces would snag onto structures such that the sprays would not dislodge them. Substantial quantities of debris likely would become trapped at locations that are protected from full spray flow due to the complexities of containment equipment, piping, etc. Because large debris would transport less easily than small debris, it was assumed that 50% of the large debris was transported. The intact debris would be less likely to transport than the large-piece debris. Based on DDTS experience, the intact pieces of debris were significantly more likely to snag on structures than the large pieces, and substantial quantities of intact debris were likely to remain attached to the original piping. It was assumed that 20% of the intact debris would transport.

VI.4.1.2.2 Erosion of Debris by CSs

Experiments conducted in support of the DDTS analysis illustrated that insulation debris could be eroded further by the flow of water. Some debris erosion could occur because of the impact of the sprays and spray drainage flows, but the amount of erosion would not be great. The DDTS concluded that <1% of the fibrous debris eroded as a result of CS operation. Debris erosion caused by condensation and condensate flow was neglected. Debris containing insulation that is still in its cover would not be expected to erode further. The erosion of debris caused by the plummeting of the break flow into the sump pool is considered as part of the sump-pool transport analysis.

It was assumed that condensate drainage would not cause further erosion of fibrous debris and that intact or covered debris would not erode further. Erosion does not apply to fine debris because the debris is already fine. It was assumed that 1% of the small- and large-piece debris that was impacted directly by the sprays would erode. It was assumed that intact pieces of debris could not erode because its canvas cover would protect the fibrous materials.

VI.4.1.3 Quantification of Fibrous-Debris Transport

The transport of fibrous debris was quantified using the models presented in Section VI.3 and the input presented in Section VI.4.1. The quantified transport results are presented in Table IX-18. The table shows the transport fractions for each size category, as well as the overall

transport fraction. It also shows the fractions of the total ZOI insulation that entered the pool, which were normalized to provide a size distribution for the debris entering the pool. About 57% of the ZOI fibrous insulation was predicted to transport to the sump pool, and nearly half of that would be the relatively transportable sizes. The transport fraction for the fines includes the erosion products from the predicted erosion of the small and large pieces of debris. The quantity of erosion products was approximately equal to 6% of the original generated fines.

Table IX-18. Fibrous-Debris-Transport Results

Debris Size Category	Category Generation Fraction	Size Category Transport Fraction	Fraction of ZOI Insulation	Distribution Entering Sump Pool
Fines	0.07	0.93	0.07	0.12
Small Pieces	0.26	0.66	0.17	0.30
Large Pieces	0.32	0.54	0.17	0.30
Intact Pieces	0.35	0.46	0.16	0.28
All Debris	1.00	0.57	0.57	1.00

VI.4.2 RMI Debris Transport

Roughly 85.7% of the insulation in the volunteer-plant containment is RMI. The debris-transport methodology discussed in Section VI.3 applies to RMI debris, as well as fibrous debris. Unfortunately, unlike the fibrous insulation, very little useful airborne transport data for RMI debris exist. Specifically, the capture fractions for the capture of RMI debris passing through structures such as gratings and of RMI debris inertially impacting surfaces have not been measured. Only secondary experience associated with RMI debris-generation experiments is applicable in this study. For RMI debris washdown, the pool transport velocities are available. Small-scale experiments suggest that RMI debris transports less easily than would the fibrous debris, primarily because the RMI debris is heavier. In addition, it would take substantially more RMI debris on the sump screen to block flow effectively through the screen than it would fibrous debris.

VI.4.2.1 RMI Blowdown Debris Transport

The capture fractions for RMI debris are likely much different from the corresponding fractions for fibrous debris. For fibrous debris, the capture fractions were very dependent on surface wetting; when the surfaces were dry, debris capture was minimal. For RMI, surface wetting may not be important. For instance, it seems likely that the capture of RMI on a grating depends on the foil folding over a bar in such a manner that it remains in place. Capture may depend on the debris remaining stuck on a structure. The amount of RMI debris that was captured by a grating could be significantly less than the amount of fibrous insulation; conversely, it could be substantially greater. Furthermore, the ability of flows to transport large cassette-like RMI debris is not known. Therefore, application of the Section VI.3 methodology required very conservative assumptions to compensate for the nearly complete lack of data.

VI.4.2.1.1 Break-Region Blowdown Debris Transport

It is conservative to overestimate the retention of debris within the SG compartments because subsequent debris washdown is more likely if the debris were in the SGs as opposed to being

dispersed throughout the containment. Because the capture rates for RMI debris passing through a grating have not been determined, it was conservatively assumed that 100% of all RMI debris impacting a grating was stopped by that grating from further forward transport. Debris stopped on the underside of a grating likely could fall back once depressurization flows subside. Because the gratings do not extend completely across the SG compartments, substantial debris still could be propelled upward into the containment dome.

Likewise, the inertial capture of RMI debris by miscellaneous structures—such as pipes, beams, or vessels—or by inertial impaction whenever the flow makes a sharp bend—has not been determined. For instance, it would seem less likely that a piece of RMI debris would stick to a wall than would a small piece of fibrous debris. The fibrous-debris capture fractions for miscellaneous structures and sharp bends were applied to the RMI debris to conservatively overpredict the retention of RMI debris within the SG compartments. Applying these assumptions to the logic charts, which are similar to Figure IX-7, results in the conservative SG capture fractions shown in Table IX-19. The values for 2- to 6-in. and the larger-than-6-in. debris categories in Table IX-19 correspond to the values for the fibrous large- and intact-category values (shown in Table IX-11): a result of similar assumptions. The assumption that the gratings capture all of the RMI debris, even the smallest pieces, predicts substantially more RMI retention within the SG compartments than likely would occur in reality. The predicted over-conservative retention was necessitated by the lack of RMI transport data.

Table IX-19. Fractional Distribution of Debris Captured and Exiting Break Region

Location	RMI Debris Category		
	<2-in. Pieces	2- to 6-in. Pieces	>6-in. Pieces
Captured within SGs 1 and 4	0.64	0.70	0.82
Expelled to Dome	0.32	0.26	0.17
Expelled to Level 832	0.01	0	0
Expelled to Level 808	0.03	0.04	0.01

VI.4.2.1.2 Dispersion Throughout the Remainder of Containment

The 24-region subdivision of the containment free volume that was used in the fibrous-debris-transport estimate (Table IX-12) also was used for the RMI debris-transport estimate. The volume weighting factors that were estimated for fibrous-debris transport (Table IX-13) also were applied to the RMI debris because no rationale was found to weight the distributions otherwise. For RMI debris, no fine debris was postulated (i.e., even the smaller pieces of RMI debris should sink readily in water, as opposed to fibrous fines, which tend to remain in suspension). The predicted dispersion of RMI debris was judged to place more debris into locations where it subsequently would be predicted to transport with the CS drainage to the sump pool. The results of the blowdown dispersion by groups of volume regions are illustrated in Figure IX-14. As modeled, a majority of the debris was retained in the break region (SGs 1 and 4). In reality, it is likely that much more of the smaller debris would be blown free of the break region and into the upper dome region, where subsequent washdown to the sump pool would be substantially less than it would be if the debris were kept within the break region. However, the lack of RMI debris-transport data necessitated the conservative assumptions leading to these results.

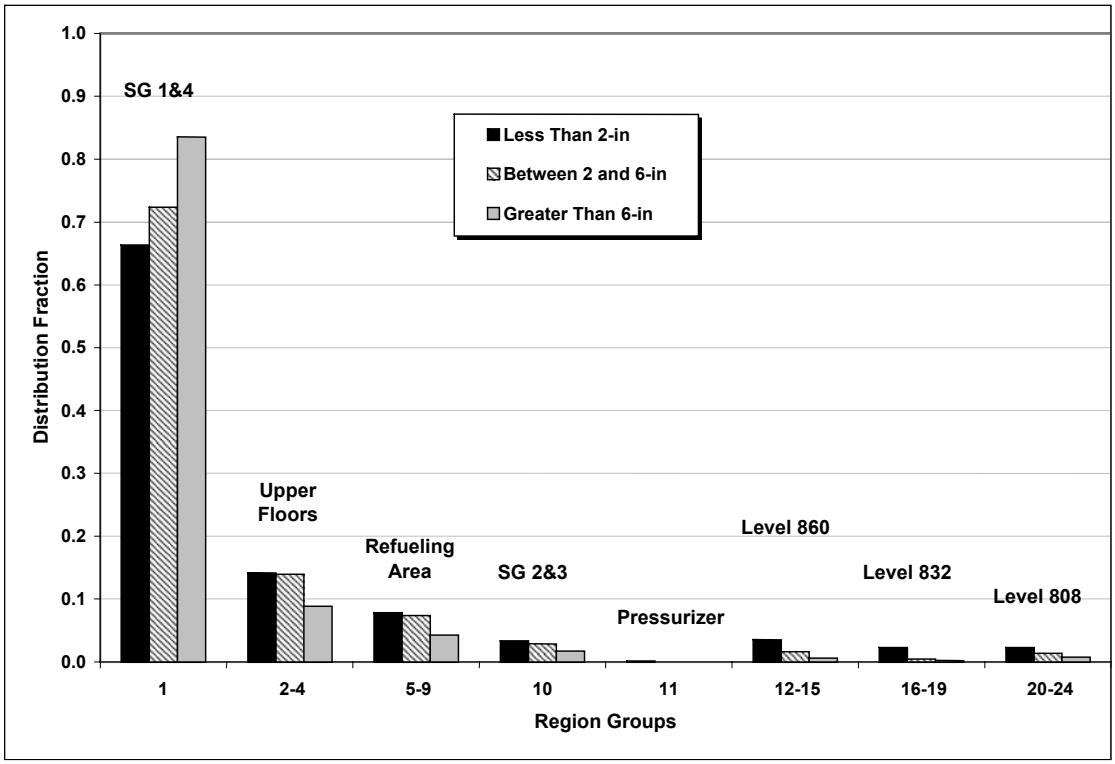

Figure IX-14. RMI Blowdown Distribution by Region Groups.

VI.4.2.1.3 Dispersion by Surface Orientation and Surface Wetness

A review of photos that were taken of RMI debris following RMI debris-generation tests indicates that RMI debris would reside preferentially on the floor surfaces [NEDO-32686, 1996, LA-UR-01-1595, 2001], although some RMI debris was caught on structures. However, the structures in these debris-generation tests were dry; therefore, it is not known if surface wetness would cause RMI to stick to wetted surfaces. Still, it is conservative to place the debris on the floors, where the subsequent washdown would be more effective. Therefore, the various surface-area-weighting factors were set to place most of the RMI debris on the volume region floors. It was assumed that 99% of the RMI debris would reside on the floor. The surface-area fractions shown in Table IX-14 apply to RMI debris as well as to fibrous debris. In these assumptions, ~99% of the RMI debris following blowdown was located where it either was impacted directly by the sprays or was located in the path of the spray drainage, leaving only 1% on surfaces that were wetted by condensation only.

VI.4.2.2 RMI Washdown Debris Transport

The RMI debris surface-retention fractions (i.e., the fraction that was not washed away) were estimated based primarily on engineering judgments and RMI pool debris-transport data. Small-scale testing of the transport of RMI debris in a pool of water demonstrated the ease or difficulty of forcing a piece of debris to move in a pool of water. Debris transport in a flowing layer of water that resides on a floor is similar to the transport of the debris in an established pool of water. Perceptions regarding the transport of RMI debris in nonpool situations are summarized

in Table IX-20. The estimated transport and corresponding retention fractions are shown in Table IX-21 and Table IX-22, respectively.

Table IX-20. RMI-Debris-Washdown Transport Trends

Debris Type	Surfaces Wetted by Condensate	Surfaces Either Sprayed or Receiving Drainage Flow	
		Without Intervening Floor Drains	With Intervening Floor Drains
<2 in.	Minority Transport	Medium Transport	
2 to 6 in.	No Significant Transport	Medium Transport	No Significant Transport
>6 in.	No Significant Transport	Minority Transport	No Significant Transport

Table IX-21. Estimated RMI-Debris-Washdown Transport Percentages

Debris Type	Surfaces Wetted by Condensate	Surfaces Either Sprayed or Receiving Drainage Flow	
		Without Intervening Floor Drains	With Intervening Floor Drains
<2 in.	1%	40%	
2 to 6 in.	0%	30%	0%
>6 in.	0%	10%	0%

Table IX-22. Estimated RMI-Debris-Washdown Retention Percentages

Debris Type	Surfaces Wetted by Condensate	Surfaces Either Sprayed or Receiving Drainage Flow	
		Without Intervening Floor Drains	With Intervening Floor Drains
<2 in.	99%	60%	
2 to 6 in.	1%	70%	1%
>6 in.	1%	90%	1%

All debris that was deposited onto the SG compartment floors and the sump-level floors automatically was assumed to have entered the sump pool; this assumption was not indicated in the tables. This assumption primarily affected the debris that was deposited onto the break-region floor during either blowdown or washdown. The actual movement of this debris from the SG compartment floor into the outer annulus would be driven by the falling and spreading break flow; this would generally be expected to be a relatively high level of transport.

Debris transport resulting from condensate drainage would be expected to affect only the smaller debris. As condensation builds on a surface, it forms a thin film that subsequently drains and typically forms small rivulets of flow. This flow usually would not move around significantly sized pieces of debris. Significant transport of RMI debris does not seem likely; however, it is possible that some of the smaller debris could move with the condensate flow until the condensate flow linked up with more substantial water drainage. It was assumed that 1% of the debris that was <2 in. and subjected only to condensate drainage ultimately would transport to

the sump pool. Furthermore, it was assumed that none of the debris that was >2 in. would transport to the sump pool.

Whenever pieces of debris <2 in. were subjected to substantial flows from impacting the CSs or from the subsequent drainage of the sprays, the flow likely would entrain a substantial portion of that debris. The evaluation of the transport of the smaller RMI debris that was exposed to sprays and/or spray drainage was based on a floor-pool drain velocity estimate and on the pool debris-transport threshold velocities. The drainage-flow velocity calculation assumed that a uniform spray was applied to an upper-level floor area corresponding to the containment-dome spray Trains A and B. A floor-area estimate indicated that ~800 ft^2 of floor area would be drained by each floor drain. A plant calculation estimated that the floor-water hold-up depth would be ~1.5 in. The separate-effect characterization of debris transport in water tests [NUREG/CR-6772, 2002] showed that a turbulent flow velocity of ~0.2 ft/s would be required to cause small stainless-steel RMI debris to tumble or slide along the floor. If it is assumed that circular drainage geometry exists, the transport estimate indicates that 60% to 80% of the floor area would not have sufficient flow velocity to transport small stainless-steel RMI debris, depending on the assumed thickness of the water layer. This conclusion resulted in the 40% transport estimate shown in Table IX-21. Because this calculation did not consider the effect of structures on the transport, which would create locations for debris entrapment, the 40% transport estimate is a reasonable number for the transport of RMI debris that is <2 in. by the CSs.

As was done for fibrous debris, pieces of RMI debris that were >2 in. were assumed not to pass through floor drains or refueling-pool drains. At locations where the larger debris would not encounter floor or refueling drains, 30% of the 2- to 6-in. debris and 10% of the >6-in. debris were assumed to transport. The corresponding fibrous-debris-transport number simply was reduced based on engineering judgment to account for the fact the RMI debris transports less easily than does fibrous debris. In any case, these two estimates affected only a relatively minor portion of the total debris.

Debris erosion of any significance would not happen to stainless-steel RMI debris; therefore, no erosion of the RMI debris by the CSs was considered in this study.

VI.4.2.3 Quantification of RMI Debris Transport

The transport of fibrous debris was quantified using the models presented in Section VI.3 and the input presented in Section VI.4.2. The quantified transport results are presented in Table IX-23. The table shows the transport fractions for each size category, as well as the overall transport fraction. It also shows the fractions of the total ZOI insulation that entered the pool. These fractions then were normalized to provide a size distribution for the debris entering the pool. Approximately 83% of the ZOI RMI was predicted to transport to the sump pool, but only ~20% of that amount was pieces <2 in.

Table IX-23. Fractional RMI Debris-Transport Results

Debris-Size Category	Category Generation Fraction	Size Category Transport Fraction	Fraction of ZOI Insulation	Distribution Entering Sump Pool
<2 in.	0.21	0.82	0.17	0.21
2 to 6 in.	0.12	0.76	0.09	0.11
>6 in.	0.67	0.85	0.57	0.68
All Debris	1.00	0.83	0.83	1.00

VI.4.3 Min-K Insulation Debris Transport

Less than 1% of the insulation in the volunteer-plant containment is Min-K insulation, a form of insulation referred to as microporous or particulate insulation. Although the transport methodology discussed in Section VI.3 also applies to Min-K insulation, a nearly complete lack of airborne transport data for this type of insulation exist, as well as debris-generation data, which were discussed in Section VI.3.2.3. Because of the lack of data for the generation of debris from Min-K insulation, the unknown erosion characteristics of this insulation, and the sparseness of the insulation within the containment (i.e., leads to a potential spatial nonuniform distribution), it was conservatively assumed that all Min-K located within the ZOI would be pulverized into a fine, highly transportable dust. If larger pieces of Min-K debris were inundated by the CSs, these pieces simply could dissolve into fine silt and transport with the spray drainage; however, this outcome is yet to be proven. Although <1% of the containment insulation is Min-K, this type of particulate debris could affect the sump-screen head losses significantly.

A conservative transport fraction for Min-K dust must be relatively high, and it seems likely that this fraction would be similar to the fraction for the transport of fibrous fines without the addition of erosion products, which was ~0.87. That is, the transport of fibrous fines generated from the ZOI to the sump pool was ~87%. (Note that the 93% value that was shown in Table IX-18 included erosion products.) Because the bulk of the 13% of fine fibers that did not transport was located on surfaces wetted only by condensate, it seems likely that a similar result would occur for the Min-K. For this study, it was assumed that 90% of the Min-K dust would transport to the sump pool.

VI.5 BLOWDOWN/WASHDOWN CONCLUSION

A methodology was developed that considers both transport phenomenology and plant features and that divides the overall complex transport problem into many smaller problems that either are amenable to solution by combining experimental data with analysis or that can be judged conservatively based on the foundation of debris-transport knowledge. The quantification of the methodology results in predicted transport fractions that are both conservative and plausible. The overall transport results are shown in Table IX-24. These transport fractions represent the fractions of the insulation by type that was initially located within the ZOI and that subsequently would transport to the sump pool. Detailed results, including size distribution information, are discussed in Sections VI.3 and VI.4.

Table IX-24. Overall Transport Results

Insulation Type	Overall Transport Fraction*	Debris-Size Distribution
Fibrous	57%	Table IX-18
RMI	83%	Table IX-23
Min-K	90%	All Dust

* Overall percentages are for demonstration only.

The overall transport fractions listed in Table IX-24 serve for demonstration purposes but are not valid for plant-specific evaluations because these fractions were calculated using LOCA-generated debris-size distributions that did not account properly for PWR jet characteristics. BWR jet characteristics were substituted for PWR jet characteristics because the PWR jet analyses had not been performed yet. When the PWR jet characteristics become available, it will be a simple matter to recalculate the overall transport fractions using PWR LOCA-generated debris-size characteristics.

Neither the debris-size distributions nor the overall transport fractions in this report are valid for plant-specific evaluations.

The transport fractions for each debris-size category are considered to be conservative for the LDFG insulation in the volunteer plant (but not necessarily for containments of other design). The fibrous-debris-transport analysis contained herein was based on LDFG insulation and may require adjusting for any high-density fiberglass insulation or mineral wool that may also be in the plant.

For the volunteer plant, a high percentage of the fine LOCA-generated debris most likely would transport to the sump pool via the spray drainage flows. The transport fractions tended to decrease as the debris size increased. A majority of the larger debris that was predicted to transport to the sump pool was stopped in the SG compartments that were associated with the break, where subsequent CS drainage was assumed to be readily capable of moving the debris downward to the pool.

The transport of the RMI and Min-K debris was skewed more conservatively toward larger transport fractions than was the fibrous debris because of the lack of transport data. Realistically speaking, the RMI might be expected to transport less readily than would the fibrous debris

because it is heavier. However, a larger fraction of the RMI debris could be trapped in the break region (SG compartments), where it could be transported subsequently into the sump pool and thus the need to skew the transport fractions conservatively. A similar discussion applies to the Min-K because of the lack of LOCA debris-generation data, lack of erosion data, and the potential nonuniform placement of Min-K in the ZOI. Therefore, most of the Min-K must be conservatively assumed to transport to the sump pool as a fine dust or silt.

Conservative engineering judgments were made in this analysis at various steps along the way. The degree of conservatism that was associated with these judgments was intended to ensure conservative final results without straying too far from realistic behavior. The judgments were not intended to be upper bounding. For example, the erosion of LDFG by CSs was assessed in the DDTS as being <1%. In reality, the erosion may be significantly <1%. The 1% value was assumed to be conservative but not far from reality. In addition, many conservative judgments tend to compound as the analysis progresses.

The analyses herein considered only one break location (SG1), although they considered a range of break sizes at that location. Plant-specific analyses must consider a range of break locations. For the volunteer plant, LOCAs can occur within an SG compartment, which is likely the most probable location. A break in the same SG but at a different level likely would have a result similar to the one analyzed because most of the break effluent still would flow to the containment dome. A break in an SG compartment different from SG1 most likely would have a similar result, except that the debris would tend to enter the sump pool at different locations. A break outside the SG compartments, such as in a main steam line, would behave differently than a break inside an SG compartment and probably should be analyzed separately. A break in the pressurizer certainly would be different because that compartment does not vent directly to the containment dome as with the SG compartments (i.e., no major upper openings exist). Therefore, a larger fraction of the debris might be driven out of the pressurizer compartment directly into the sump area, but the total quantity of debris might be substantially less than a primary-loop piping break. Neither a pressurizer-line break nor a main steam-line break was analyzed herein.

In performing blowdown/washdown analyses, it is important that

- the debris-size categories match the characteristics of the debris-transport behavior;
- the break region is analyzed in substantial detail because so much of the debris capture is likely to occur in this region;
- the debris capture along the primary exits from the break region also should be analyzed in substantial detail;
- CS drainage patterns should be determined to support the washdown analysis and to indicate where the debris would enter the sump pool and how the spray drainage would impact sump pool turbulence; and
- vulnerable spray-drainage pathways, where potential debris blockage might occur, should be identified.

VI.6 REFERENCES

1. [NUREG/CR-6772, 2002] D. V. Rao, B. C. Letellier, A. K. Maji, and B. Marshall, “GSI-191: Separate-Effects Characterization of Debris Transport in Water,“ NUREG/CR-6772, LA-UR-01-6882, August 2002.

2. [NUREG/CR-6773, 2002] D. V. Rao, C. Shaffer, B. C. Letellier, A. K. Maji, and L. Bartlein, “GSI-191: Integrated Debris-Transport Tests in Water Using Simulated Containment Floor Geometries,“ NUREG/CR-6773, LA-UR-02-6786, December 2002.

3. [NUREG/CR-6762, Vol. 2, 2002] D. V. Rao, B. Letellier, K. W. Ross, L. Bartlein, and M. T. Leonard, “GSI-191 Technical Assessment: Summary and Analysis of US Pressurized Water Reactor Industry Survey Response and Responses to GL 97-04,“ Volume 2, LA-UR-01-1800, Los Alamos National Laboratory, August 2002.

4. [LA-UR-99-3371, 1999] B. E. Boyack, T. S. Andreychek, P. Griffith, F. E. Haskin, and J. Tills, “PWR Debris Transport in Dry Ambient Containments—Phenomena Identification and Ranking Tables (PIRTs),“ LA-UR-99-3371, Revision 2, December 14, 1999.

5. [LA-UR-01-1595, 2001] D. V. Rao, Clinton J. Shaffer, and Robert Elliott, “BWR ECCS Strainer Blockage Issue: Summary of Research and Resolution Actions,“ prepared for the US Nuclear Regulatory Commission, Los Alamos National Laboratory, LA-UR-01-1595, March 21, 2001.

6. [NUREG/CR-6369-1, 1999] D. V. Rao, C. Shaffer, and E. Haskin, “Drywell Debris Transport Study,“ NUREG/CR-6369, Volume 1, SEA97-3501-A:14, September 1999.

7. [NUREG/CR-6369-2, 1999] D. V. Rao, C. Shaffer, B. Carpenter, D. Cremer, J. Brideau, G. Hecker, M. Padmanabhan, and P. Stacey, “Drywell Debris Transport Study: Experimental Work,“ NUREG/CR-6369, Volume 2, SEA97-3501-A:15, September 1999.

8. [NUREG/CR-6369-3, 1999] C. Shaffer, D. V. Rao, and J. Brideau, “Drywell Debris Transport Study: Computational Work,“ NUREG/CR-6369, Volume 3, SEA97-3501-A:17, September 1999.

9. [NUREG/CR-6808, 2003] C. J. Shaffer, D. V. Rao, M. T. Leonard, and K. W. Ross, “Knowledge Base for the Effect of Debris on Pressurized Water Reactor Emergency Core Cooling Sump Performance,“ NUREG/CR-6808, LA-UR-03-0880, February 2003.

10. [NEDO-32686, 1996], “Utility Resolution Guidance for ECCS Suction Strainer Blockage,“ BWROG, NEDO-32686, Rev. 0, November 1996.

11. [NRC-SER-URG, 1998], “Safety Evaluation by the Office of Nuclear Reactor Regulation Related to NRC Bulletin 96-03 Boiling Water Reactor Owners Group Topical Report NEDO-32686, ‘Utility Resolution Guidance for ECCS Suction Strainer Blockage,’“ Docket No. PROJ0691, August 20, 1998.

12. [OPG, 2001] John Russell, “Jet Impact Tests—Preliminary Results and Their Application,“ N-REP-34320-10000, Revision R00, April 18, 2001.

13. [NUREG/CR-6762, Vol. 3, 2002] D. V. Rao, C. J. Shaffer, and S. G. Ashbaugh, “GSI-191 Technical Assessment: Development of Debris-Generation Quantities in Support of the Parametric Evaluation,“ LA-UR-01-6640, Los Alamos National Laboratory, August 2002.

14. [NUREG/CR-6762, Vol. 1, 2002] D. V. Rao, B. C. Letellier, C. Shaffer, S. Ashbaugh, and L. S. Bertlein, “GSI-191 Technical Assessment: Parametric Evaluations for Pressurized Water Reactor Recirculation Sump Performance,“ LA-UR-01-4083, Los Alamos National Laboratory, August 2002.

15. [SEA-95-970-01-A:2, 1996] Gilbert Zigler et al., “Experimental Investigation of Head Loss and Sedimentation Characteristics of Reflective Metallic Insulation Debris,“ draft letter report, prepared for the US Nuclear Regulatory Commission, SEA No. 95-970-01-A:2, May 1996.

Attachment 1 to APPENDIX VI:

VOLUNTEER-PLANT SPRAY-WATER DRAINAGE ANALYSIS

INTRODUCTION numbered headings throughout attachment?

A postulated LOCA in the volunteer plant would distribute insulation debris throughout the containment, whereby the subsequent drainage of spray water following the LOCA would transport portions of this insulation debris toward the recirculation sump screens. A best estimate of how the water would drain to the sump was performed to support subsequent debris-transport calculations. The analysis will help to identify spaces and surfaces where insulation debris likely would not be washed away by sprays or drainage flow (e.g., an area that was not impacted by sprays and has too little drainage flow to transport debris). The analysis will help to determine how the drainage water enters the sump pool, which in turn will affect debris transport within that pool.

SYSTEM DESCRIPTIONS

The CS systems in the volunteer plant consist of two independent trains (Trains A and B), with headers located in four containment regions. Spray nozzles are located in one of four regions of the containment:

- Region A—Containment dome spraying down toward Level 905;
- Region B—Below Level 905 spraying Level 860;
- Region C—Below Level 860 spraying Level 832; and
- Region D—Below Level 832 spraying Level 808.

The specifications are shown in Table 1 **consistently number by section? e.g., VI-1?**for both trains in Unit 1, combined. Spray Train B has one more nozzle in the dome than Train A; therefore, the flows that are associated with single train operations constitute essentially half of the flows shown for both trains. Unit 1 has seven more nozzles than Unit 2. The drainage estimate performed for Unit 1 is applicable also to Unit 2.

Table 1. Unit 1 Spray Nozzle Summary

Spray Region	Number of Nozzles	Nozzle Flow (gpm)	Region Flow (gpm)
A	545	20	10,900
B	134	20	2680
C	28	20	560
D	54	20	1080
Total	761	20	15,220

The containment was designed to drain the spray water down to the containment recirculation sumps. Furthermore, the containment apparently was designed to minimize water holdup,

thereby maximizing the depth of the sump pool. Several features of the containment determine the primary drainage pathways in the containment. These features include the following.

Floor Drains—A primary means of draining spray water is the floor drains that drain water from one floor directly down to the next floor. A typical drain, which is ~6 1/2 in. in diameter, is shown in Figure 1. **consistently number by section? e.g., VI-1?**At the top of this figure, another type of drain is shown that drains directly to the containment sump. Floor surfaces are sloped to channel water into the drains.

Figure 1. Typical Floor Drain.

Water Barriers—Water drainage is controlled by water barriers (curbs)—both concrete and metallic types—that are placed around floor-area perimeters to prevent water from draining from those perimeters. However, these barriers do not cover the entire perimeter of a floor. Gaps exist in the barriers at locations such as the areas around walkways and ladders. In many places, water can flow from a floor perimeter onto another floor, into the gap between the internal structures and the outer wall, into an SG compartment, into a stairwell, etc. A typical curb is shown in Figure 2. Figure 3 shows another curb next to an SG compartment that illustrates a discontinuity in a curb.

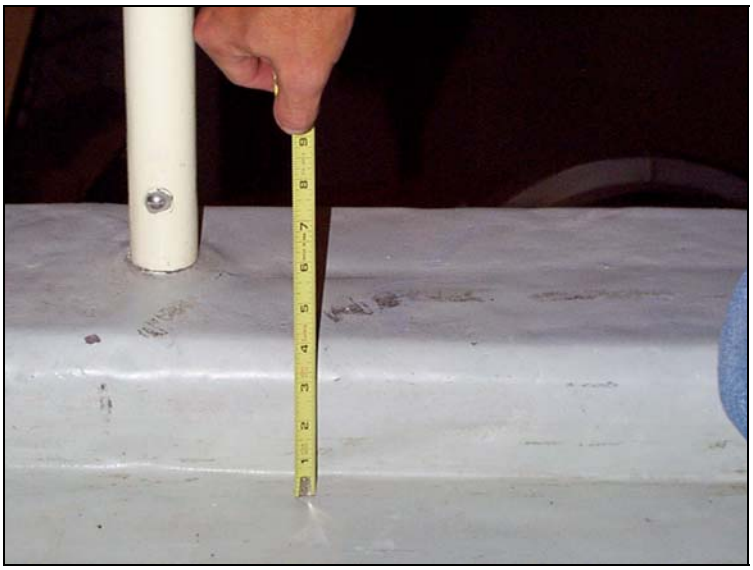

Figure 2. Typical Concrete Curb.

Figure 3. Gap in Concrete Curb Surrounding an SG Compartment.

Refueling Pool Drains—A substantial portion of the dome sprays will fall into the refueling cavity and accumulate in the three pool areas of the cavity. During normal operation, the pool drains are open, allowing spray water to drain down to the sump. The pool drains consist of 4-in. and 6-in. sizes. Figure 4 shows the drains in the pool that are used to store the reactor vessel lower internals during refueling. A 4-in. drain with a cover screen (with holes ~1/4 to 1/2 in. in diameter) is shown near the center of the photo. Two 6-in. drains also are shown in the upper-right (cover off) and lower-right corners (cover in place). These 6-in. drains are closed off with blind flanges during refueling and are uncovered during normal operations. The 4-in. drains drain down into the labyrinth of rooms on Level 808, which is located directly below the refueling pools. The two 6-in. drains drain to SGs 3 and 4. The pool that is used to store and transfer fuel is drained to Level 808 by a single 4-in. drain. The pool that is used to store reactor vessel

upper internals during refueling has a single 4-in. drain, which drains into the pool that stores the lower internals.

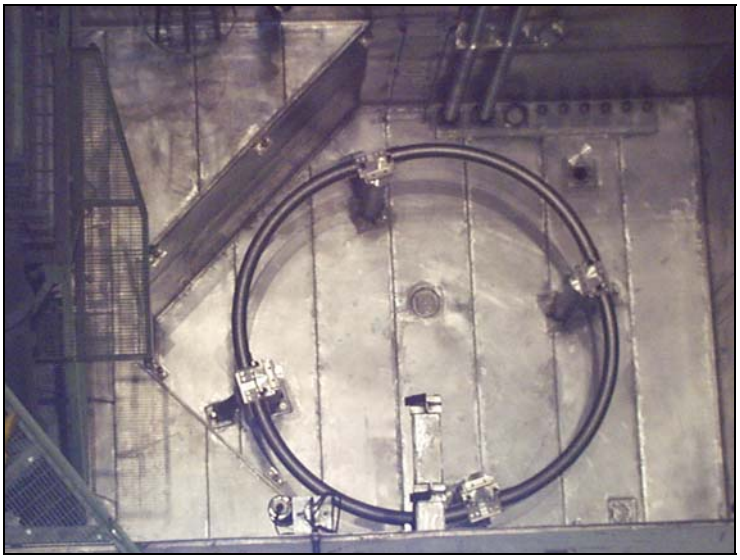

Figure 4. Refueling Pool Drains.

Floor Gratings—Water drainage between floors also occurs through the floor gratings that cover several open areas in the floors (e.g., the equipment-transfer floor hatches).

Stairwells—At several staircases, water can drain from one floor to the next. Two primary staircases extend all the way from sump Level 808 up to the top floor at Level 905.

APPROACH number as heading?

A review of containment drawings and plant documents led to many general observations.*

- Little, if any, water is expected to drain down the elevator shaft by way of the elevator doors. The elevator shaft was not treated as a wetted drain perimeter in the plant's minimum pool calculation, and the floors generally slope away from elevator. Furthermore, elevator doors may prevent water entry into the elevator shaft.

- The pressurizer compartment should remain essentially dry. A roof covers the compartment so that sprays do not enter this compartment. Drains and sloping floors generally prevent water flow into this compartment at other entrances.

- Water entering the SG compartments consists of dome-spray droplets falling directly into those compartments. Droplets falling onto the wall-tops and floor that are located between or near the SG compartments likely will flow into the SG compartments. Also, the two 6-in. refueling-pool drains flow directly into the SG compartments.

*The most useful drawings were floor layouts that showed floor slopes, water barriers, and floor drains. The most useful document was a plant calculation of the minimum sump-pool height.

- Water entering the stairwells consists of spray droplets falling directly into stairwells and of some water overflowing a floor perimeter.

- Water entering the refueling cavity consists of spray droplets falling directly into the cavity. This water includes droplets that are falling onto walkways surrounding the refueling pool and that subsequently would flow into the pool.

- Water entering the gap between the inner containment structure and the containment outer wall consists of spray droplets impinging the outer containment wall and subsequently flowing down the liner and of water from gaps in the water barriers along the floor perimeters.

- Substantial quantities of water are intended to drain from one floor to the next by way of the floor drains between the floors.

Because of the complexity of the water drainage, many simplifying assumptions and engineering judgments were necessary. The primary assumptions include the following.

- All spray systems were active (only one possible spray scenario was evaluated).[*]

- No blockage of drain flows by debris was postulated.[†]

- Dome spray droplets fall vertically and distribute uniformly across the containment cross section before encountering any containment structure. Distribution was based on cross-sectional areas.

- Crosswalks on Level 905 that are directly between the refueling cavity and the SG compartments drain into those compartments.`

- Refueling cavity walkways on Level 860 drain into pools.

- Levels 873 and 851 do not have floor drains (floor drains not shown in drawing).

- Water draining onto Level 849 from Level 860 subsequently drains to Level 832.

- Water drains that drain directly to a containment sump (e.g., the one shown in the upper portion of Figure 1) are neglected. These specialized drains were not delineated in the drawings and are assumed to be substantially fewer in number than the main floor drains.

Engineering judgments were necessary where insufficient data were available to estimate drainage accurately.

The calculational approach included the following steps:

- the locations of all spray nozzles were identified;

[*]The scenario where one train operates and one train is inactive can be estimated by dividing all flows for both trains by a factor of 2.

[†]Insulation debris could block a floor drain or a refueling pool drain.

- the dome spray impacting and running down the containment liner was estimated;
- the main floor areas on Levels 808, 832, 860, and 905 were nodalized into three sections for each floor;
- the locations where the spray droplets would settle were identified; and
- the drainage process was tracked from the uppermost surfaces down to Level 808.

The dome spray nozzles, arranged around four rings for each of the two trains, are aimed in four different directions. Some of the nozzles apparently are aimed to spray the dome liner. A portion of this spray impacting the liner subsequently should drain down the liner itself. The number of nozzles aimed in each of the four directions was tabulated for each ring. Then the spray impact and runoff was judged for each ring location. Of the 10,900-gpm total dome spray flow, 700 gpm was estimated to flow down the liner.

Figure 5 illustrates the subdivision of the main floors. Section 1 includes the side of the containment where the main steam and feedwater lines penetrate the containment. Drainage on this side would be distinctly different from the remainder of the containment. Section 2 includes unique features such as Level 849 and Level 832; sprays do not extend into this section. Section 3 includes the remainder of the floors.

To estimate the distribution of settled dome spray water, the containment cross-sectional area was estimated for each section of floor, refueling cavity, SG compartment, open area, etc. It was assumed that the spray droplets would fall uniformly onto these areas. Once the settled flows were determined, the drainage from floor to floor was estimated, starting with the uppermost floor surface. For each floor section, a drainage distribution was estimated, based on floor sloping relative to drainage pathways.

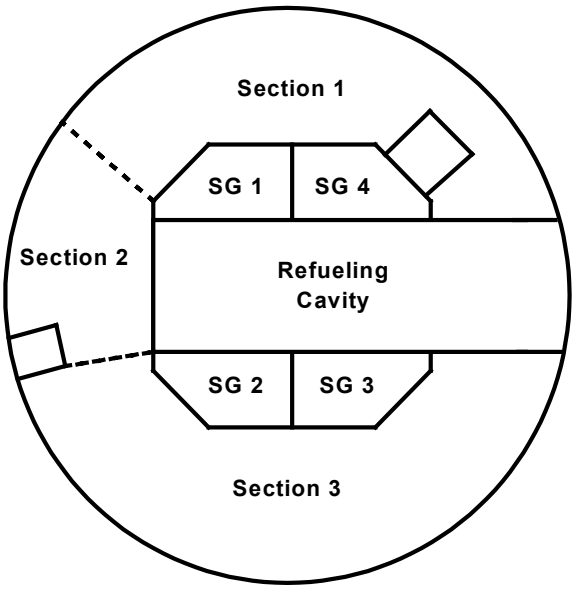

Figure 5. Schematic of Floor Sections.

The overall spray drainage is shown in Figure 6. The dashed lines represent spray droplets falling onto a surface[*] (the arrow head indicates the surface receiving the droplets). The numbers indicate flow rates in gallons per minute. The solid lines indicate water draining from one surface to another or water falling into and through a stairwell or the outer wall gap. A diagram illustrating where the water enters the Level 808 sump pool is shown in Figure 7.

[*] The surfaces are not drawn to scale.

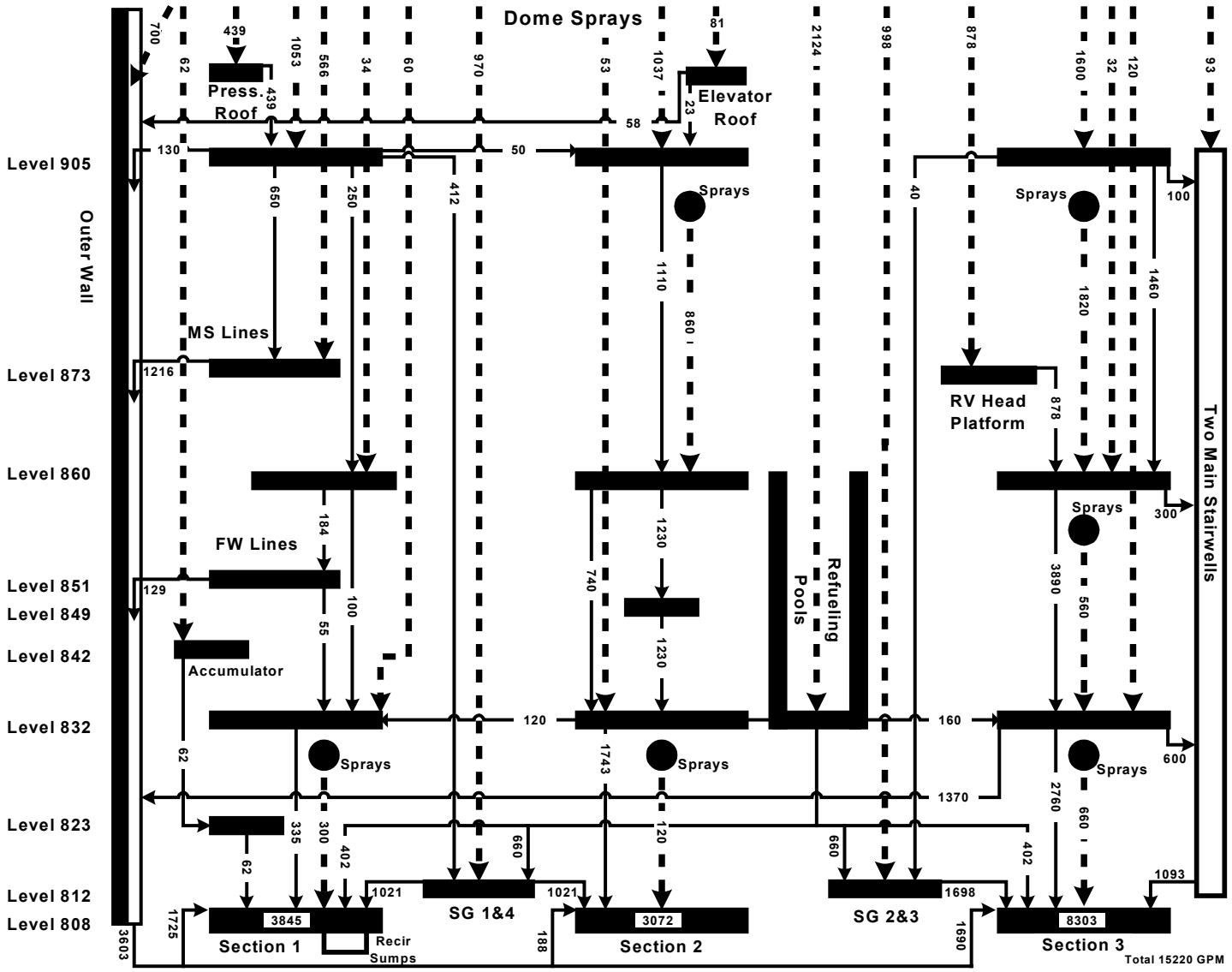

Figure 6. Spray-Water Drainage Schematic.

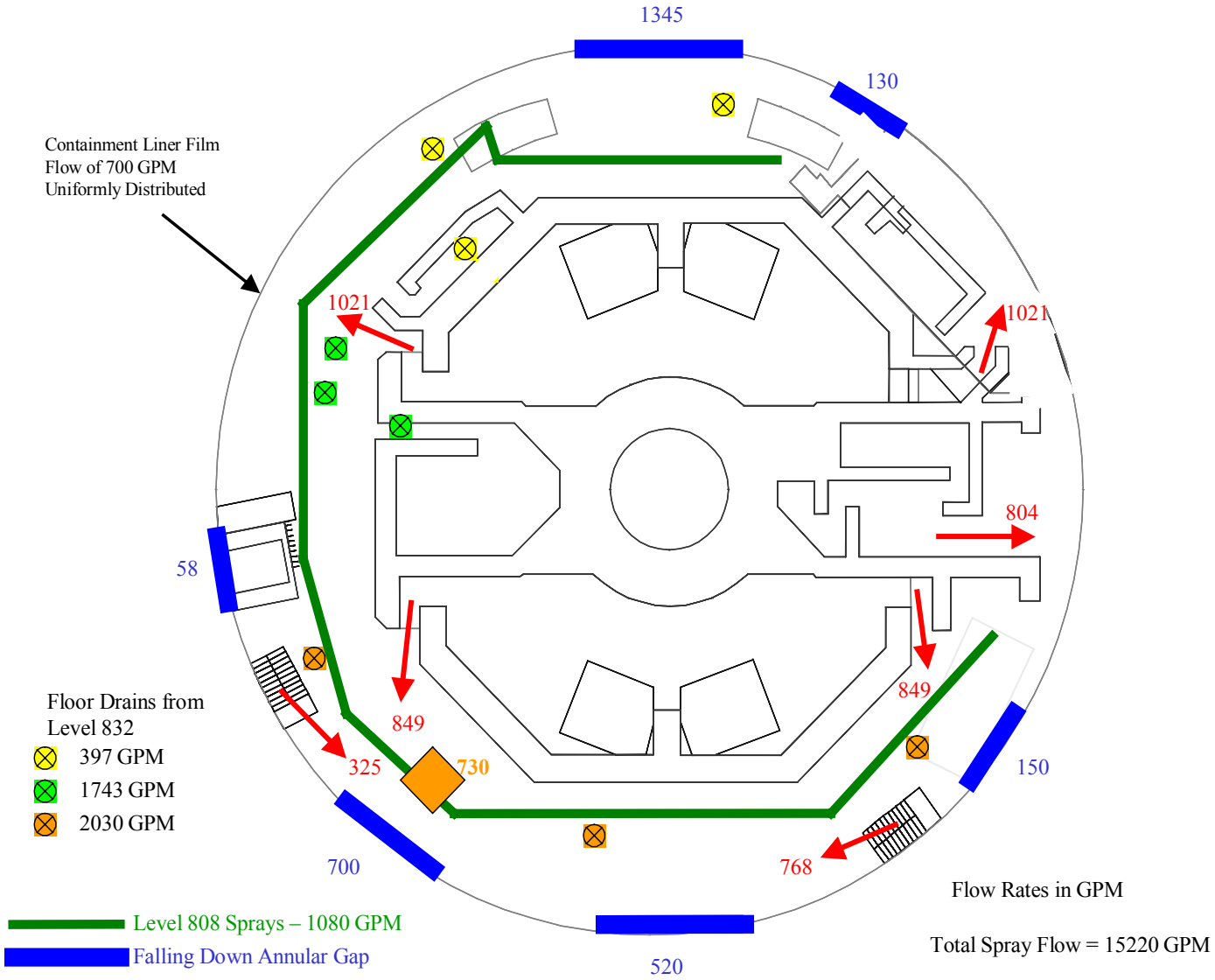

Figure 7. Spray-Water Drainage to Level 808 Sump Pool.

APPENDIX VII: Characterization of PWR Latent Debris

The United States (US) Nuclear Regulatory Commission (NRC) has recently initiated a study conducted through Los Alamos National Laboratory (LANL) and the University of New Mexico (UNM) to characterize latent debris samples collected at five individual volunteer plants. The focus of this work is to study physical attributes of dust and dirt, such as particulate-to-fiber mass ratio, size distributions of particulate, material and bulk densities, and hydraulic parameters, including the specific surface area. Because of variations in plant collection methods and sampling schemes, it is not possible to make estimates of total latent-debris inventories. [trh1]This appendix documents preliminary results of that study that are relevant to the supplementary guidance provided by the staff in Section 3.5 of the safety evaluation report (SER).

A total of five sets of samples were received at LANL for analysis, but only four were totally characterized. The fifth set was not characterized fully because it was dominated by paint chips generated from pressure washing and was therefore deemed to be unrepresentative of pressurized-water-reactor (PWR) containment debris. Material property data collected for the latent-debris samples establish the basis for preparation of a particulate-debris simulant that is suitable for large-scale head-loss testing at UNM. The objective of head-loss testing is to quantify the hydraulic properties of latent debris that are needed for the proper application of the NUREG/CR-6224 debris-bed head-loss correlation.

The experimental scope for sample characterization was as follows.

1. The debris was removed from its shipping container and transferred to plastic laboratory containers for gamma-spectrum counting.

2. The “fiber“ and “particle“ fractions were separated from the remaining (or “other“) debris items by manual manipulation, sieving, and water rinsing.

3. Particulate size distributions were obtained by graduated sieving.

4. The weight of fine particles attached to swiping (masslin) **need to correct throughout SER** cloth or filter paper was determined by mass balance and comparisons of clean collection media to soiled collection media.

5. The fiber thickness/diameter was determined by scanning electron microscopy (SEM) and microphotographic statistics.

6. The material and bulk densities of fibers were estimated by mass measurement combined with volume estimates obtained from water displacement and direct measurement in graduated columns, respectively.

7. Particle surface area and density measurements were taken using state-of-the-art nitrogen adsorption techniques.

8. Scanning electron microscope/energy-dispersive spectroscopy (EDS) methods were used to characterize the chemical composition of representative particulate and fiber samples.

Figure VII-1 illustrates a typical variety of composition and proportion between particulate, fiber, and other larger pieces that are assumed to have minimal transport potential. All plants submitted multiple samples ranging from a few grams to several thousand grams that exhibited similar characteristics. For some plants, the samples had to be combined to obtain meaningful measurements; for others, each individual sample could be fully characterized.

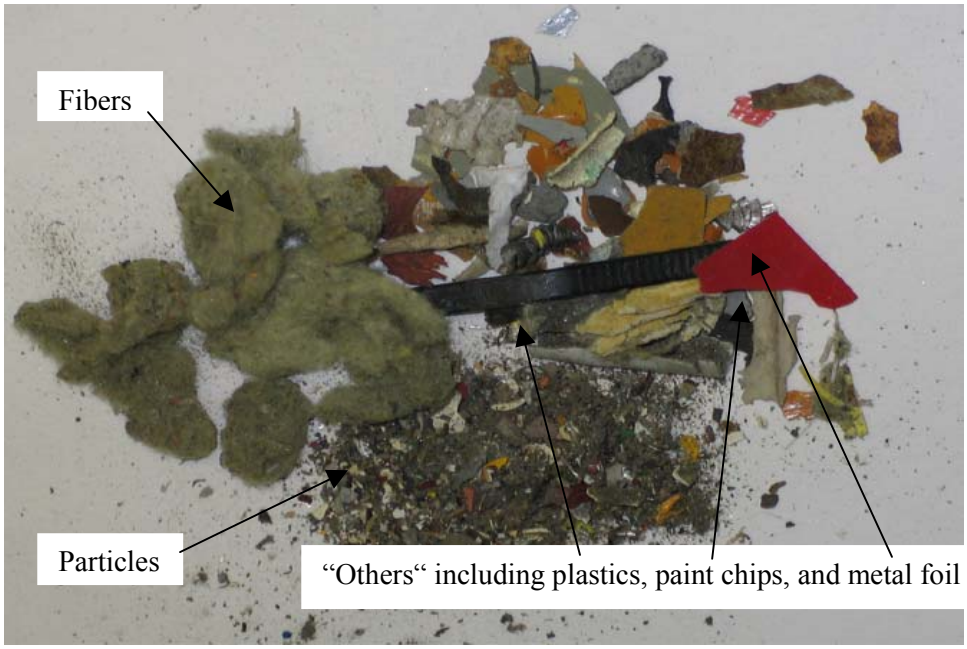

Figure VII-1. Representative Latent-Debris Components from a Single Volunteer Plant.

Objects larger than a 0.132-in.-mesh-size sieve were classified as a debris type "other" than particulate or fiber. This category of size, composition, and characteristics should be removed from any plant-specific samples that are collected before applying any mass fractions reported in this appendix. Larger latent debris types are not assumed to be transportable at recirculation pool velocities and so do not contribute to long-term increases in sump-screen head loss. However, any of this debris category that is present on the sump-pool floor may readily transport to the sump during pool fill-up. Table VII-1 presents the range of particulate and fiber mass fractions that were measured for samples that were characterized after the larger pieces were removed. From these data come the generic recommendation that 15% of the transportable latent debris be assumed to be fiber.

Each volunteer plant used a different collection method and sampling scheme. When separating particulates by wet sieving into fractions (>2 mm, 500 μm to 2 mm, 75 μm to 500 μm, and <75 μm), it became apparent by comparing plants that scraping and bristle-brush collection were not effective at capturing the smaller particulate fractions. This conclusion was further reinforced by SEM photos of filter papers and cloth swipes that showed significant loadings of particles <10 μm in diameter. High-efficiency particulate air (HEPA) filter vacuuming with the brush attachments or manual swiping with lint-free (masslin) cloth are recommended collection methods for characterizing plant-specific latent debris loadings.

Table VII-1. Particulate and Fiber Mass Fractions for Volunteer Plants A–D

Plant	Particle Weight	Fiber Weight	% Particle	% Fiber
A	5.42	1.04	84	16
B1	214	20	91	9
B2	369	64	85	15
B3	390	37	91	9
B4	592	47	93	7
B5	792	34	96	4
B6	122	50	71	29
B Total	2479	252	91	9
C	13.77	0.76	95	5
D1	2.51	0.47	84	16
D2	0.29	0	100	0
D3	12.45	0.28	97	3
D4	34.34	2.20	94	6
D6	5.56	0.1	98	2
D8	9.15	0.09	99	1
D10	11.98	0.74	94	6
D15	74.92	7.0	91	9
D Total	151.2	10.88	93	7
Sample Range	Total Particulate	71%–100%		
	Total Fiber	0%–29%		
Plant Range	Particulate	84%–95%		
	Fiber	5%–16%		

The material density of characterized fibers was found by water displacement measurements of 10 plant samples to range between 1.0 to 1.9 g/cm^3. The mean value of 1.5 g/cm^3 is recommended for use if needed in generic latent-debris assessments. However, a more relevant parameter of fiber is the dry-bed bulk density that can be used to estimate the volume of fiber needed to form a 1/8-in.-thick thin bed across the wetted-screen area of a given sump configuration. This property and the suggested application is comparable to the use of the as-manufactured bulk density for fiberglass insulation.

The dry-bed density of latent fiber depends greatly on the amount of compaction applied for the measurement. Several alternatives were tried, but ultimately the staff recommends using the fiberglass density of 2.4 lbm/ft^3 = 38.4 kg/m^3 as a surrogate for dry latent debris. Similarly, fiberglass hydraulic properties should also be used as a surrogate for latent fiber. These recommendations are supported by the following rationale. First, in cases where fiberglass debris is present on the screen, minor inaccuracies in the latent fiber properties will not affect head-loss calculations. Second, where latent fiber is the dominant fibrous debris source and there is sufficient quantity to form a thin-bed filter, maximum head loss will be dominated by the properties of particulates captured on the fiber bed. Again, the difference between the actual hydraulic behavior of latent fiber and the presumed properties of fiberglass will not affect head-loss calculations adversely.

Particulate densities for each size fraction and volunteer plant were measured very accurately using the Brunauer-Emmett-Teller (BET) nitrogen adsorption method. Densities of particulates in the debris range from 2 to 4 g/cm^3 with only a few exceptions, and densities for most of the

samples range between 2.5 and 3.0 g/cm^3, regardless of their particle size. These data form the basis of the recommendation for a nominal latent particulate density of 2.7 g/cm^3.

A nominal size distribution of particulates found in the latent debris samples was used as a starting point to develop a formula for surrogate particulate debris that could be tested in a vertical-flow test loop at UNM. This apparatus permits measurement of pressure drop across a debris bed of known composition under a range of water velocities. Hydraulic parameters of the debris bed can then be inferred from differential pressure data by iteratively applying predictive correlations until the model results envelop a range of observed data. Material-specific parameter values, such as the specific surface area that are inferred in this manner, are only appropriate for use with the particular head-loss formula with which they were derived. In this case, the NUREG/CR-6224 head-loss correlation was applied. Microporous flow-resistance tests were performed on both the latent-debris samples and the surrogate formula to confirm that the surrogate could produce reasonably representative yet conservative hydraulic behavior.

Equivalent mass fractions of common sand and clay-based soil were used to recreate the size distribution of the latent particulate. Over a set of well-conditioned head-loss tests where the surrogate particulate was tested in combination with fiberglass insulation, the specific surface area of the surrogate was estimated to be 106,000 ft^2/ft^3. Analyses of these tests were complicated by penetration of the debris bed by extremely fine clay silt that continued to circulate in the test loop. Within the range of the tests where flow velocities at the screen are <0.2 ft/s (uncompressed fiber bed) and the estimated particulate-to-fiber mass ratios cannot exceed 3, the estimated particulate loading on a postulated debris bed can be reduced by 7.5% (one-quarter of the <75-μm mass fraction) to accommodate realistic debris-bed penetration of latent fine particulates.

The surrogate debris formula was further refined by eliminating the latent-debris fraction with nominal dimensions >2 mm because the particles (sand grains) are not likely to transport at pool velocities <0.5 ft/s that may exist near the screen under recirculation conditions. This size fraction represents ~22% of the particulate mass on average that can be discounted from the particulate inventory that is available for long-term transport under recirculation. This size fraction may be subjected to high-velocity transport during fill-up, and so the fractional decrease was only recommended for latent-particulate inventories residing above the flood level.